LASER SURFACE STRUCTURING OF BIOCOMPATIBLE POLYMER FILMS FOR POTENTIAL USE IN TISSUE ENGINEERING APPLICATIONS

TIAW KAY SIANG

(B.Eng. (Hons), NUS)

A THESIS SUBMITTED

FOR THE DEGREE OF DOCTOR OF PHILOSOPHY

DEPARTMENT OF MECHANICAL ENGINEERING

NATIONAL UNIVERSITY OF SINGAPORE

2009

Preface

The thesis is submitted for the degree of Doctor of Philosophy in the Department of Mechanical Engineering at the National University of Singapore under the supervision of Professor Teoh Swee Hin and Associate Professor Hong Minghui. No part of this thesis has been submitted for other degree at other university or institution. To the author's best knowledge, all the work presented in this thesis is original unless reference is made to other works. Parts of this thesis have been published or presented in the List of Publications shown in page xvi:

Acknowledgements

The author would like to express his most sincere gratitude Professor Teoh Swee Hin and Associate Professor Hong Minghui, for their advice, support and guidance throughout the entire course of his research study. He is very grateful for the encouraging comments during the difficult times he has encountered. Through this research, I believed I have discovered some of my strong points and managed to improve on my weaknesses. Most importantly, I hope I have met my supervisors' expectations, and to embark on my career milestone henceforth.

He would like to extend his gratitude to Professor Seeram Ramakrishna and his staffs for providing experimental facilities, such as the VCA-optima Surface Analysis System for water contact angle measurement and the Perkin-Elmer Pyris-6 DSC for thermal properties measurement. He would also like to thank Dr. Zhang Yanzhong for his support and assistance in the carrying out the measurement of tensile properties of PCL films using the Instrom Universal Tensile Tester.

Last but not least, he would like to express his most sincere thanks to all graduate and undergraduate students in BIOMAT, including Mr. Chong Seow Khoon, Mark, Mr. Chen Fenghao, Dr. Wen Feng, Dr. Bina Rai for their help, advices and encouragement along the way.

Table of Contents

Chapter 3

Synthesis of PCL thin films

Chapter 4

Theoretical Simulation of Heat Accumulation during Laser Ablation of PCL Films

Summary

The research scope encompasses the different methods of fabricating the biocompatible and biodegradable poly(ε-caprolactone) (PCL) thin films through simultaneous bi-axially drawn films prepared via: 1) conventional solution casting, 2) spin casting and 3) solvent-free method of hot roll-milling. The purpose of biaxial drawing is to enhance the mechanical properties of the film. PCL films were shown to be suitable for membrane tissue engineering applications. However, prior treatment of sodium hydroxide solution or plasma was required to provide better affinity for cells. Alternative method to treat the PCL films using different lasers to modify the surface by creating micro-structures were carried out. In this study, the mathematical modeling of temperature-rise and heat propagation on the PCL film during the impingement of laser using different wavelengths and pulse duration was studied and compared with the actual results. The scope of this thesis ended with the degradation study of PCL films caused by the irradiation of the lasers.

Biaxial drawing of the PCL sheets into ultra-thin films enhanced both the tensile strength and modulus. This was largely due to the polymer chain extension and orientation during the biaxial stretching process. As the thickness of the PCL films were substantially reduced by the biaxial drawing, the water vapour transmission rate increased significantly, which subsequently allows better bidirectional gas and moisture diffusion through the film.

Laser micro-processing on PCL films by Nd:YAG (Neodymium-doped yttrium aluminium garnate) lasers to create micro-structures and micro-trenches was carried out. The thickness of the PCL films was found to play an important role in the degree of melting around the laser spot due to a larger volume at higher thickness. Temperature-rise modeling of the laser irradiation on PCL film was evaluated and the results showed that different focusing spot sizes delivered through different lens played an important role in the cooling rate of the material significantly. The laser which was delivered through plano-convex lens with long focal length and smaller numerical aperture experienced a cooling time constant of 2 ms., while an objective lens with short focal length and high numerical aperture experienced a cooling time constant of 8.4 μs. A slow cooling rate is found to be able to register a high temperature rise of up to 1200 K while a fast cooling rate registers a temperature rise of 88 K. The different heat rise can in turn affect the dimensions of the micro-holes produced and the radial heat flow around the micro-holes region. These theoretical simulation results of heat propagation explain the actual results of the laser micro-processing on the PCL thin films.

Femtosecond laser and KrF excimer laser was used to modify the surface by producing arrays of micro-perforations. Higher pulse energy increased the width of the Gaussian bean profile and enlarged the micro-pores drilled on the PCL film while lower pulse number increased the deposition of ejected materials back on the film surface. These micro-pores, together with the material deposits, were believed to have caused the rupture of thin liquid membrane that resulted in substantial reduction in the water contact angle by up to 30%, hence enhancing the surface wettability.

Lasers can also be used to induce chemical modifications through photo-chemical reactions. This is especially so for UV laser which can cause the breakdown of polymer chain by the high energy photon absorption. Photo-chemical oxidative degradation was believed to be the main breakdown mechanism for PCL films exposed to KrF excimer laser as it exhibited the highest amount of degradation, resulting in large reduction in number-average molecular weight (M_n) and weighted-average molecular weight (M_w), and hence an increase in polydispersity index. Conversely, thermo-oxidative degradation was found to have taken place in PCL films processed by Nd:YAG lasers and the results showed less surface oxidation and changes to the values of M_n and M_w and hence, relatively unchanged polydispersity index.

In conclusion, the work presented in the thesis showed the versatile use of lasers as a tool for laser micro-structuring and inducing chemical changes on self-developed PCL thin films. The processed films can be suitable for use on wide array of applications such as flexible membrane tissue engineering matrices, drug delivery and cell encapsulation.

List of Tables

List of Figures

List of Publications:

International journals:

1. K.S. Tiaw, P.S. Tan, M.H. Hong, Z.B. Wang, S.H. Teoh. *Effect of nanosecond and femtosecond pulse duration of laser processing of thin biodegradable polymeric film*. Proceedings of SPIE, **2004**, 5662: p. 684-688.

2. K.S. Tiaw, S.W. Goh, M.H. Hong, Z. Wang, B. Lan, and S.H. Teoh, *Laser surface modification of poly(e-caprolactone) (PCL) membrane for tissue engineering applications.* Biomaterials, **2005**. 26(7): p. 763-769.

3. M.H. Hong, Q. Xie, K.S. Tiaw and T.C. Chong. *Laser Singulation of Thin Wafers & Difficult Processed Substrates: A Niche Area over Saw Dicing.* Journal of Laser Micro/Nanoengineering, **2006**. 1(1): p. 84-88.

4. K. S. Tiaw, S.H. Teoh, R. Chen and M.H. Hong, Processing Methods of Ultrathin Poly(ε-caprolactone) Films for Tissue Engineering Applications. Biomacromolecules, **2007**: 8(3): p. 807-816

5. K.S. Tiaw, M.H. Hong and S.H. Teoh. *Precision laser microprocessing of polymers*. Journal of Alloys and Compounds, **2008.** 449(1-2): p. 228–231.

6. K.S. Tiaw, M.H. Hong and S.H. Teoh, Laser Microstructuring of Poly(ε-caprolactone) Thin Films: Study of Surface Chemistry, Degradability and Potential Applications in Tissue Engineering. **2009**. *(Submitted)*

Conferences:

1. M.H. Hong, S.M. Huang, W.J. Wang, K.S. Tiaw, S.H. Teoh, B. Luk'yanchuk, and C.T. Chong. *Unique functional micro/nano-structures created by femtosecond laser irradiation*. Proceedings in Advanced Optical Processing of Materials held at the MRS Spring Meeting. April 22 - 23, **2003**

2. K.S. Tiaw, S.W. Goh, M.H. Hong, Z. Wang, B. Lan, and S.H. Teoh. *Laser surface modification of poly(e-caprolactone) (PCL) membrane for tissue engineering applications*. Proceedings in International Conference on Materials for Advanced Technologies. December 7 - 12, **2003**. Singapore. (Oral)

3. K.S. Tiaw, P.S. Tan, M.H. Hong, Z. Wang, and S.H. Teoh. *Effect of nanosecond and femtosecond pulse duration of laser processing of polymeric membrane*. Proceedings in 5th International Symposium on Laser Precision Microfabrication - Science and Applications. May 11 - 14, **2004**. Nara, Japan. (Poster)

4. K.S. Tiaw, S.H. Teoh, and M.H. Hong. *Ultra-short pulse laser processing of ultra-thin poly(e-caprolactone) films*. Proceedings in 1st Nano-Engineering and Nano-Science Congress. July 7 - 9, **2004**. Singapore. (Poster)

5. K.S. Tiaw, M.H. Hong, T.S. Ong, Q. Xie, S.H. Teoh, *Laser Micro-structuring of Newly-developed Ultra-thin Poly(ε-caprolactone) Films.* Proceedings in 6th International Symposium on Laser Precision Microfabrication - Science and Applications. April 4 - 8, **2005**. Williamsburg, Va, USA. (Poster)

6. K.S.Tiaw, M.H. Hong, S.H. Teoh, *Precision Laser Micro-processing of Polymers*. Proceedings in 1st International Symposium on Functional Materials. December 6 – 8, **2005**. Kuala Lumpur, Malaysia. (Poster)

Chapter 1:
Introduction

1.1 General Background

Current applications of biomaterials for tissue engineering (TE) involve the combination of a scaffold with cells and/or biomolecules that promote the repair and regeneration of tissues. These TE constructs are under vigorous exploration and have resulted in the incessant emergence of diverse strategies. However, despite intense efforts, the ideal tissue engineered construct has yet to be discovered. From an engineering perspective, significant advances in scaffold design and fabrication have evolved in the past decade. Our interdisciplinary group at the National University of Singapore has evaluated and patented the parameters necessary to process polycaprolactone (PCL) and PCL-based composites by fused deposition modeling (FDM). Other cutting-edge technologies, such as biaxial-stretching and electro-spinning, have also been utilized to manufacture PCL-based biomaterials with unique macro- and nano-architectures that are useful for drug, growth factor and cell delivery applications. Lasers are also used to modify the surface of the biaxially drawn PCL films to enhance its purpose.

1.2 Current progress of laser treatment in biopolymers

At present, polymers are becoming very versatile and are used in various industries, such as the food, electronics, automobile, medical and other manufacturing industries [1].

Polymers are gaining more attention as their physical properties can be enhanced for higher load-bearing applications, light weight, cheaper to produce and widely available. To extend its functional usage, research in the surface modifications of the polymers has become more intense. Most polymers surfaces are inert, hydrophobic in nature, and usually have a low surface energy. Therefore, they do not possess specific surface properties that are needed in some applications. The purpose of surface treatment are: to modify the surface layer of a polymer by introducing some functional groups into the surface to increase surface energy, to introduce surface cross-linking, to improve its wettability, to modify sealability, to adjust dye uptake and to be resistance to glazing. All these surface treatments are carried out while the desirable bulk properties of the polymers are retained [2]. Surface treatment can also be used to improve the barrier characteristics of polymers and impart it with antimicrobial properties.

Surfaces of polymeric membranes have been modified by chemical means for years, but these methods require rigorous process control and can lead to undesirable surface changes, such as severe surface roughening, excessive surface damage (cracks, pitting, etc.) and surface contamination. They may also cause environmental problems due to the chemical agents used.

Laser treatments offer advantages over both chemical and other physical methods. They enable precise modification of certain surfaces that are difficult to treat with conventional chemical methods. The resulting modified surfaces are free from contaminants. Most importantly, the bulk properties of the material remain intact. They are therefore rather simple techniques, easily controlled and environmentally clean and safe. Due to these striking properties that laser treatments have and the development of industrially applicable laser systems, laser-assisted modification of polymer surfaces is a rapidly growing and developing field that has gained considerable interest among scientists in the past decade.

Surface modification using a laser can be carried out in a variety of ways, such as: etching, ablation, deposition, evaporation and surface functionalization. The types of laser to be used, the ambient conditions and the materials to be treated are also important factors to be considered. Therefore, a large number of lasers that are capable of operating at different wavelengths and operation modes (continuous wave or pulsed) are available for the surface modification of various materials, depending on the properties required of the final products.

A substantial number of experiments and studies have been carried out by using lasers to alter the surface property of polymers. The surface of polydimethysiloxone (PDMS) membrane of 0.3 mm thickness was successfully treated with pulsed CO_2 laser to create a super-hydrophobic polymer while keeping the bulk properties of the substrate intact [3]. This laser treatment introduced peroxide groups onto the PDMS surface, which is capable of initiating graft polymerization of 2-

hydroxyethylmethacrylate (HEMA) onto the PDMS [4]. Poly(HEMA) is known as a hydrogel with high hydrophilicity and good biomedical properties. The result of this laser-induced graft polymerization of HEMA onto PDMS surface has provided an adequate surface to reduce platelet adhesion. Pulsed CO_2 laser-induced surface modification of polyethylene terephalate (PET) membrane with a thickness of 70 μm was carried out and that the morphology and contact angle changed with laser irradiation are different at different wavelengths and laser pulses [5].

In the biomedical field, the use of polymeric biomaterials has been carried out extensively in recent years because of its favourable mechanical properties, transformation processes and low cost. Modifying the surfaces of biocompatible polymers can lead to improved interactions between the polymer surface and the surface of cells. Thin membrane of a biocompatible polymer blends made of polycarbonate (PC) and polymethylmethacrylate (PMMA), with a thickness of 3 μm and irradiated with KrF excimer laser was successfully patterned [6]. Results showed morphological changes which was accompanied with enhanced wetting and adhesion properties.

1.3 Research aim and proposal outline

Current techniques of the fabrication of PCL thin films through solvent-cast and hot-roll milling can allow the thickness of the film to be drawn to a minimum of 10 μm thick. One of the objectives is to be able to reduce the film thickness so as to introduce less foreign material and be resorbed into the body system quickly. In order for this to be carried out, spin-casting technique is developed in which the thickness of the PCL films can be further reduced to approximately 1 μm.

Upon successfully fabricating the PCL films, the inherent hydrophobic property needs to be addressed. It is required to improve the wettability of the film to enhance cell-biomaterial surface interaction. Surface treatments through chemicals and plasma are known to be effective but such methods may not be able to retain its favourable physical bulk properties. Surface texturing on the films such as creating micro-size pores, wells and trenches using lasers would help to increase the surface roughness and hence its wettability. As this process is highly localized, the bulk properties of the material can therefore be retained.

The PCL films fabricated do not have pores that are sufficiently large enough to be able to allow the bi-directional diffusion of dissolved solute and gaseous particles. This property is especially important for applications in multi-layer tissue engineering so that nutrients and oxygen are able to diffuse into the inner lying layers while the respiratory by-products can be removed. The creation of the micro-pores on the film will therefore help to improve on the exchange and transport of these solute and

gaseous particles. There is also potential in promoting angiogenesis in multi-layer membrane tissue engineering.

Through the understanding of the challenges faced in the use of biodegradable PCL film for membrane tissue engineering, this research aims to overcome these limitations through the use of improved PCL film fabrication technique and laser technology. Hence, this thesis will emphasize on the following selected areas, namely:

- The fabrication of the biocompatible and biodegradable PCL membrane through unique simultaneous bi-axially drawn films prepared via conventional solution casting, spin casting and solvent-free method of hot roll-milling.

- The exploration of the use of lasers to modify the surface of PCL films and understanding the mechanisms behind it, and the effect of the physical and chemical changes imparted during the laser irradiation.

- Further insight in the degradation study of PCL films by the irradiation of laser at different wavelengths.

- Theoretical simulation of heat propagation on the PCL film during the impingement of laser using different wavelengths and number of laser pulses.

Chapter 2:
Literature Review

2.1 Biomaterials engineering

Biomaterials engineering is concerned with the application of biomaterials science in the design and engineering aspects of medical devices' fabrication. The study of biomaterials focuses on issues such as biocompatibility, host-tissue response to implants, cyto-toxicity, and basic structure-property relationships [7-14]. These issues provide a strong scientific basis for a clear understanding of successful biomedical devices, such as vascular stents, assisted devices and heart valves.

Biomaterials must possess unique properties that can be tailored to meet its specific application. For example, a biomaterial must encompass properties such as biocompatibility, biodegradability, non-carcinogenic, low toxicity and resistant to both corrosion and wear [12, 13]. However, differing requirements may arise and sometimes, these requirements can be completely opposite. Hence, the understanding of biomaterials science engineering is of great importance due to its specific nature of the targeted applications.

Generally, the requirements of biomaterials can be grouped into four broad categories:

1. Biocompatibility: The material must not disturb or induce un-welcoming response from the host, but rather promote harmony and good tissue-implant integration. An

initial burst of inflammatory response is expected and is sometimes considered essential in the healing process. However, prolonged inflammation is not desirable as it may indicate tissue necrosis or incompatibility.

2. Sterilizability: The material must be able to undergo sterilization. Sterilization techniques include gamma, gas (ethylene oxide (ETO)) and steam autoclaving. Some polymers, such as polyacetal, will depolymerise and give off the toxic gas formaldehyde when subjected under high energy radiation by gamma. These polymers are thus best sterilized by ETO.

3. Functionability: The functionability of a medical device depends on the ability of the material to be shaped to suit a particular function. The material must therefore be able to be shaped economically using engineering fabrication processes. The success of the coronary artery stent — which has been considered the most widely used medical device — can be attributed to the efficient fabrication process of stainless steel from heat treatment to cold working to improve its durability.

4. Manufacturability: It is often said that there are many candidate materials that are biocompatible. However it is often the last step, the manufacturability of the material that hinders the actual production of the medical devices. It is in this last step that engineers can contribute significantly.

Biomaterials can broadly be classified as biological and synthetic biomaterials. Biological materials [7, 8] can be further classified into soft and hard tissue types. In the case of synthetic materials, it is further classified into metallic, polymeric, ceramic

and composite biomaterials. Appendix 1 shows the various classifications examples of biomaterials.

The mechanical properties of a biomaterial can best be described by the following:

- Modulus of elasticity – the stiffness of the material and is usually obtained from the slope of a stress-strain diagram.
- Ultimate tensile strength – the ability of the material to withstand a load before it fails.
- Elongation to failure – the amount of strain the material can bear before it fails.
- Fracture toughness – the measure of the material's resistance to crack propagation.

Fig. 2.1 – 2.4 show the comparisons amongst different classes of biomaterials with respect to the four properties mentioned above [15]. It can be seen that metals are generally very stiff and have high strength and fracture toughness. In sharp contrast to the metals are the polymers, which have fairly low stiffness, strength and fracture toughness. Polymers generally do also exhibit high elongation to failure, and this is an important property that is used to enhance the strength and fracture toughness through drawing.

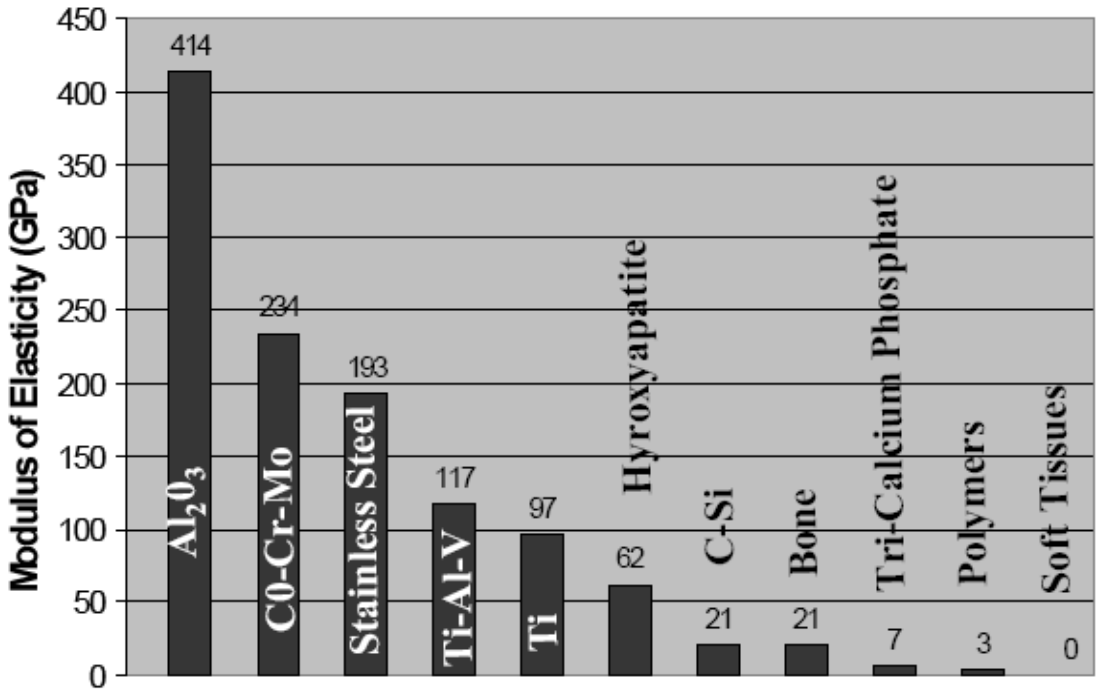

Fig. 2.1 Comparison of moduli of elasticity of biomaterials [15].

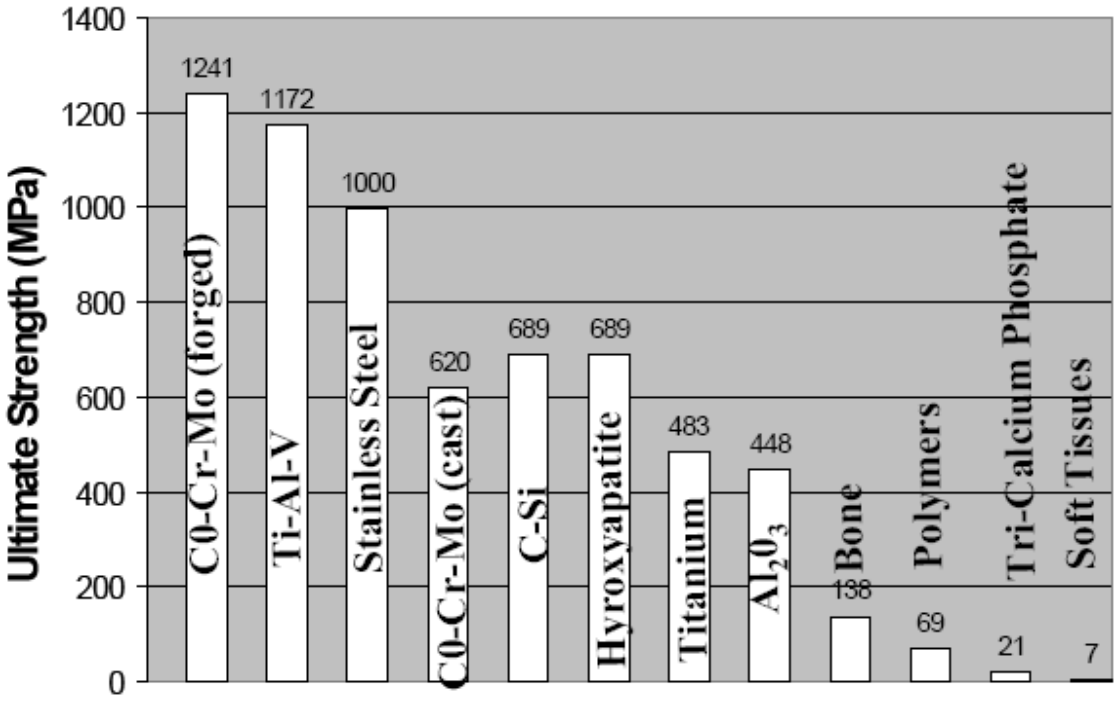

Fig. 2.2 Comparison of ultimate tensile strengths of biomaterials [15].

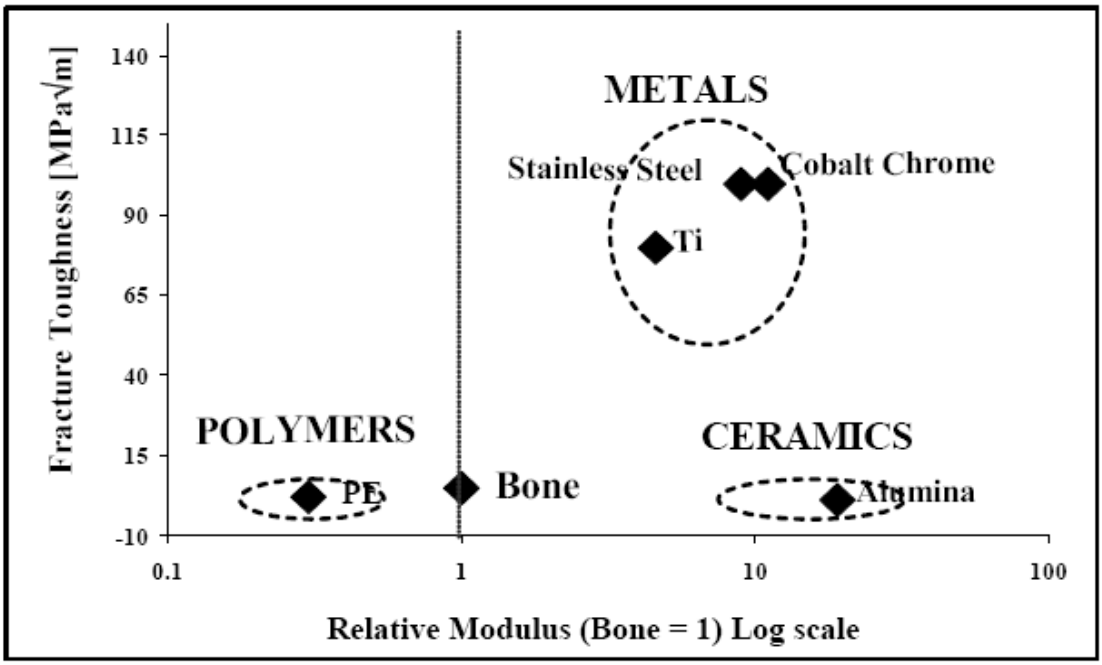

Fig. 2.3 Comparison of fracture toughness of biomaterials relative to the log (Young's modulus) with bone as the reference [15].

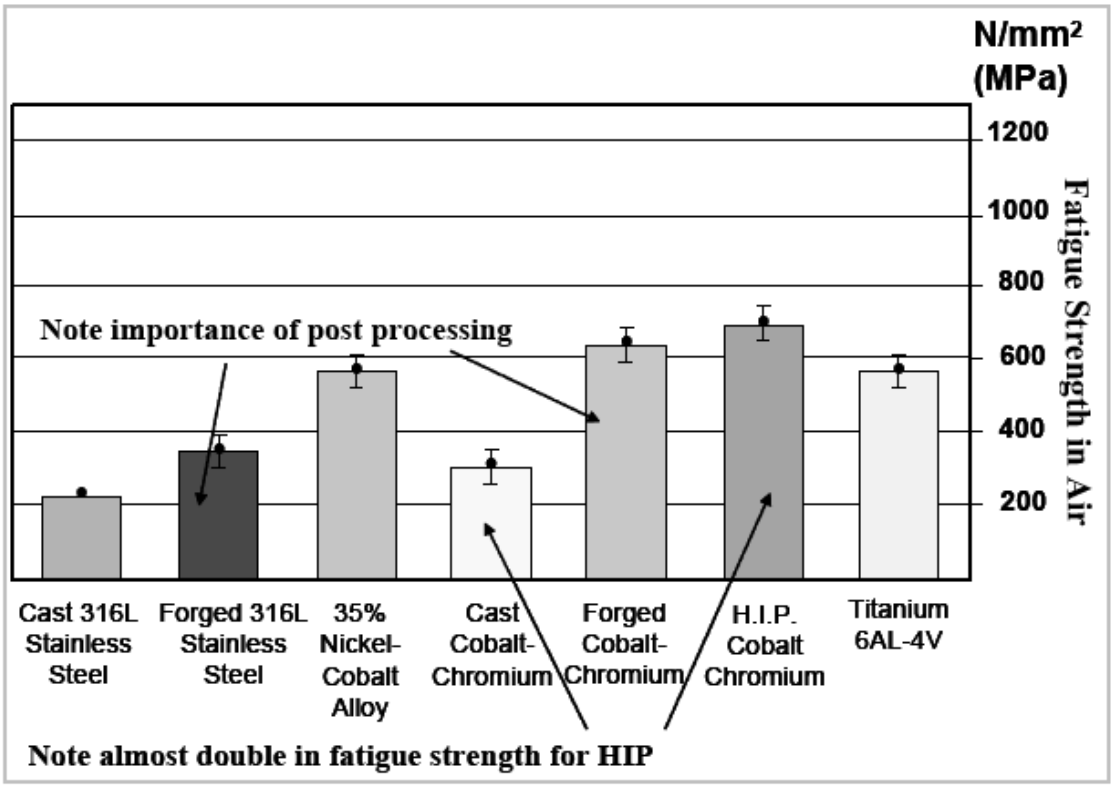

Fig. 2.4 Fatigue strengths (in air) of common alloys used as implants [15].

2.2 Significance and Importance of Tissue Engineering

The growing affluent and the sedentary lifestyle of people have led to many illnesses that cause the malfunctions of organs such as the heart, liver and kidney. Treatment in the early stages can actually prevent further deterioration or even cure the disease. However, some of these symptoms are detected late into the stages and may have resulted in irreparable damage to the organs. When this happens, replacement of the diseased organ may be the only option to cure the illness. However, current technology for organ and tissue replacement has its own limitations. These include donor scarcity, adverse immunological response from the host tissue, biocompatibility, infection, pathogen transfer, and high cost to patients. Then, there is the perennial deficiency of synthetic materials to provide the multifunctional requirement of organ. The aim of tissue engineering is to restore tissue and organ functions with minimal host rejection. This arose from the need to develop an alternative method of treating patients suffering from tissue loss or organ failure. Tissue engineering has been heralded as the new wave to revolutionize the healthcare-biotechnology industry. It is a multidisciplinary field and involves the integration of engineering principles, basic life sciences, and molecular cell biology.

The success of tissue engineering shown in Fig. 2.5 lies in five key technologies: 1) Biomaterials; 2) Cells; 3) Scaffolds; 4) Bioreactors; and 5) Medical Imaging technology. It is vital to select the biomaterials with suitable mechanical and chemical properties for use in the required applications. This chosen material can be fabricated into scaffolds that are able to act as a “housing” that is strong enough to support the loading and growth of cells. The cells chosen to colonise the scaffold can

be carefully extracted from the patient. The use of stem cells has also become a popular choice as they can be differentiated into any kinds of cells, and hence has evolved into an important stem-cell technology. In order for the cells to be grown and proliferate over the scaffold properly, this has to be carried out over a bioreactor in which the optimal conditions for growth are carefully designed and considered. The scaffold will next be characterized commonly through imaging methods of scanning electron microscopy, confocal microscopy and computed tomography to assess the growth of the tissue over the scaffold.

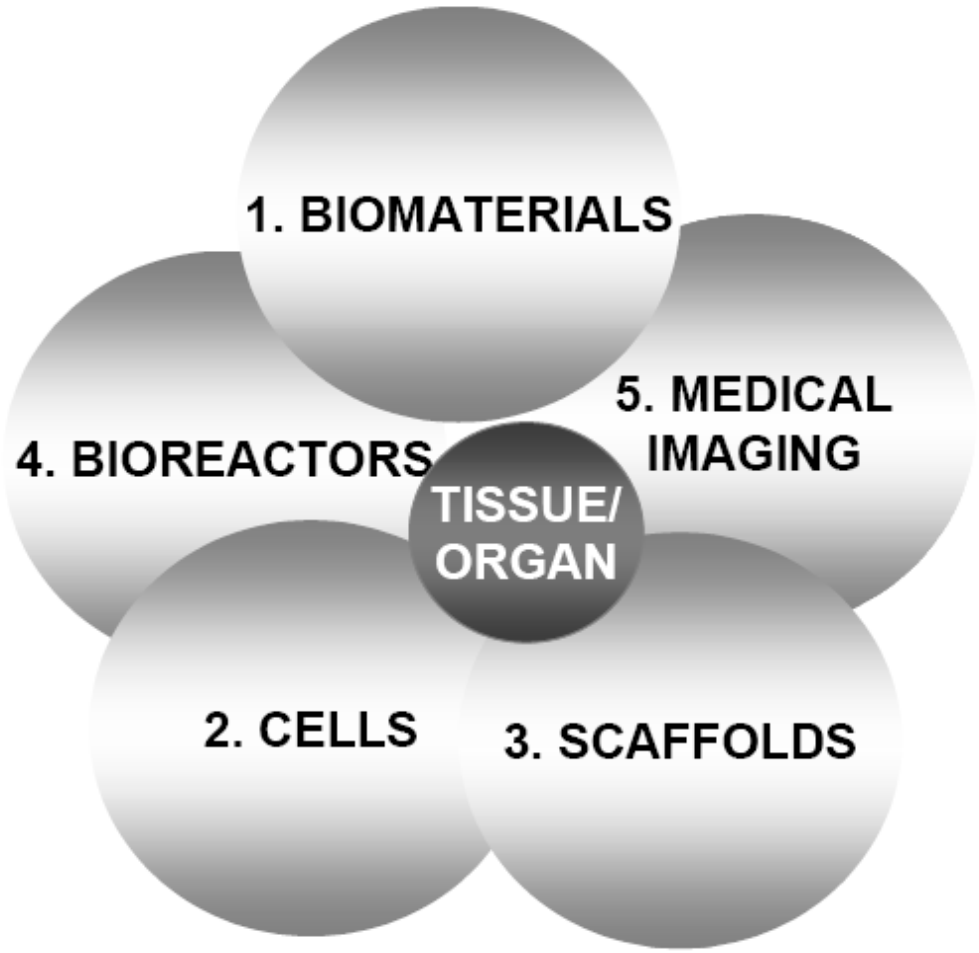

Fig. 2.5 Five core technologies (biomaterials, cells, scaffolds, bioreactors, and medical imaging) required for tissue engineering [15].

Tissue engineering of bone is one recent breakthrough that has been made in the development of a platform technology which integrates medical imaging, computational mechanics, biomaterials, and advanced manufacturing to produce three-dimensional, porous load bearing scaffolds [16]. The three-dimensional scaffold reported has interconnected pores that enables good cells entrapment, facilitates easy flow path for nutrients and waste removal, and demonstrates long-term cell viability.

In tissue engineering, there are certainly issues and challenges which are yet to be resolved. These issues range from cell-biomaterial interactions, stem cells technology to methods in scaffolds manufacturing. For example, in the case of cell-biomaterial interactions, though single cell sheets can be grown, it is difficult to understand how the cells in composite tissues (such as the heart valve leaflets) recognize their own boundaries and hence, do not cross and violate each other. Apart from the biochemical effects such as growth factors that will affect the cell-biomaterial interactions, there is also a need to study the mechano-induction effects. This is because the manner in which cells differentiate, proliferate, and express their extracellular matrix (ECM) is also a function of the stress fields they experience.

Stem cells and scaffolds technologies also pose some challenges. Recently, some work on human blood vessels was done by Auger's group [17] in Canada; They showed that by growing the cells in sheets and then rolling them into a tube helps to eliminate immunological mismatch. This is because smooth muscles cells (SMCs) re-expressed desmin, a differentiation marker known to be lost under culture conditions. As a result, large amounts of ECM were produced and the structural integrity maintained. However, the handling of the sheets is delicate and it is not clear if the

material would survive the viscoelastic compliance mismatch in long-term *in vivo* physiological environment. Okano's group [18] has developed an interesting cell sheets technology where cells were able to grow on culture surfaces grafted with temperature-responsive polymer, poly(N−isopropylacrylamide) (PIPAAm). Instead of using enzymatic treatment, confluent cells simply detached from the polymer as a cell sheet simply by just lowering the temperature. Layered cell sheets of cardiomyocytes then began to pulse simultaneously and morphological communication via connexin 43 was established between the sheets. When the sheets were layered, engineered constructs were macroscopically observed to pulse spontaneously too. The examples quoted above point to the fact that tissue engineering breakthroughs will further gravitate towards even greater challenges ahead.

For a material to be used as a biomaterial, it must first possess the mandatory properties of being biocompatibility and sterilizability. Biomaterial must also be malleable and ductile because it is important for the biomaterial to be able to be pulled or pressed into shape for the medical device to function. When it comes to the manufacturability of a biomaterial, processing techniques often affect the final property of the biomaterial — which means affecting the durability of the device. On this note, engineers need to examine the various processing effects that stem from grain refinement of steel to molding conditions and irradiation on ultra-high molecular weight polyethylene (UHMWPE).

Future direction seems to lead us to nanolaminate composites, which give better properties such as fracture toughness and wear enhancement. The era of tissue engineering also paves the way for new biomaterial processes to be developed and

invented. The integration of different modalities from cells, biomaterials to medical imaging has opened up new challenges in the healthcare industry.

2.3 Poly(ε-caprolactone) thin films and matrices

PCL is a semi-crystalline and biodegradable polymer. It has a melting point of 60 ^{o}C and a low transition temperature at –60 ^{o}C that allows it to be relatively ductile at room temperature. As a homopolymer belonging to the aliphatic polyester family, PCL consists of 5 non-polar methylene group and a single relatively polar ester group. Fig. 2.6 shows a structure of PCL. Due to its high olefinic content, PCL exhibits mechanical properties similar to that of polyolefin. The presence of the hydrolytically unstable aliphatic-ester linkage has attributed to the biodegradability of PCL [19]. PCL is also by nature a hydrophobic material as a result of the linear chains of the methylene group. The PCL also possesses a high decomposition temperature of 350^{o}C, a tensile modulus of 0.45 GPa and a melt viscosity of 443 Pa s at 150^{o}C.

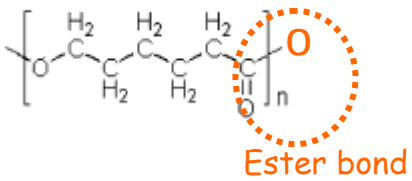

Fig. 2.6 Chemical Structure of PCL and its ester linkage

The biocompatibility of PCL has been confirmed through extensive *in vitro* and *in vivo* studies [20] and approved by US Food and Drug Administration (FDA). Besides being bioresorbable and biocompatible, the polymer can also be processed with ease into many shapes and forms. Presently, PCL has been regarded as a soft and hard tissue compatible material for applications in resorbable suture, drug delivery

system and bone graft substitutes. Its susceptibility of its aliphatic ester linkages to auto-catalysed bulk hydrolysis has allow it to be used for sutures as the products generated are either metabolised via the tricarboxylic cycle (TCA) or eliminated by direct renal secretion [21]. The rubbery characteristics of PCL results in high permeability, which is exploited for the use of drug delivery system. However, the semi-crystalline nature of PCL has extended its resorption time to more than 2 years as the closed packed macromolecular arrays retard fluid ingress [22]. The applications of PCL have been limited due to its slow resorption and degradation kinetics cause by its hydrophobic character and high crystallinity. PCL has also been used in bone repair. Marra et al. [23] has reported that PCL is a comparable substrate or supporting cell growth resulting from two-dimensional bone marrow stromal cell culture .

PCL is compatible with numerous other polymers and PCL polymer blends such as PCL-TCP, which is a blend of polycaprolactone with tri-calcium phosphate. This has greatly increased the usage of PCL in the biomedical field. PCL/PLA blend disc incorporated with hydroxyapatite is feasible as scaffolds for bone tissue engineering. Heath et al. [24] tested the coating effect of tissue transglutaminase on the surface of PCL to enhance the biocompatibility of PCL. Tissue transglutaminase is a novel cell adhesion protein that binds with high affinity to fibronectin in pericellular matrix.

2.4 Current progress of poly(ε-caprolactone) in biomedical engineering

Thin polymer membranes can be fabricated via many existing methods; each of them brings about different properties and characteristics to the films in terms of

strength, stiffness, thickness and etc. In industrial applications, common methods to produce films include the familiar extrusion, calendaring and blowing. In biomedical applications, membranes were often produced through solution or precipitation casting methods. However, films prepared through these methods may not have sufficient strength to withstand mechanical loading, or the thickness of the film may be undesirable for use. Physically drawing the films can reduce the thickness of the films substantially to give ultra-thin membranes. Hence, this allows minimal material to be introduced into the body. At the same time, the tensile strength and modulus can be greatly enhanced caused by the induced orientation of the fibrils [25].

While uniaxial drawing improves the physical properties of the film along its drawing direction, it is important to take note that the use of uniaxial drawn films has to be exercised with caution as wrong direction of the applied load may cause failure. On the other hand, biaxial drawing, either sequentially or simultaneously, produces films that are mechanically strong in both the longitudinal and lateral directions [26]. This superior quality of biaxial drawn films over uniaxial ones leads to the extensive use of biaxial drawing in the polymer industry, especially in the production of packaging films.

The properties of biaxial drawn films of commercially important polymers have been well studied: Sakai *et al* investigated structural changes [27], development of fibrillar morphology [28] and mechanical properties [29] in the biaxial drawing of UHMWPE films. Taraiya's group investigated the barrier properties [30] whereas Chu *et al* studied the formation of microvoids [31] in the studies on biaxial drawn polypropylene, Gerrits *et al* [32] and Zhu *et al* [33] evaluated the micro-porosity

generated in drawn UHMWPE and polypropylene, respectively. The correlation between orientation and properties of biaxial stretched polystyrene has also been studied by Zhang and Ajji [34]. However, none of the polymers studied above is biocompatible and biodegradable.

The use of biaxially-drawn biodegradable and biocompatible polymer films has been well documented in recent times. Several research efforts that have made use of biaxially-drawn PCL membranes include Teoh and Hutmacher's group in which human dermal fibroblasts [35] and keratinocytes [36] was cultured on solvent-cast and biaxial stretched PCL films. The results indicate that the PCL membranes would support the attachment and proliferation of human keratinocytes and have the potential to be applied as a matrix material for tissue engineering an epidermal equivalent. The same group has also shown that the PCL membranes supported attachment, growth, and osteogenic differentiation of human primary osteoblast-like cells and hence feasible for bone reconstruction [37]. Serrano *et al* recommended the suitability of hot-pressed PCL membranes as scaffolds for vascular graft development [38] after the evaluation with L929 mouse fibroblasts. These studies demonstrated the versatility of the membranes for reconstructing different tissues.

The underlying concept of TE is the isolation of cells and their expansion and proliferation under *in vitro* conditions. The resultant TE construct is then grafted back *in vivo* to function as the introduced replacement tissue [39]. Hence, an artificial extra-cellular matrix, or scaffold, is required to accommodate cells and guide their growth and tissues regeneration outside the body.

Biocompatible polymer thin membranes have become a favorable field of investigation by numerous research groups [35, 40, 41] in the past decade as thin membranes introduce minimal foreign substances into the biological system and thus fewer degradation products. As a result, adverse host-tissue responses can be reduced. The challenge in the area of membrane tissue engineering lies in the fabrication of a film of minimal thickness and with reasonable mechanical properties. Thin films in the scale of nanometer thickness have been successfully achieved using spin cast technique [42]. However, such a method produces films which are very strongly adhered to the substrate surface, such as glass or silicon, due to electrostatic attraction. Hence, removing the thin films from the substrate surface at such nanometer scale thickness without tearing it could prove to be quite a challenge. With biaxial drawing combined with spin casting, minimal thickness has become possible with acceptable level of mechanical strength retained. This method is going to be reported and investigated in the later part of this thesis. In addition, thin films give higher degree of flexibility [43] to allow for the formation of different shapes of tissues. Moreover, the excellent mechanical properties of biaxially stretched PCL films make them more durable scaffolds and also allow for easier handling for research work and for surgical implantation

The combination of the membrane matrix concept and the excellent biocompatibility and degradation characteristics of PCL appears to be an attractive option for the field of tissue regeneration. Due to its low glass transition temperature of approximately -60 ºC, PCL is always rubbery at room temperature which gives the material a high degree of drawability [26]. This increases the ease of processing to the

polymer and facilitates the fabrication of thin membranes through deformation and orientation processes such as uniaxial or biaxial drawing methods.

Due to poor hydrophilicity of the PCL membranes, surface treatments are often performed in order to further enhance the cell-membrane interaction and to facilitate cell attachment and proliferation during *in vitro* cell culture. Some of the surface modifications include the immobilization of biomacromolecules [44] such as various amino groups or collagen, coating of the membranes with fibrin [36], surface treatment with sodium hydroxide or plasma of gases, and grafting of other polymers such as acrylic acid [45]. Lasers have also been used in modifying the physical and chemical properties of the film surface. More details on laser processing of PCL films will be discussed in the later sections.

2.5 Introduction to lasers and technology

Laser, acronym for light amplification by stimulated emission of radiation, is a device that creates and amplifies narrow intense beam of coherent light. They are widely available in a continuous wave or pulsed mode and can be easily, efficiently and reliably manipulated and controlled [46]. Laser exists in the visible, infra-red (IR), or ultra-violet (UV) parts of the electromagnetic spectrum. Laser differentiates itself from the rest through the medium, which can be in the form of solid, liquid or gases, in which light is transmitted and possesses its own unique set of characteristics. There are basically three main families of lasers; they are gas lasers, solid-state lasers and semiconductor (or diode) lasers [1].

Lasers are becoming very widely used in the field of medicines because of its high accuracy and precision in surgery as well as its intrinsic sterile and haemostatic property. Its clinical applications include ophthalmology, dermatology, neurosurgery, gynecology and urology [47]. The effects of using lasers in applications can be classified under thermal, electromechanical, photochemical and photoablation [48]. Thermal effect is simply the absorption of light energy by the irradiated material, which consequently causes heating. In electromechanical effect, breaking of chemical bonds and ionization takes place at a very high fluence and this subsequently leads to electric breakdown of the medium. Photoablation is the breaking down of chemical bonds without heating the material. This happens when the photon energy released by electronic excitation is equal or larger than the bond energy. Photoablation is performed by lasers emitting ultraviolet rays, such as excimer lasers. During bond-breaking, part of the energy exists as thermal energy. This energy is sufficient to allow the rapid detachment of the molecules into the gas phase, thus giving rise to the ablation of the material. The principles of photochemical effects are similar to photoablation, and the main difference between these two effects is based on the fact that electronic excitation leads to electronically excited states, whose chemical reactivity is different from non-excited states.

2.6 Laser Processing and Ablation of Materials

Laser ablation is the vigorous material ejection from a solid surface that occurred when pulsed laser light is focused onto the surface of a solid material [49]. Pulsed laser ablation has been well established as a universal tool for surface processing of organic polymeric materials [50]. The dynamics of the removal process is influenced by a

variety of parameters originating from material properties, the parameters of the laser pulse and the laser irradiation environment. The parameters of the laser radiation and properties of the material govern the possible physical processes, such as optical absorption, heat conduction, phase transitions, evaporation kinetics and plasma dynamics, which can determine the final properties of the processed materials [51]. Lasers, in general, can be classified as long pulse laser or short pulse laser. Long pulse lasers, such as Nd:YAG (355 nm, 8-10 ns) and the KrF excimer laser (248 nm, 8 ns), usually refer to lasers with pulses longer than 10 ps while the short pulse lasers, namely femtosecond laser (800 nm, 80-110 fs), refer to lasers with pulses shorter than 10 ps.

Laser ablation can be brought about by exposure to intense excimer laser light [52], by exposure of doped polymers to low UV laser light [53] and by using infrared nanosecond laser pulses [54, 55]. Under these conditions, the polymeric material is photochemically and photothermally degraded. The ultraviolet-pulsed laser treatment of polymer blends is expected to induce local changes in the chemical composition and roughness of the polymer surface, depending on the way these two polymers absorb the UV radiation on the surface. This controlled surface modification allows decoupling of the surface properties of the material from its bulk properties [56]. The ablative photo-decomposition is of great interest as it leads to the physical structuring of the morphology of normally smooth polymer surfaces [57]. This directly influences the polymer properties such as wetting and adhesion properties. Fig. 2.7 shows how a UV excimer laser pulse rapidly breaks chemical bonds within a restricted volume, causing mini-explosions and ejection of the ablated materials [58]. Fig. 2.8 shows a model of photochemical ablation proposed by Srinivasan and Braren.

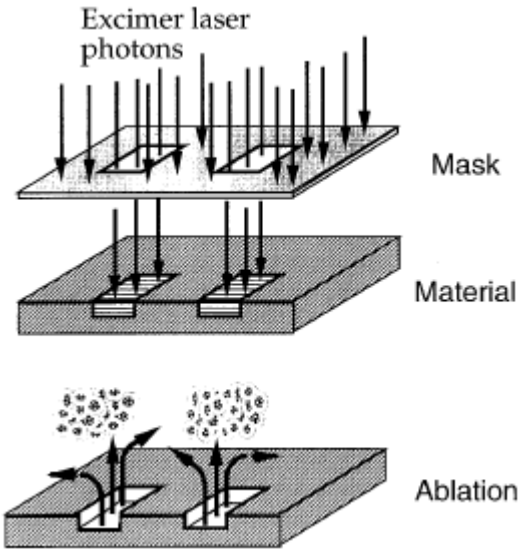

Fig. 2.7 UV laser micro-machining process [58].

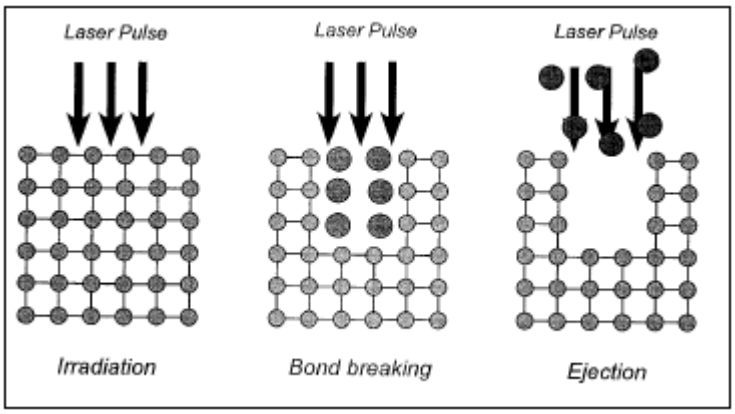

Fig. 2.8 Simplified photo-chemical ablation model [58].

Comparing the physical conditions during material processing, it has been reported that short pulse lasers offer more advantages in the treatment of the polymer surfaces than long pulse lasers. The main advantage of using ultra-short pulse lasers for laser ablation of the polymeric materials is that there is negligible amount of heat diffusion into the polymer. Thus, high precision patterning of the polymer can be done without causing any thermal damage to the surrounding regions of the patterned holes.

Hence, a structure that is free from thermal and mechanical damages, such as melting, formation of burr and cracks and spalling, can be obtained [59].

Fig. 2.9 shows the numerous physical phenomena that are present when a material is processed with a long laser pulse. The absorption of the long laser pulse leads to melting and then sputtering, evaporation of the material which can contaminate the surrounding area, producing micro-cracks, and removing material over dimensions much larger than the intended laser spot size. Other adverse effects include damage to adjacent structures, delamination, formation of recast material and poor shot-to-shot reproducibility [22]. Fig. 2.10 shows the ablation of material using an ultra-short laser pulse. Physical processes, such as heat conduction, do not have sufficient time to dissipate the energy from the process of plasma formation which lead to eventual material ejection [60].

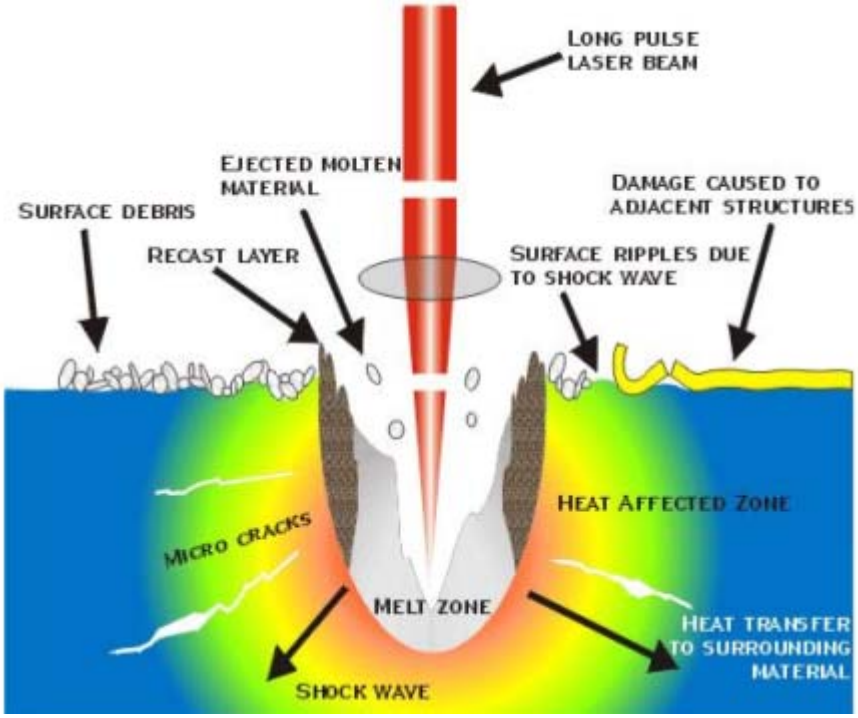

Fig. 2.9 Ablation of material by a long pulse laser at a pulse duration > 10 ps [60]

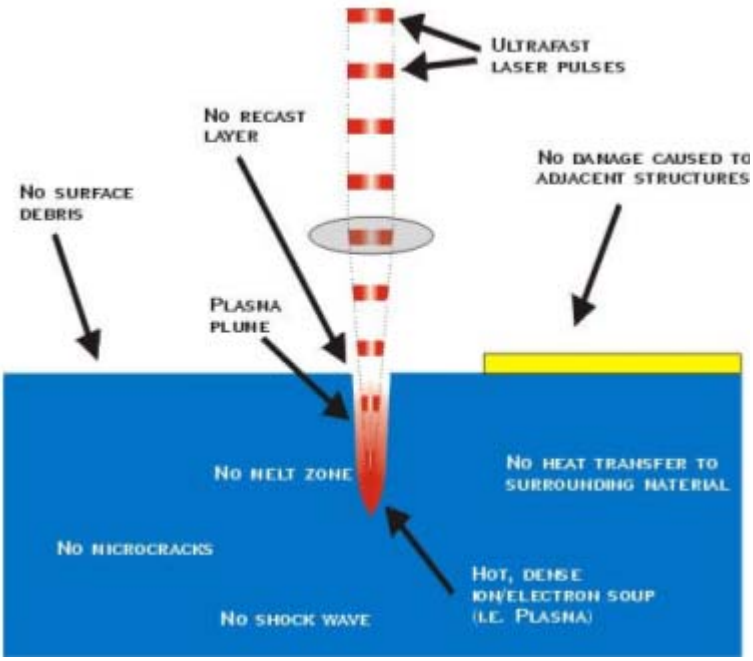

Fig. 2.10 Ablation of material by ultra-short pulse laser at a pulse duration < 10 ps [60].

The surface micro-structuring and modification of PCL through the use of lasers has not been reported with much detail. This research thesis highlights and investigates the cause and effect of using various lasers to create micro-structures, such as micro-pores, micro-wells and micro-channels, on the PCL bi-axial drawn film.

Chapter 3:
Synthesis of Poly(ε-caprolactone) Thin Films

3.1 Introduction

Development and fabrication of thin polymer films through a variety of methods has spawned wide applications in industry and biomedical sciences. Although there are different methods in the fabrication of thin polymeric films, each method brings about different properties and characteristics to the films in terms of strength, ductility and permeability. Extrusion, calendaring and blowing are the common industrial methods for fabricating polymer sheets and thin films [61, 62], of thickness ranging from tens to hundreds of micrometers. These methods usually produce low to moderate level of chain orientation and are only suitable for low to moderate load-bearing applications. There is also a limitation to how thin the films can be fabricated through these methods. This limitation can be overcome by drawing the films to substantially reduce the film thickness and at the same time, improve the tensile strength and modulus caused by the induced orientation of the fibrils [25].

With increasing interest in the use of biodegradable polymers in the area of biomedical science, extensive research has been carried out. Biodegradable polymers include poly(lactide), poly(glycolide), poly(ethylene glycolide) and poly(ε-caprolactone). These biodegradable materials are suitable for pharmaceutical products, such as wound dressings which require durability, stress resistance, flexibility and good elasticity. The surface chemistry of the biodegradable polymers can also be modified to provide good and uniform adherence and conform to the wound

topography. This can help to prevent accumulation of air or liquid pockets at the interface. Besides good adherence, it must also provide a barrier to prevent infections that can be caused by bacteria penetration. The water vapour permeability is another important aspect to consider. This property helps to regulate the diffusion of water vapour through the membrane such that it not only helps to prevent fluid accumulation under the dressing, it can also maintain an optimum moist condition [63, 64]. The criteria to minimize adverse long term host-tissue response to foreign materials is to consider the use of thin membrane structure. For membrane tissue engineering in ophthalmology, dermatology and even vascular graft engineering, polymer films are seen as favourable matrices because less material is administered and hence will invoke minimal adverse host-tissue response. Also, the use of such think polymer films as stromal substitutes has been reported to support cell growth; this is an important development as the use of allogenic biological materials as substrates can be completely phased out, hence overcoming problems of disease transmission or allograft rejection [65, 66].

Ultra-thin films of 10 μm thickness fabricated through biaxial drawing of PCL films has been developed successfully by Teoh's group [26] and subsequent tests have proven that the PCL thin films are suitable for membrane tissue engineering [35, 38, 67]. The excellent mechanical properties of PCL thin films also allow easy handling for in vitro and in vivo research works. Further treatment of the PCL films was also carried out to enhance cell-biomaterial interaction [43, 45, 67, 68].

Fabrication of films with sub-micrometer thickness with reasonable mechanical properties and adequate handling capabilities will be a challenge in the area of

membrane tissue engineering. Thin films in the scale of nanometer thickness have been successfully constructed by using spin cast technique [39, 69]. However, such this technique produces films which are very strongly adhered to a substrate surface such as glass or silicon. This results in the inability of the thin films to be removed from the substrate surface.

This chapter reports on the methods of achieving ultrathin PCL films in the region of sub-micrometer thickness through a two-step process. The polymer solution was first spin cast to achieve films with approximately thickness of 6.3 ± 1.4 μm. The spin cast films were then subjected to biaxial drawing to obtain ultra-thin PCL films of 1.2 ± 0.5 μm thick. PCL films fabricated through two-roll milling and standard solution casting followed by bi-axially drawn were also compared. The physical, mechanical, water moisture permeability and thermal characteristics of the biaxial drawn and undrawn films were investigated and discussed.

3.2 Experimental Procedures

3.2.1 Materials

The PCL pellets used was purchased from Sigma-Aldrich. and has a density of 1.145 g/cm^3 of number average molecular weight (M_n) of 80,000. The polydispersity of PCL as determined by gel permeation chromatography was 1.51. The glass transition temperature and melting temperature of PCL are -60 ^oC and 60 ^oC respectively. Since PCL has a low glass transition temperature, it exists in a rubbery state at room temperature, and explains its excellent tensile-drawing ability.

3.2.2 Methods of PCL Thin Film Preparation.

PCL ultra-thin films were fabricated using three techniques, namely solvent casting, two-roll milling and spin casting. Solvent was not required using two-roll milling whereas the other two methods of spin casting and solvent casting required the use of solvent for the polymer solution to flow and precipitate into thin sheets. The initial steps of the film preparation were represented in Fig. 3.1 and described as follows.

Solvent Casting: Polymer solution was prepared by dissolving PCL pellets in methylene chloride at a concentration of 3 wt% and casted over glass moulds. A metal foil was placed on the top of the moulds to allow slow evaporation of the solvent. The solvent casted films obtained were further dried in a vacuum oven at 40 ^{o}C to remove any remnants of the solvent. Solvent casted films of thickness 120 μm was uniformly achieved.

Two-Roll Milling: PCL pellets were gradually fed in between the rolls, which were heated up to 80 ºC at a rolling speed of 1 rpm. The pellets melted completely and formed a highly viscous liquid layer that adhered to the surface of the rolls. The layer of this viscous PCL on the surface of the rolls was collected by scrapping using a blade. The scrapped off PCL was allowed to cool and solidify into a uniform solid piece. The solid piece was then cut into smaller pieces to be ready for melt pressing.

Spin Casting: This method to fabricate the PCL films was evolved from the idea of a spin-coating machine for coating photo-resist polymer in the semi-conductor industry. A simple and effective spin cast device was self-developed by mounting a rotating platform on to the rotor of a speed control motor. Polymer solution was then placed on the platform and covered with a bell jar before the rotating platform was set to spin at the desired rate of revolution. The initial preparation was similar to solvent casting where PCL pellets were dissolved in methylene chloride to give a polymer solution at a concentration 3 wt%. 5 cm^3 of the solution was spread over an area of approximately 20 cm^2 on a metal sheet which was attached to a rotating platform. The platform was then set to rotate at a revolution of 500 rpm for 5 minutes. Uniformly spin cast PCL films of thickness approximately 6.3 ± 1.4 μm were produced and the spin cast films were next placed in a vacuum oven for similar reasons.

Upon the completion of the initial preparation stages of the three methods, heat treatment and simultaneous biaxial drawing of the film followed, as shown in Fig. 3.2. Either of the solvent cast film, roll-mill piece or spin-cast film was sandwiched between two stainless steel sheets and melt-pressed at 80 ^oC at a pressure of 30 MPa. After 10 minutes, the sandwiched film was allowed to slow cool at the same pressure for 12 hours. The melt-pressed film obtained was then pre-heated before bi-axially drawn in a temperature-controlled chamber at a temperature of 58 ^oC, which was just 2 ^oC below the melting point of PCL. After drawing, the film was annealed at the same temperature for a further 6 hours.

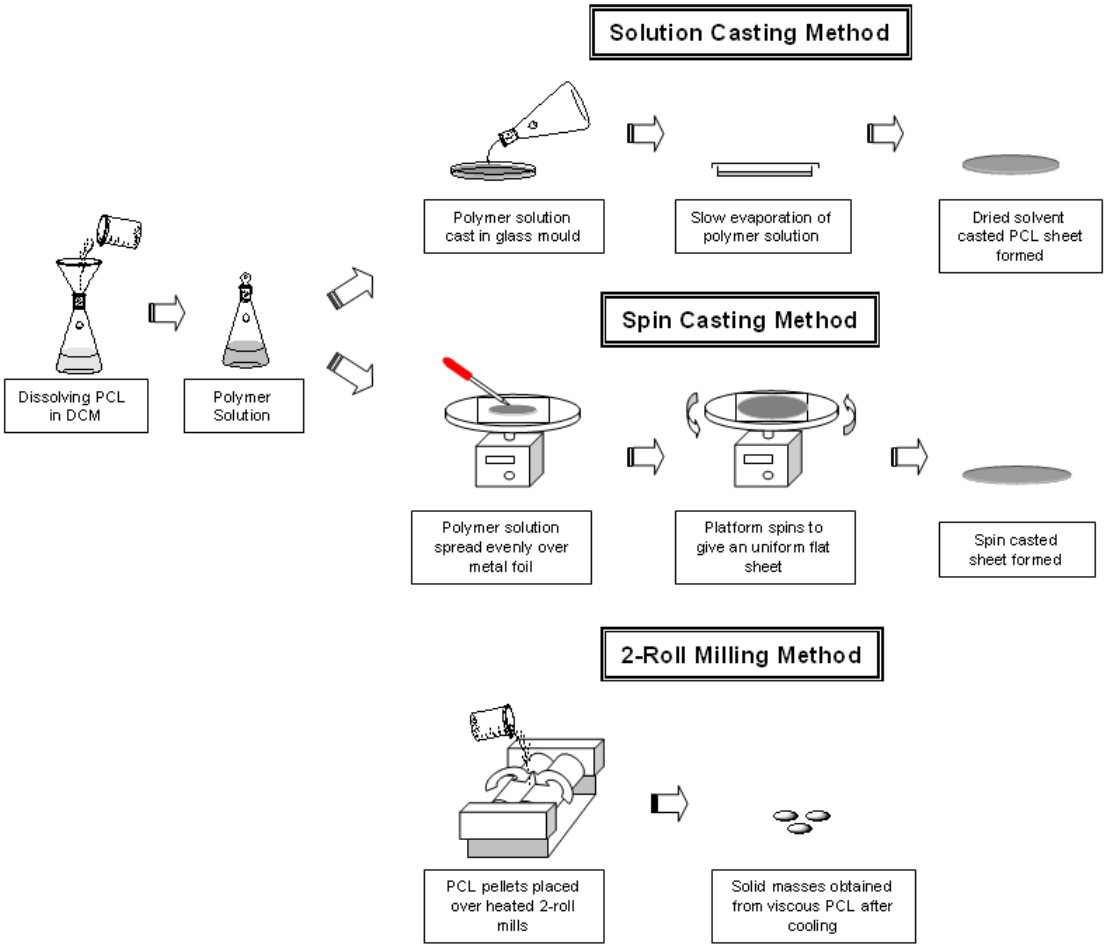

Fig. 3.1 Schematic drawing showing the stages of initial preparation of PCL thin films using methods of solvent casting, two-roll milling and spin casting.

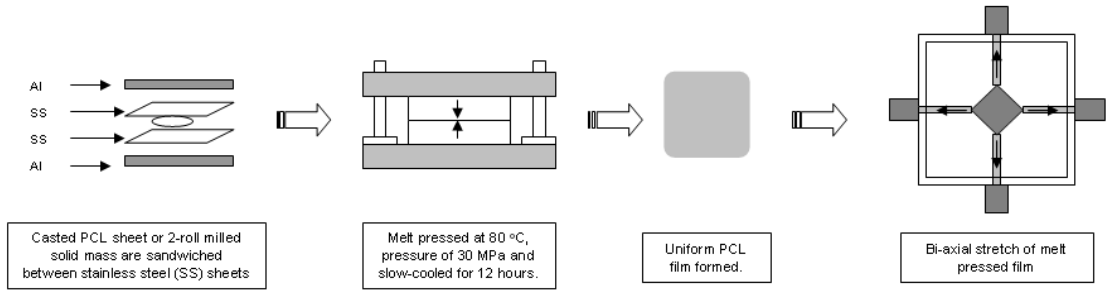

Fig. 3.2. Stages of heat treatment and biaxial drawing.

3.3 Film Characterization

3.3.1 Optical Microscopy:

The morphology of the PCL films was examined using a Nikon Optiphot-Pol Polarizing microscope. The optical images were captured using a Nikon Coolpix 4500 digital camera attached to the microscope with a Nikon Coolpix MDC lens mounted on the phototube. Fine details of the microstructures of the PCL films were examined using an atomic force microscopy (Digital Instrument Nanoscope 111a AFM) tapping over an area of 20 μm x 20 μm and 5 μm x 5 μm.

3.3.2 Differential Scannning Calorimetry (DSC):

The thermal properties (peak temperature and enthalpy of fusion) of PCL films were studied using a Perkin-Elmer Pyris-6 DSC. The instrument was calibrated with In and Zn standards. The PCL film samples were scanned from 20 ^{o}C to 80 ^{o}C at a heating rate of 5 ^{o}C/min in a nitrogen atmosphere. The percentage crystallinity of the samples was estimated by comparing with 100% crystalline PCL with enthalpy of fusion of 139.5 J/g [70].

3.3.3 Water Permeability:

Permeability to water moisture of the films was determined by the water vapour transmission rate across the films. This experiment was carried out in accordance to ASTM E96-00 E. The films were wrapped round the opening of

centrifuge tubes with a cross sectional area of 113 mm^2. The tubes were filled with 15 ml of deionised water (to about 95% full) with an air gap of 5 mm. An environment chamber (Contherm® 5200 RHS, New Zealand) was used to maintain ambient temperature and relative humidity. The temperature and relative humidity of the chamber were set at 32 ^oC and 50% respectively. 5 samples for each specimen group were used to conduct the experiment. The experiment was conducted over a period of 21 days and the mass of water loss was recorded.

The water vapour transmission rate was determined by the following equation [71]:

$$\text{WVTR} = \frac{\left(G/t\right)}{A} = \frac{Flux}{Area}, \qquad \text{(Eq. 3.1)}$$

where G, t and A represent weight change (g), time during which G occurred (hr) and the opening area of centrifuge tube (m^2), respectively. $\left(G/t\right)$ can also be represented as the flux of the water vapour across the film thickness.

3.3.4 Modulus (E), ultimate tensile strength σ_{UTS} and elongation (λ):

Tensile properties of the PCL films were determined using an Instron Universal tensile tester conducted at standard room conditions. The samples were cut into strips of width measuring 10 mm and were mounted onto pneumatic grips. The grip separation was set at 30 mm and a testing speed of 5 mm/min was used. The thickness of the films was measured using an electronic length measuring equipment with an accuracy of 0.1 μm (Carycompar B Vertical comparator - V150) from TESA

TECHNOLOGY. The samples were subjected to tensile stress till breakage and stress-strain curves were plotted from the data generated. The modulus (E), ultimate tensile strength σ_{UTS} and elongation (λ) were then subsequently extracted.

3.4 Results and Discussion

3.4.1 Drawing Ability of Films.

The films were biaxially drawn to its limit near the melting temperature of PCL. The amount of biaxial drawing was dependent on the temperature at which the polymer was drawn [72]. Films produced by different techniques were found to exhibit different drawing ratios at the same drawing temperature, as shown in Table 3.1. Before biaxial drawing, the thickness of the heat-pressed films produced by two-roll milling and solvent casting was approximately 95.0 μm while that of spin cast films was approximately 6.3 μm. Films produced using two-roll milling had the largest drawing ratio of 4 x 4, followed by solvent cast of 3 x 3 and spin cast of 2 x 2.

Table 3.1. Thickness of non-biaxial and biaxial drawn PCL films produced by different methods

Method	Mean Film thickness (μm)	
	Non-biaxial Drawn	Biaxial Drawn
Spin casting	6.3	1.2
Two-roll milling	95.0	9.3
Solvent Casting		15.0

One of the reasons for the difference in draw ratio between films fabricated through two-roll milling and solvent casting, despite similar film thickness, could be due to the incomplete removal of solvent used in solvent casting during the stage of evaporation. The remains of the solvent residing within the solvent-cast film introduced defects such as nano pores and could be the reason for its lower draw ratio than two-roll mill film. The three methods produced different microstructures (especially in fibrils thickness) of these PCL films, as shown in Figure 3. The thick fibrils of the biaxial drawn 2-roll mill film allowed a better drawing ratio as compared to the thinner fibrils of the biaxial drawn solvent cast films. Films produced by spin cast before drawing was 15 times thinner than that of for solvent cast and 2-roll mill films. Although these films had a relatively low drawing ratio as compared to the rest, very thin films of thickness approximately 1.2 μm was successfully created.

The drawing ratio of the films could also be affected by its molecular weight M_n. Polymer chain with a higher M_n was known to have a higher tensile strength and elongation than one with a lower M_n. In order for thermal degradation of PCL to take place, temperatures of 230 ^oC and 355 ^oC would be required for PCL with M_n of 1800 and 42450 respectively [73]. Thermal degradation of PCL with a higher M_n of 80000 took place at an even higher temperature of up to 430 ^oC [74-76]. Hence, melt pressing at 80 ^oC should not trigger degradation to cause chain reduction to PCL. Therefore, the PCL films reported here that had previously undergone melt-pressing at a temperature much below the degradation temperature would not have resulted in any significant degradation.

3.4.2 Film Surface Morphology

The polarized optical micrographs of the PCL films processed using different techniques were shown in Fig. 3.3. This figure showed images of biaxially drawn films by the method of spin casting (A), two-roll milling (B) and solvent casting (C) at regions

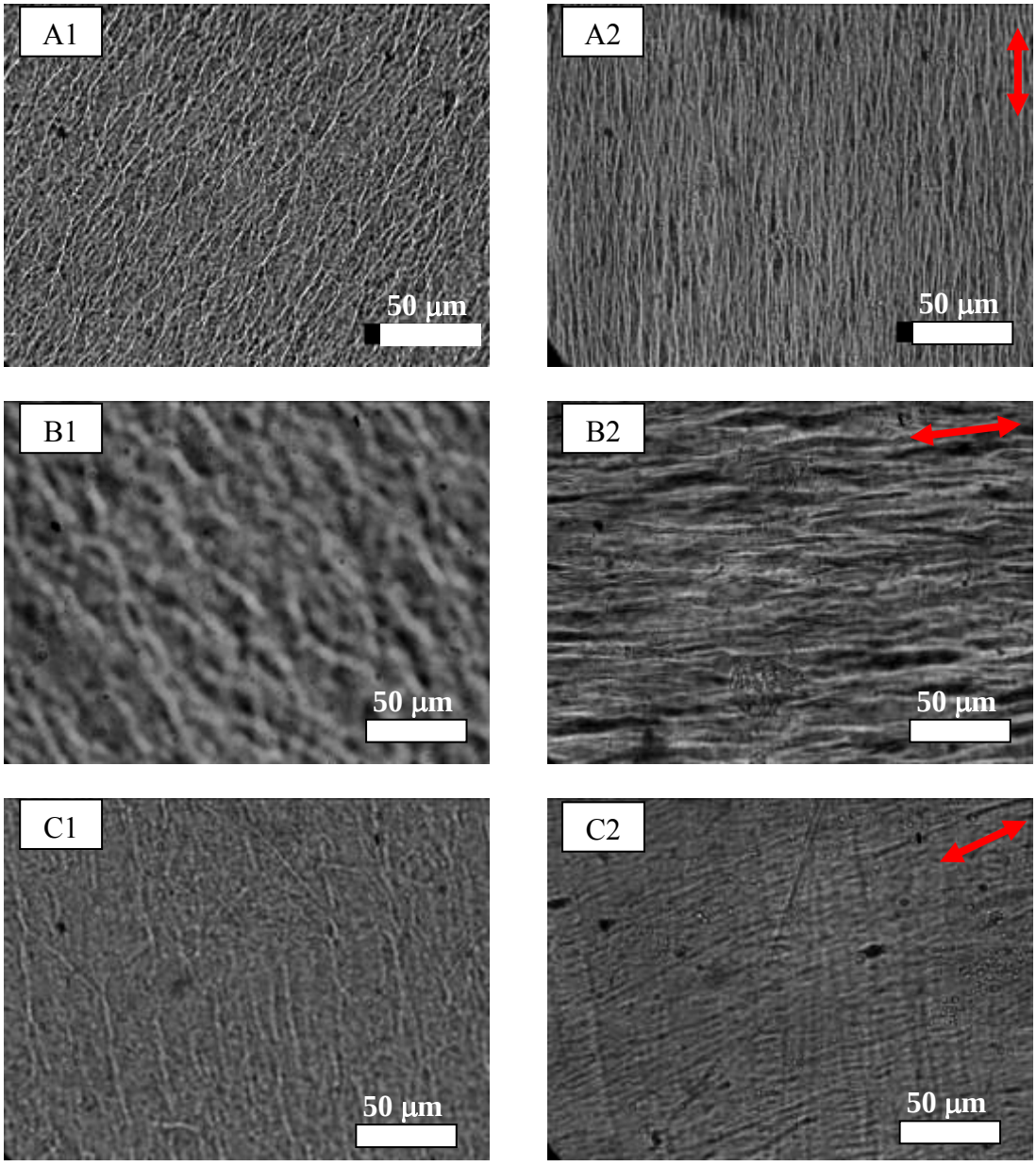

Fig. 3.3 Morphology from polarizing microscope showing different orientations of the fibrillar network of the biaxial drawn films by different fabrication methods. (A: spin casting; B: two-roll milling; C: solvent casting) at centre (1) and side (2).)

of centre (1) and side (2). A very dense network of fibrillar structures were observed in all the optical images. The orientation of the fibrils at the centre regions for all films did not follow a particular orientation. Generally it was quite isotropic. This was expected as the centre region of the film was subjected to near biaxial straining of the fibrils. As compared to the side regions, the fibrils were strongly aligned in a unidirectional manner, as shown in the arrows at the top right corner. This was because the side of the film was subjected to a more unidirectional drawing process. This was also observed in the study of biaxial elongation of semi-crystalline poly(ethylene terephthalate) (PET) by Marco and co-workers [77]. A distinct difference in diameters of the fibrils of different fabrication methods was observed. Drawn spin cast film showed a very fine network of fibrils while that of two-roll mill film showed a coarser network. Drawn solvent-cast film also showed a network of fibrils intermediate in size. The difference in the size of the fibrils could be due to the different sizes of the spherulites formed at different cooling rates. The spin-cast films, which were allowed to dry at room conditions, experienced a higher cooling rate than the two-roll mill and solvent-cast films. As a result of fast cooling, the spin-cast films had smaller spherulites and the fibrils formed from drawing would thus be significantly thinner.

Uniform biaxial drawn films were achieved with good repeatability using methods of two-roll milling and solvent casting. Undrawn material was not observed under the microscope, showing that the drawing ratio of both film types was sufficient in transforming the lamellar structures into fibrils. However, for the spin cast films, regions of undrawn materials were found. Fig. 3.4 showed the centre region of the biaxial drawn spin cast PCL film with fibrils extending radially outwards from the undrawn material. The existence of the undrawn materials could be due to inefficient

transfer of the drawing forces to the fibrils as stress transfer over a very thin structures was difficult due to thickness variations.

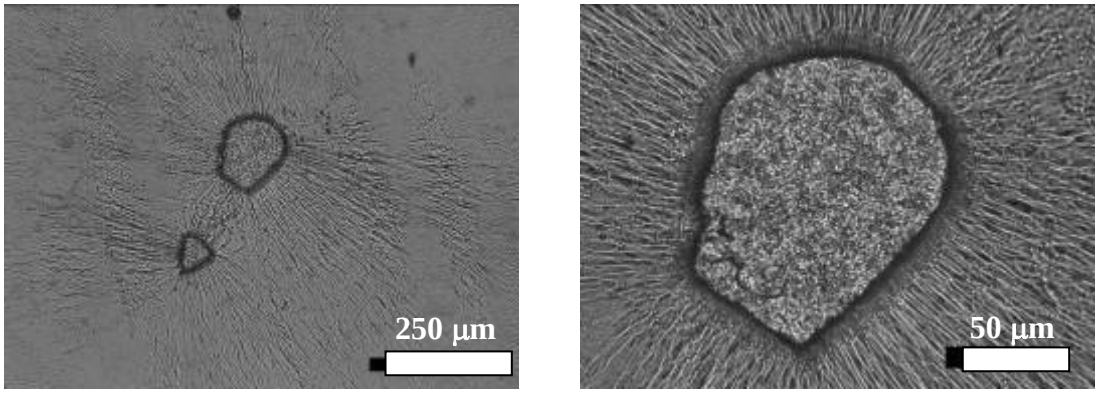

Fig. 3.4. Morphology from polarizing microscope showing fibrils extending radially outwards from the undrawn material of biaxial stretched spin cast PCL films at the centre region.

AFM images of drawn PCL films at the side regions were shown in Fig. 3.5 and those in the centre region were shown in Fig. 3.6. In Fig. 3.5, all three types of PCL films showed a unidirectional alignment of fibrils and were similar to the microstructures as shown previously in Fig. 3.3. The thick rod like structures shown in Fig. 3.5 A1 and B1 could be the macrofibrils and when scanned at a higher resolution of 5 μm x 5 μm as shown in A2 and B2, the macrofibrils could be seen thinning and slipping away to form microfibrils in a unidirectional orientation.

Fig. 3.6 showed the AFM images in the centre regions of the drawn PCL films. Fibrillar networks were observed and the fibrils were also no longer aligned unidirectionally and were seen to be oriented non-preferentially. These results were in agreement with the images shown by the polarized optical microscopy in Fig. 3.3.

However, biaxial or radial alignment of the fibrils was not as obvious as the image shown in Fig. 3(d) where the radial fibrils were seen extending from the undrawn material. This happened when the biaxial force at the four corners of the film was released after the drawing process, and subsequently the fibrils experienced a stress relaxation that caused the fibrils to coil back from its biaxial drawn direction. Such relaxation, which can cause shrinkage, was reported by Zhang in the biaxial drawing of polystyrene [34].

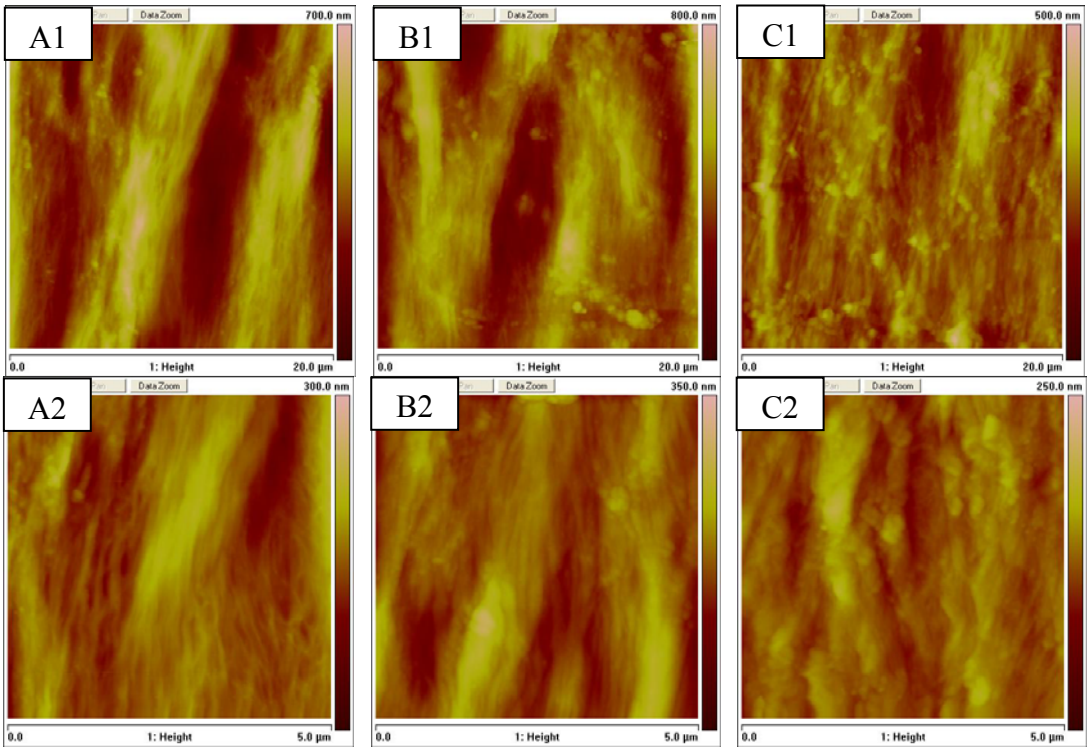

Fig. 3.5. AFM images of the biaxial drawn films by different fabrication methods (A: spin-casting; B: two-roll milling; C: solvent casting) at the side regions.

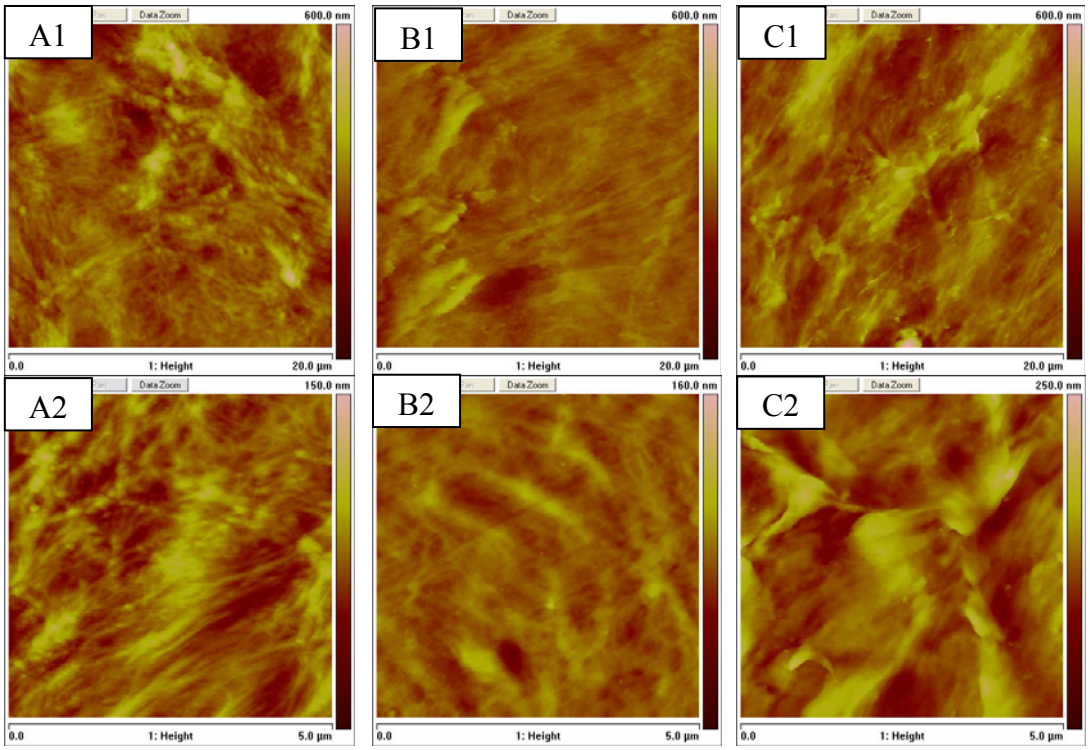

Fig. 3.6. AFM images of the biaxial drawn films by different fabrication methods (A: spin-casting; B: two-roll milling; C: solvent casting) at the centre regions.

3.4.3 Thermal Properties of PCL films (DSC)

Biaxial drawing produced a significant effect on the melting behaviour of the films. This was expected due to structural changes by biaxial drawing, and these were indicated in the melting endotherms shown in Fig. 3.7 and the melting temperature, enthalpies and percentage crystallinities tabulated in Table 3.2. Fig. 3.7 showed a series of DSC traces of drawn and non-biaxial drawn PCL films. The traces showed very well defined profiles of a material with a typical semi-crystalline characteristic. The non-biaxial drawn PCL films melted at 62.0 ^{o}C for spin-cast film, 62.2 ^{o}C for solvent-cast film and 62.9 ^{o}C for two-roll mill film. These three types of undrawn films showed similar melting temperature. After bi-axial drawing, the melting temperatures of the films were found to be 63.6 ^{o}C for spin-cast film, 63.3 ^{o}C for solvent-cast film

and 62.5 ^{o}C for two-roll mill film. No notable change in melting temperatures was observed after two-roll mill films were drawn. An increase of 1.1 ^{o}C was observed in drawn solvent-cast film while an increase of 1.6 ^{o}C was observed in drawn spin-cast film. Increase in melting temperature after biaxial drawing of polymers was also reported elsewhere [26, 27, 78]. Since melting temperature is dependent on crystalite sizes, the increase in melting temperature suggested that larger and thicker lamellae were formed during the biaxial drawing at near melting temperature of the PCL.

The melting profiles of the films fabricated by method of solvent-casting and two-roll milling showed a reduction and broadening in the peaks after biaxial drawing, as compared with pointed and narrow peaks before biaxial drawing. The biaxial drawing process broke up the lamellae and widened the lamellae size distribution, which was evident by the broadening of the melting trace since crystallite sizes affect glass transition temperatures. For spin cast films, the peak remained relatively unchanged after biaxial drawing but a slight shift of the melting peak at higher temperatures was observed.

Table 3.2 showed the peak temperatures, melting enthalpies and percentage crystallinities of the PCL films. The percentage crystallinity of the film was calculated against the melting enthalpy of 100% crystalline PCL at 139.5 J/g [70]. The degree of crystallinity was observed to be 4 ~ 6 % lower after biaxial drawing for all three types of films. This indicated the destruction of crystalline material as the large lamellae (folded chain structures) were subjected to drawing to form micro-fibrils (extended chain structures).

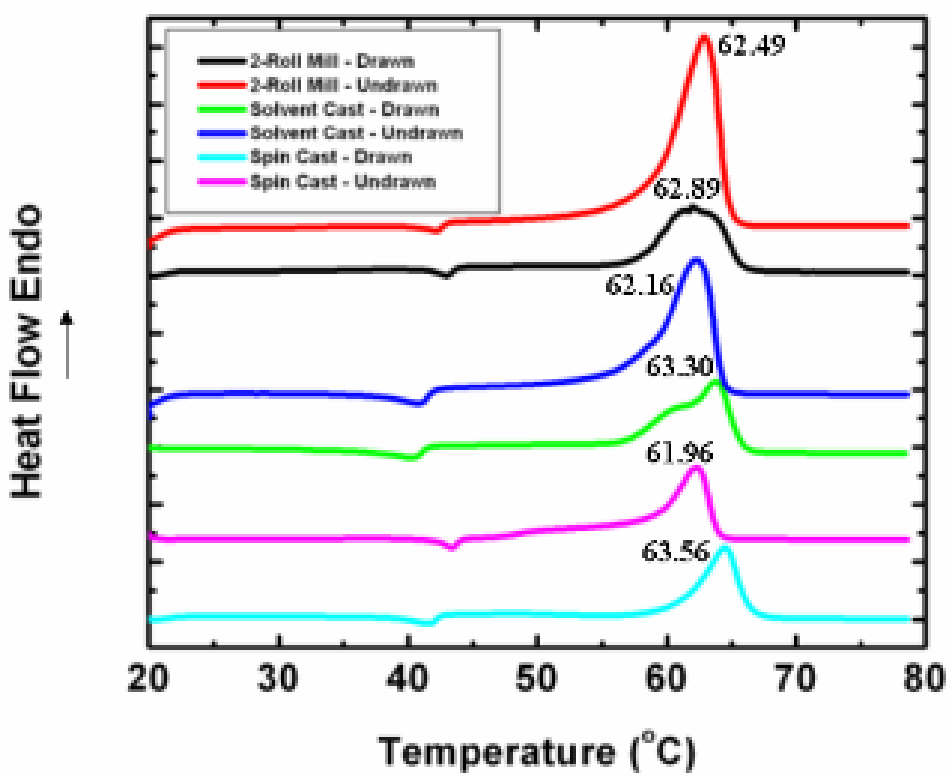

Fig. 3.7. DSC profiles of drawn and undrawn PCL films.

Table 3.2 . Peak temperature, melting enthalpy and percentage crystallinity of the drawn and undrawn PCL films.

	Film Types	Peak Temp. (°C)	Enthalpy (J/g)	% Cryst.
Non-biaxial drawn films	spin-cast	62.0	73.8	52.9
	two-roll mill	62.9	69.6	49.9
	solvent-cast	62.2	68.0	48.7
Biaxial drawn films	spin-cast	63.6	65.2	46.7
	two-roll mill	62.5	65.5	47.0
	Solvent-cast	63.3	62.8	45.0

These results appeared to be different from the findings by Ng and co-workers [26], who reported an increase in the melting enthalpy of the biaxial drawn films. This difference could be due to adopting different cooling techniques. Slow cooling after melt pressing was carried out in this experiment while Ng et al adopted quenching of melt-pressed films in ice water.

It is important to note that the different methods in cooling can affect the size of the lamellae formed. The lamella thickness L is related to cooling rate ΔT [79] by

$$L = \frac{2\sigma_e T_m^O}{\Delta H_f \Delta T} + \delta L \quad , \qquad \text{(Eq. 3.2)}$$

where σ_e , ΔH_f , T_m^O and δL are the fold surface energy, heat of fusion, equilibrium melting temperature and a quantity arising from the kinetic theory (which varies slowly with cooling rate), respectively. From Eq. 3.2, slow cooling produces larger and thicker lamellae while fast cooling, like quenching, produces smaller and thinner lamellae and lower crystallinity. Smaller lamellae may suggest a more ordered fibrillar structure after biaxial drawing while larger lamellae from slow cooling may produce a less ordered fibrillar structure.

3.4.4 Water Vapour Transmission Rate (WVTR)

One of the critical concerns in the search for good tissue engineering scaffolds is the mass transport issue. Cells need supplies of nutrients and other vital substances, such as oxygen, to survive. This transport is accomplished through blood vessels and capillaries *in vivo*; under *in vitro* conditions where the tissue grown is avascular, physical diffusion and permeation are the only possible routes to provide these

substances. Therefore, permeable scaffolds are more suitable for healthy tissue growth. As a result, the testing for transport of small molecules, such as water vapour, through the films becomes indispensable in our assessment of the membranes via the water vapour permeability test.

There are possible sources of errors in water vapour permeability tests, such as local defects, leakage, resistance to transmission from the still air layer between water surface and film and resistance of the two surfaces of the film [80]. For permeable thin films, these sources of error may cause significant difference to the vapour transmission rates measured. In the experiments conducted, leakage was minimized by carefully sealing the opening circumference of the tube using parafilms to prevent vapour from escaping; still air gap between water surface to the film surface was kept at a minimum; and the surfaces of the films were carefully cleaned with ethanol to minimize contamination which could potentially increase surface resistance.

The WVTR test was first performed for four types of PCL films, namely bi-axial drawn two-roll mill film, solvent-cast film, spin-cast film and non-biaxial drawn spin-cast film. The values of the WVTRs obtained were tabulated in Table 3.3. The results showed that the single layer biaxial drawn solvent-cast films had the lowest WVTR at 38.24 g/h.m^2 while the biaxial drawn spin-cast PCL films had the highest WVTR at 74.96 g/h.m^2. The WVTR was 43.10 g/h.m^2 for biaxial drawn two-roll mill films. However, Htay and co-workers [43] had reported a WVTR of 30.5 g/h.m^2 for 10.4 μm thick biaxially drawn solvent-cast PCL films. Judging from the results in Table 3.3, one would have expected Htay's films to have a WVTR that was higher than the biaxial drawn solvent-cast PCL films or close to the value registered by

Table 3.3. Values of thicknesses and WVTR of different PCL films.

Film type	**Mean Film Thickness (μm)**	**WVTR (g/(h.m^2))**
	-	171.9
Biaxial drawn spin-cast	1.15	74.96
Non-biaxial drawn spin-cast before heat treatment	1.58	67.77
Non-biaxial drawn spin-cast after heat treatment	2.68	46.88
Biaxial drawn two-roll mill	10.7	43.10
Biaxial drawn solvent-cast	14.0	38.24
Biaxial drawn two-roll mill (Double layer)	23.67	33.43
Biaxial drawn solvent-cast film reported by Htay [43]	10.4	30.50

biaxial drawn two-roll mill PCL films. One of the reasons for the lower WVTR recorded by Htay *et al* could be due to the larger resistance to water vapour transmission caused by the depth of the air gap below the film. In this experiment, the air gap was kept at a minimum to 5 mm as compared to Htay's 45 mm. This big difference thus played a significant role in the difference recorded. Another reason for such discrepancy would be due to the size of the spherulites. In Htay's experiment, his PCL membrane was subjected to ice water quenching immediately after it was heat-pressed, since his PCL membrane was fabricated in the same manner as described by Ng *et al*. However, the PCL films tested here was slow cooled after melt-pressed. As

mentioned previously, slow cooling produces larger and thicker lamellae, and a less ordered fibrillar structure after biaxial drawing while quenching produces smaller and thinner lamellae and a more ordered fibrillar structure after biaxial drawing. As a result, a much more compact and dense structure would be expected in the quenched PCL films and hence it provided a larger resistance for water molecules to diffuse through, thereby having a WVTR that was significantly lower than the PCL films that were allowed to slow-cool.

An ideal correlation between thickness and WVTR for homogeneous film types is governed by Fick's Law of steady state transport. Strictly speaking, the wet cup test in accordance to ASTM E96-00 E requires a steady state of water vapour transport to be established across the barrier membrane. For this condition to be achieved, it is required that the relative humidity (RH) levels on both surfaces of the film be maintained constant such that the outside surface facing the air is kept at 50 % RH by the humidity chamber and the inner surface facing distilled water is maintained at 100 % RH by the evaporation of water [81].

Under this steady state condition, the transport of water vapour through the film governed by Fick's law of steady state diffusion [82] can be concisely expressed by the following relation:

$$\text{Flux} = -\wp \frac{\text{dP}}{\text{dx}} = \frac{G}{t}, \qquad \text{(Eq. 3.3)}$$

where $\wp$ is the permeability coefficient of the material that depends on material characteristics, $\frac{dP}{dx}$ the gradient of the driving force of transport, G the weight change and t the time during which G occured. Under steady state, this gradient is equal

to $\frac{\Delta P}{l}$, where ΔP is the pressure or concentration or potential difference across the film and l the thickness. Since WVTR is flux divided by the cross-sectional area, it can be deduced that WVTR is proportional to $\frac{\Delta P}{l}$ under steady state conditions, which leads to the conclusion that WVTR should be inversely proportional to film thickness l if fabrication methods have no influence on the material permeability $\wp$.

The WTVR of free water surface was determined at 171.90 g/(hr.m^2), and this result matches closely to the value of 167.75 g/(hr.m^2) established [43], hence verifying the matching accuracy of this test setup. A wide range of PCL film types were fabricated and used in this test. Stacking of two-roll mill films were also carried out to explore WVTR at higher thickness. As mentioned earlier, Fick's Law states that the WVTR is inversely proportional to the film thickness provided the films are homogenous. Since the films were fabricated by different techniques, these films could not be homogenous. However, judging from the difference between biaxial drawn two-roll mill film and biaxial drawn solvent-cast film by Htay *et al*, we could allow the values of the WVTR to be plotted against film thickness based on the fact that error margin caused by the non-homogeneity of different film processing techniques accounted for less than 50%. Fig. 3.8 showed the WVTR versus thickness.

The results from Fig. 3.8 showed that an exponential decay between WVTR and film thicknesses could be established. This predicted accurately that WVTR was inversely proportional to its thickness. The relative magnitudes of WVTR values of the available films could be concluded such that biaxial drawn spin-cast films always give the highest level of water vapour transmission rate as compared to other films,

possibly due to its lowest thickness and/or structural differences. Spin-cast films were believed to have undergone rather limited amount of drawing such that the fibrillar structure is not fully formed as undrawn materials were observed under the microscope. Drawing defects might have also caused the presence of many micro-voids in the structure such that the micro-pores formed allow the direct flow of water vapour through the membrane instead of diffusion and sorption. Thus, these micro-voids could have possibly enhanced the transmission rate of water vapour.

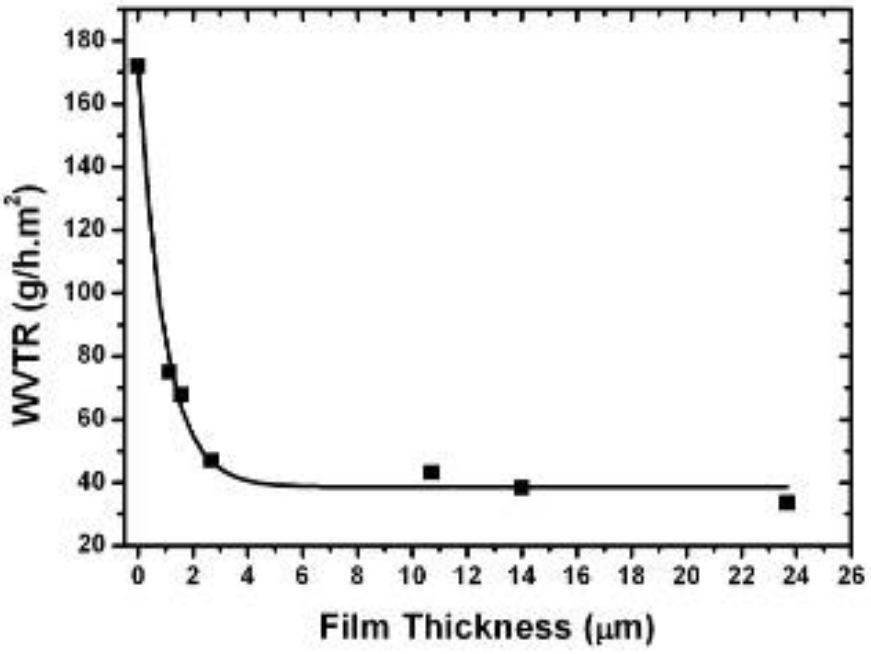

Fig. 3.8. WVTR plotted against film thickness for various film types.

3.4.5 Tensile Properties

The stress-strain curves of the PCL films were shown in Fig. 3.9. Distinct differences in the tensile strength and elongation could be seen from the graph upon biaxial drawing of the films. Biaxial drawn films exhibited higher tensile strength while non-biaxial drawn films exhibited greater elongation.

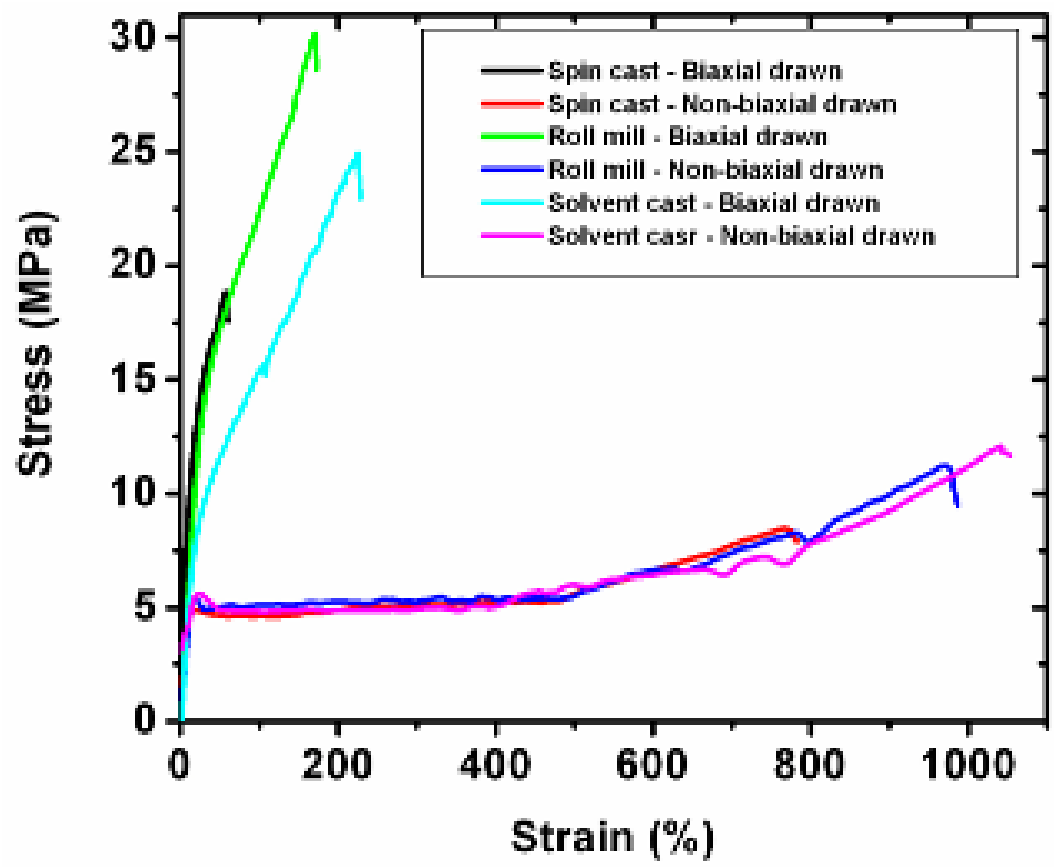

Fig. 3.9. Stress-strain curves of PCL films fabricated by different methods.

For non-biaxial drawn films, all three fabrication methods yielded similar tensile characteristics. Yielding took place at a stress of about 5 MPa which was followed by cold drawing till it reached strain of 500 %. At this stage of cold drawing, the spherulites were drawn to form macro-fibrils, similar to what happened to the PCL structures during biaxial drawing. At strain of 500% and beyond, strain hardening took place. A higher tensile force was required to stretch further the fully extended macro-fibrils into micro-fibrils, and the films finally fractured beyond its tensile strength of 8.2 MPa, 11.4 MPa and 10.9 MPa for spin cast, roll mill and solvent cast films respectively. Two-roll mill and solvent-cast films had almost the same elongation at

break of about 1000 % while spin cast films had a lower elongation at break of 720%. The lower tensile strength and elongation for spin cast film were expected due to non-uniform microstructure as compared to the rest of the films and the smaller spherulites formed caused by fast evaporation of solvent.

Upon biaxial drawing, the elongation was reduced to 59.6 %, 183.0 % and 229.5 % for spin-cast, two-roll mill and solvent-cast films, respectively. The elongation became very much smaller as compared to their non-biaxial drawn counterparts because after biaxial drawing, the micro-fibrils were almost fully stretched to its limit. At this point when all the spherulites had strain-hardened to form micro-fibrils, elongation will become substantially reduced and any force applied will be utilized to deform and fracture the micro-fibrils. Hence this explained the reduction in the elongation at break. At the same time, the modulus of the films increased due to the strain-hardening. The modulus of spin-cast films was increased by approximately 58% from 223.2 MPa to 352.8 MPa while that of the two-roll mill films increased by about 25% from 273.3 MPa to 339.3 MPa. However, the solvent-cast films registered a reduction in modulus from 262.3 MPa to 214.5 MPa.

In biaxial drawn films, greater force was required to stretch and deform the strain-hardened micro-fibrils as compared to non-biaxial drawn films where less force was required to draw the spherulites into macro-fibrils. Strain hardening upon biaxial drawing also resulted in the tensile strength of all PCL films to increase by approximately 2.5 folds. The tensile strength of spin-cast, two-roll mill and solvent-cast PCL films increased to 20.7 MPa, 30.6 MPa and 24.8 MPa respectively. The distinct enhancement in the modulus and tensile strength of the biaxial drawn PCL

films could be attributed to the effect of annealing after biaxial drawing where the stress imposed on the micro-fibrils was relaxed. As mentioned earlier, the increase in melting temperature after biaxial drawing at near melting temperature and annealing resulted in the growth of thicker lamellae; this aspect further substantiated the results for the increase in tensile strength and modulus of the films.

Table 3.4 summarized the tensile characteristics of all types of PCL films before and after bi-axial drawing. Biaxial drawn spin-cast films were found to have a higher modulus, hence stiffer, than the other two types of biaxial drawn films. Biaxial drawn spin-cast films were also found to have the least tensile strength.

Table 3.4. Values of modulus (E), ultimate tensile strength σ_{UTS} and elongation (λ) of all types of PCL films.[42]

	Films Types	**E (MPa)**	**σ_{UTS} (MPa)**	**λ (%)**
Non-biaxial drawn films	Spin-cast	223.2	8.2	720.6
	Two-roll mill	273.3	11.4	978.7
	Solvent-cast	262.3	10.9	1000.6
Biaxial drawn films	Spin-cast	352.8	20.7	59.6
	Two-roll mill	339.3	30.6	183.0
	Solvent-cast	214.5	24.8	229.5

3.5 Summary

- The fabrication of sub-micrometer ultra-thin PCL films was successfully carried out through biaxial drawing of the spin-cast films. All films were biaxially drawn

to its limit and were found that films made from two-roll mill have the highest drawing ratio while that of spin cast films has the lowest drawing ratio.

- The morphology of all the biaxial drawn films studied showed similar fibrillar networks due to chain orientation induced by biaxial drawing.

- Thermal analysis revealed an increase in the melting peak temperature of the films upon biaxial drawing but a drop in the percentage crystallinity.

- The WVTR was found to be inversely proportional to film thickness and can be dependent on the effect of quenching. Biaxial drawn spin-cast film, being the least thick, therefore has the highest WVTR as compared to the rest of the biaxial drawn films.

- The mechanical properties determined through the tensile test showed that upon biaxial drawing, all films exhibited a reduction in elongation, increase in tensile strength and increase in modulus. However, for solvent cast films, the modulus decreased.

Chapter 4:
Theoretical Simulation of Heat Accumulation during Laser Ablation of PCL Films

4.1 Introduction:

In Chapter 3, the techniques of the fabrication of PCL films, through the initial steps of dissolution, spin-casting and two-roll milling, followed by compression into thin, uniform and homogenous sheets, and finally the bi-axial drawing of the sheets into ultra-thin membranes, have been carried out. The mechanical properties of the biaxially drawn PCL thin films have become enhanced as it shows an increase in both tensile strength and modulus. Due to the reduction in film thickness, the water vapour transmission rate has also increased significantly to allow better bidirectional gas and moisture diffusion through the film. Upon the successful fabrication of the PCL films, these films were next processed with lasers to create micro-structures on the films, as well as study the chemical changes induced on it.

Excimer lasers such as KrF (λ = 248 nm) and ArF (λ = 198 nm) and ultra-fast femtosecond lasers were widely reported to be an efficient tool for precision micro-structuring of polymer materials [50, 83-85]. Excimer lasers make use of the photo-chemical effect [86] whereby polymer chains are broken down by the high energy photon absorption while the femtosecond laser causes material breakdown through multi-photon absorption (MPA) [87, 88]. These two ablation mechanisms would result in minimal photo-thermal effect, and are suitable for precision laser micro-fabrication of materials. But for excimer laser, problems sometimes do arise. The photon energy will initially breakdown the polymer chain and then followed by material removal.

Recently, 3rd harmonic diode-pumped solid state (DPSS) Nd:YAG laser had proved to be also able to produce precise micro-features on polymer films at a low cost and high processing speed. This was made possible through the use of high magnification objective lens which help to tightly focus the laser beam spot, and hence was able to produce exceptionally high laser fluence even at low laser output power. This greatly improved the quality of micro-features that were to be produced on polymers, such as micro-pores, micro-wells and micro-trenches..

In this study, micro-structures were created in biaxially drawn PCL films by laser micro-processing. Many research studies [26, 35, 37, 45, 67, 68, 89] have been focusing on utilizing and developing thin PCL films. The ability to micro-structure the film surface with micro-pores, lines or other patterns are known to induce cell orientation, proliferation and hence differentiation [90-92]. This research in surface modification of biodegradable polymer films, therefore, proves to be important in areas of biomedical applications. In this paper, precision laser micro-processing of polymer films was investigated through the use of the 3rd harmonic DPSS Nd:YAG laser delivered through a high magnification objective lens and a typical plano-convex lens.

4.2 Experimental Setup:

4.2.1 Laser setup

The laser used in this work was carried out by a Coherent AVIA 355-1500 3rd harmonic diode-pumped solid-state (DPSS) Nd:YAG laser (355nm, 30ns) and a Lightwave 2nd harmonic generation Nd:YAG laser (532 nm, 10 ns). A Mitutoyo M Plan NUV-Plan objective lens of 50X magnification with focal length of 4 mm and a numerical aperture (NA) of 0.40 was used for the micro-processing of the thin PCL

polymer films. A plano-convex lens with a focal length of 50 mm was also used. Linear motion of the stage was controlled by AeroTech motorized stage with 3 axes. A CCD was configured to monitor the process. Fig. 4.1 showed the schematic setup for the laser processing of PCL films.

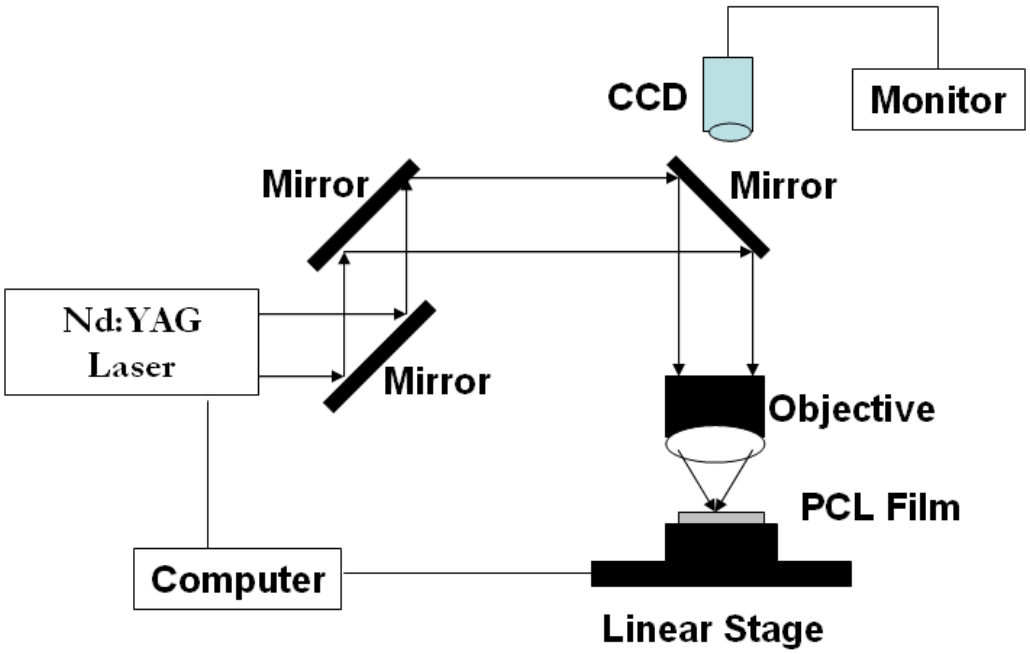

Fig. 4.1 Schematic setup for the laser micro-processing of PCL films.

4.3 Results and Discusion:

4.3.1 Laser micro-drilling and melt-related issues on PCL films using Nd:YAG lasers

Micro-drilling using Nd:YAG laser was carried out on PCL film of 9 μm thickness fabricated by hot roll-milling followed by biaxial drawing, as described previously in Chapter 3. A plano-convex lens with a focal length of 50 mm was used in this micro-drilling at a laser fluence of 25 J/cm^2 and a repetition rate of 4000 Hz. It was shown in Fig. 4.2 that the micro-holes produced were of below-par quality. The

micro-holes drilled varied in shape to a certain extent and the dimension of the micro-pores was about 100 μm in diameter throughout. The annulus ring of material was observed to be smooth and extended over a larger area, which was caused by melting and material flow. The effective pore size drilled was about 85 ~ 90 μm while the width of the annulus ring caused by melting was about 25 ~ 30 μm. No re-deposition of the material was spotted at the circumferential regions of the pores after the laser micro-drilling.

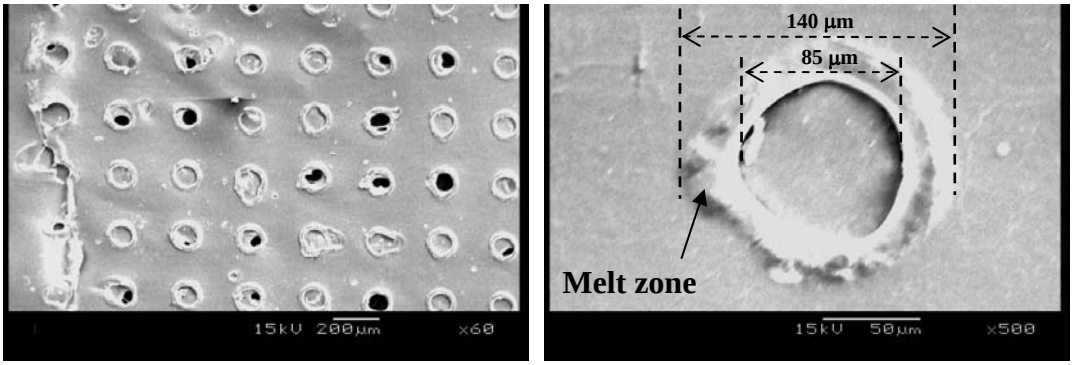

Fig. 4.2. Laser micro-drilling of micro-pores on bi-axial drawn PCL film at a laser fluence of 25 J/cm^2 and pulse repetition rate of 4000 Hz for 2000 pulses using a plano-convex lens with a focal length of 50 mm.

In order to reduce the pore size, an objective lens with a focal length of 4 mm was used for the laser micro-drilling on the same bi-axially drawn roll-mill film. The SEM results were shown in Fig. 4.3. The change of optical lens to one with a much smaller focal length allowed producing micro-size pores in the region of 7 ~ 9 μm at a laser fluence of 25 J/cm^2 for 5000 laser pulses at a repetition rate of 10 kHz. Similarly, it was observed to have suffered from melting as evident from the smooth annulus ring of width 8 ~ 10 μm formed on each pore. With a reduction in the focal length from 50

mm to 4 mm, the pore size was reduced by close to 10 times while the width of annulus ring of melted polymer was reduced by approximately 6 times.

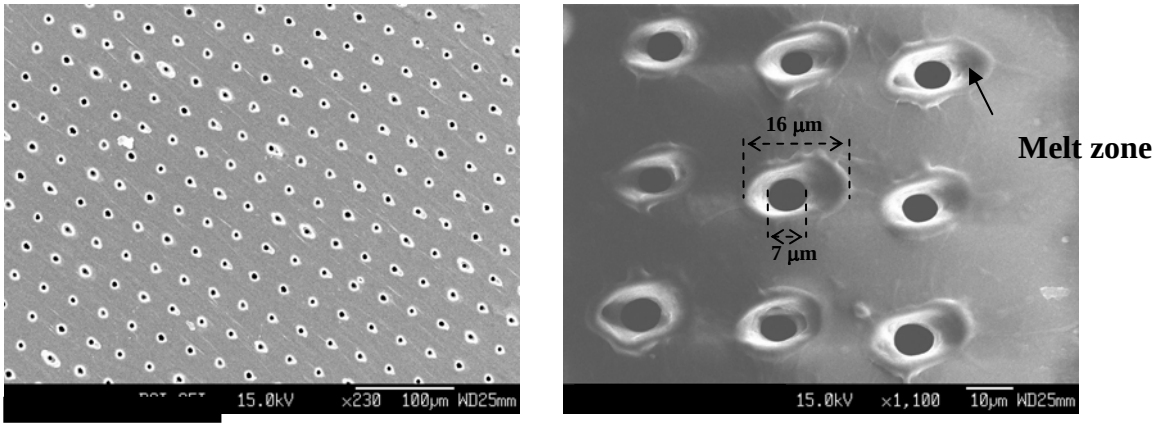

Fig. 4.3. Laser micro-drilling of micro-pores on bi-axial drawn PCL film at a laser fluence of 25 J/cm^2 and pulse repetition rate of 10000 Hz for 5000 pulses using an objective lens with a focal length of 4 mm.

Laser micro-drilling of micro-pores on approximately 2 μm thick spin cast film was next carried out and the SEM results were shown in Fig. 4.4. It was found that the average size of the micro-pores drilled was approximately 5 ~ 7 μm, which was about 25 % reduction in pore dimension as compared to using thicker 10 μm thick bi-axial drawn film. It was also found that there was no visible signs of melting as observed in previous cases.

4.3.2 Theoretical simulation of laser-drilled hole sizes on PCL films

Base on the above-mentioned results, there seemed to be a relationship between film thickness, the dimension of the micro-pores and the degree of melting that resulted in forming an annulus ring around the pore. At more than 10 μm thick,

melting was observed for both sets of optical lens used. A smaller micro-pore dimension and melted region were formed when used with objective lens. When the experiment was conducted using a 2 μm thick film instead, the pore dimension decreased further with no smooth annulus ring formed from melting. The minimum spot size of a laser beam is known to be dependent on the focal length of the lens used, as shown in Eq. 4.1 [93]. Base on this relation, the reduction in focused beam is as large as 12 times.

$$2w_o = \left(\frac{4\lambda}{\pi}\right)\left(\frac{F}{D}\right), \qquad \text{(Eq. 4.1)}$$

where λ is the wavelength of laser, F the laser fluence and D the diameter of laser beam entering the lens.

This corresponded closely with the dimension of the pores drilled as shown in Fig. 4.6 and Fig. 4.7, which was approximately 10 ~ 12 times difference.

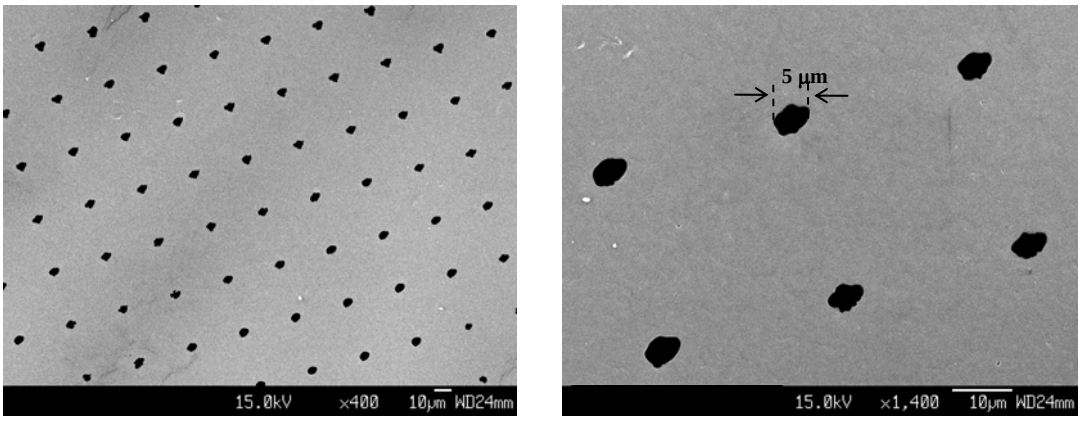

Fig. 4.4 Laser micro-drilling of micro-pores on 1 μm thick spin-cast PCL film at a laser fluence of 25 J/cm^2 and pulse repetition rate of 10000 Hz for 5000 pulses using an objective lens with a focal length of 4 mm.

Other than a reduction in the pore size, the depth of focus was also substantially reduced when an objective lens was used, as defined by Eq. 4.2 [93]:

$$\text{Depth of Focus, DOF} = 2.44\lambda\left(\frac{f}{D}\right)^2, \qquad \text{(Eq. 4.2)}$$

where λ is the wavelength of laser, *f* the focal length of the lens and D the diameter of laser beam entering the lens.

From a focal length of 50 mm to 4 mm, the depth of focus was reduced by a significant $(50/4)^2$ or approximately 155 times to about 3 μm. This clearly showed that the depth of the focused beam using the objective lens was not sufficiently long enough to penetrate through the thicker bi-axial drawn PCL film to allow complete drill-through of the micro-pores, unless the exposure time or the pulse repetition rate was increased. However, increasing the exposure time would have induced more melt to occur and subsequently led to tearing of the film. Hence, increasing the repetition rate to 10000 Hz from the previous 4000 Hz was preferred instead. At a high repetition rate of 10000 Hz, the quality of micro-drilling on 2 μm thick film would not deviate much from one with a lower repetition rate. For film with thickness up to 9 μm, the edge of the pore will be subjected to more intense melting due to a more confined melting zone (approximately 5 μm in diameter) when the laser beam was more tightly focused by the objective lens, as compared to using a plano-convex lens approximately which was 30 μm in diameter. The confine melting space would have restricted the volume expansion of the polymer melt and this resulted in the purging of material from the surface as melt re-deposition, as shown in Fig. 4.3.

In order to gain a clearer understanding of the relationship between PCL film thickness on the dimension of the micro-pores and the degree of melting, two PCL films with thicknesses of 9 μm and 2 μm were used for laser micro-drilling at different laser fluence. The results were shown in Fig. 4.5. The minimum and maximum pore size drilled for 9 μm thick film were about 3.5 μm and 8.2 μm respectively while for 2 μm thick film were about 2.9 μm and 8.9 μm respectively. It was impossible to drill micro-pores on 9 μm thick film below 20 J/cm^2 due to insufficient laser fluence. Micro-pores drilled were slightly larger in 2 μm thin film as compared to 9 μm thick film at the same laser fluence. This was because the stress imposed on the thin film caused some degree of tearing when a micro-pore was drilled. As for the thicker film, there was enough mass to withstand the stress to prevent the tearing from happening. Apart from the slight difference in size of the micro-pores drilled, both films showed increase in pore size with increasing laser fluence.

The size of the micro-pores drilled was determined to be related to the laser fluence as determined by a Gaussian profile [93] shown in Eq. 4.3:

$$
\begin{aligned}
F &= F_0 e^{-\frac{2r^2}{w_0^2}} \\
&= F_0 e^{-\frac{2\left(\frac{D}{2}\right)^2}{w_0^2}} \\
e^{-\frac{D^2}{2w_0^2}} &= \frac{F}{F_0} \\
D^2 &= 2w_0^2 \ln\left(\frac{F}{F_0}\right)
\end{aligned}
\quad , \qquad \text{(Eq. 4.3)}
$$

where F, F_0, r^2, w_0 and D are the laser fluence, laser threshold fluence, output radius, Gaussian beam radius and size of micro-pore, respectively. Clearly, the square of the micro-pore dimension D^2 is directly proportional to the logarithmic of the laser fluence, and this was shown in Fig. 4.5.

The melt width was observed to increase with increasing laser fluence, as shown in Fig. 4.6. The melt width (or the heat affected zone) surrounding the micro-pores was also noted to be related to the thickness of the film. At 9 μm thick, the melt width of the film reached a maximum of 9 μm while for the 2 μm thin film, the melt width reached a maximum of approximately 2 μm at increasing laser fluence.

Investigation on the number of laser pulses affecting the micro-pore drilling at a constant laser fluence was also conducted. Fig. 4.7 showed the dimension and melt width of the micro-pore at a laser fluence of 50 J/cm^2 at varying pulse numbers. When the number of laser pulses was varied while the laser fluence was kept constant, the pore sizes were found to increase almost linearly with increasing number of pulses. There was not much difference in the sizes of the micro-pores on PCL films of different thicknesses. Similarly, the melt width increased with increasing number of laser pulses for a 9 μm thick film but stayed relatively constant at about 1.6 μm for a 2 μm thick film. Similarly, the melt width was also observed not to exceed the thickness of the films as the number of laser pulses was increased.

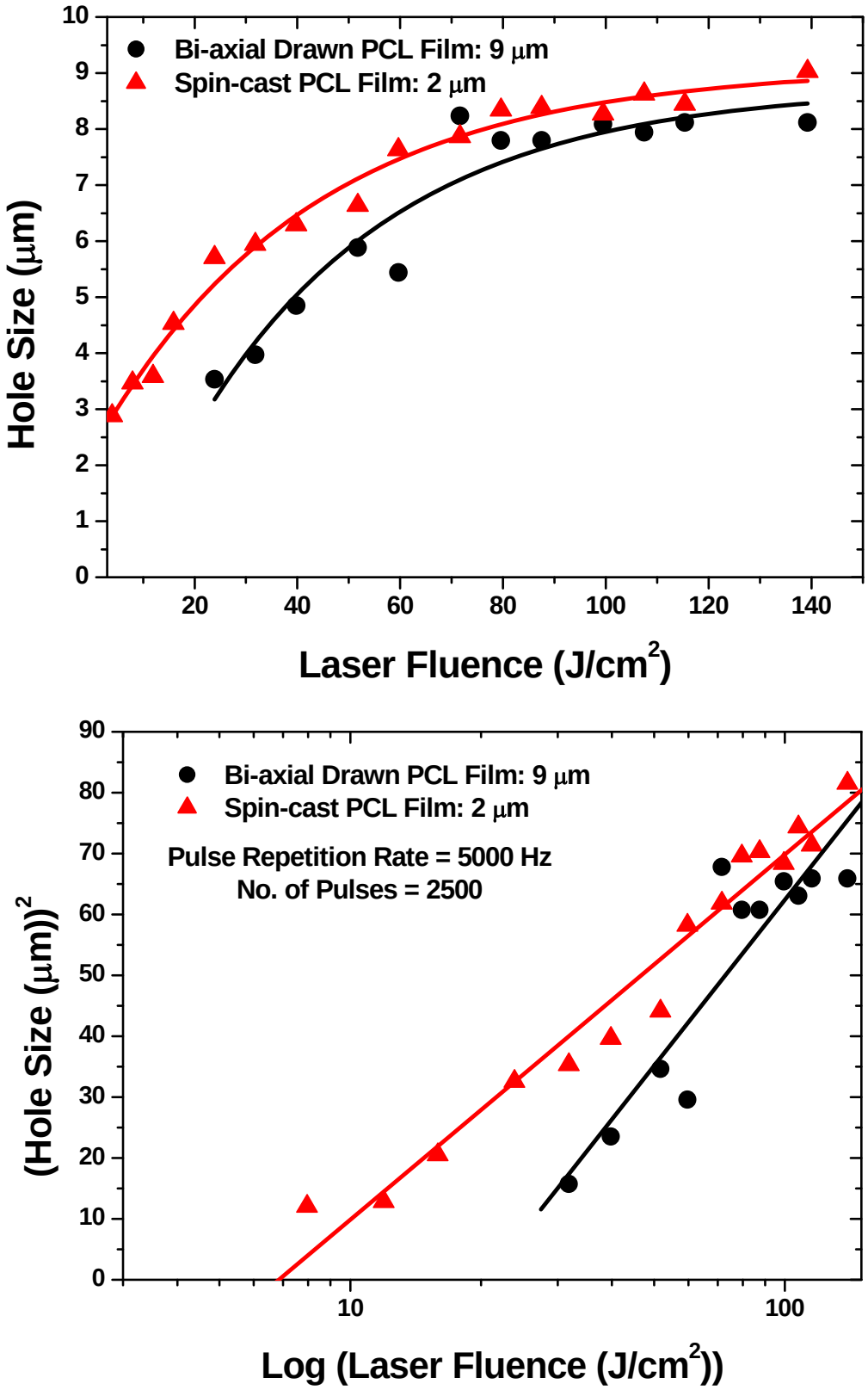

Fig. 4.5. Relationship between the dimension of the micro-pore with laser fluence, using 9 μm and 2 μm thick PCL films for 2500 pulses at a repetition rate of 5000 Hz.

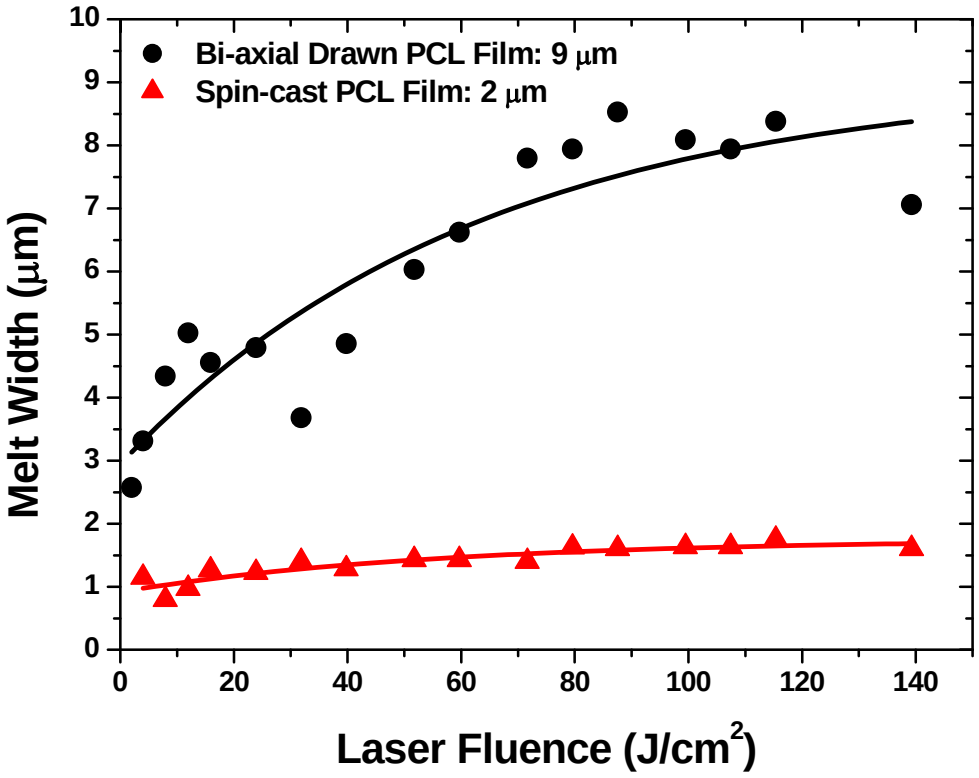

Fig. 4.6. Relationship between the dimension of the melt-width with laser fluence using 9 μm and 2 μm thick PCL films for 2500 pulses at a repetition rate of 5000 Hz.

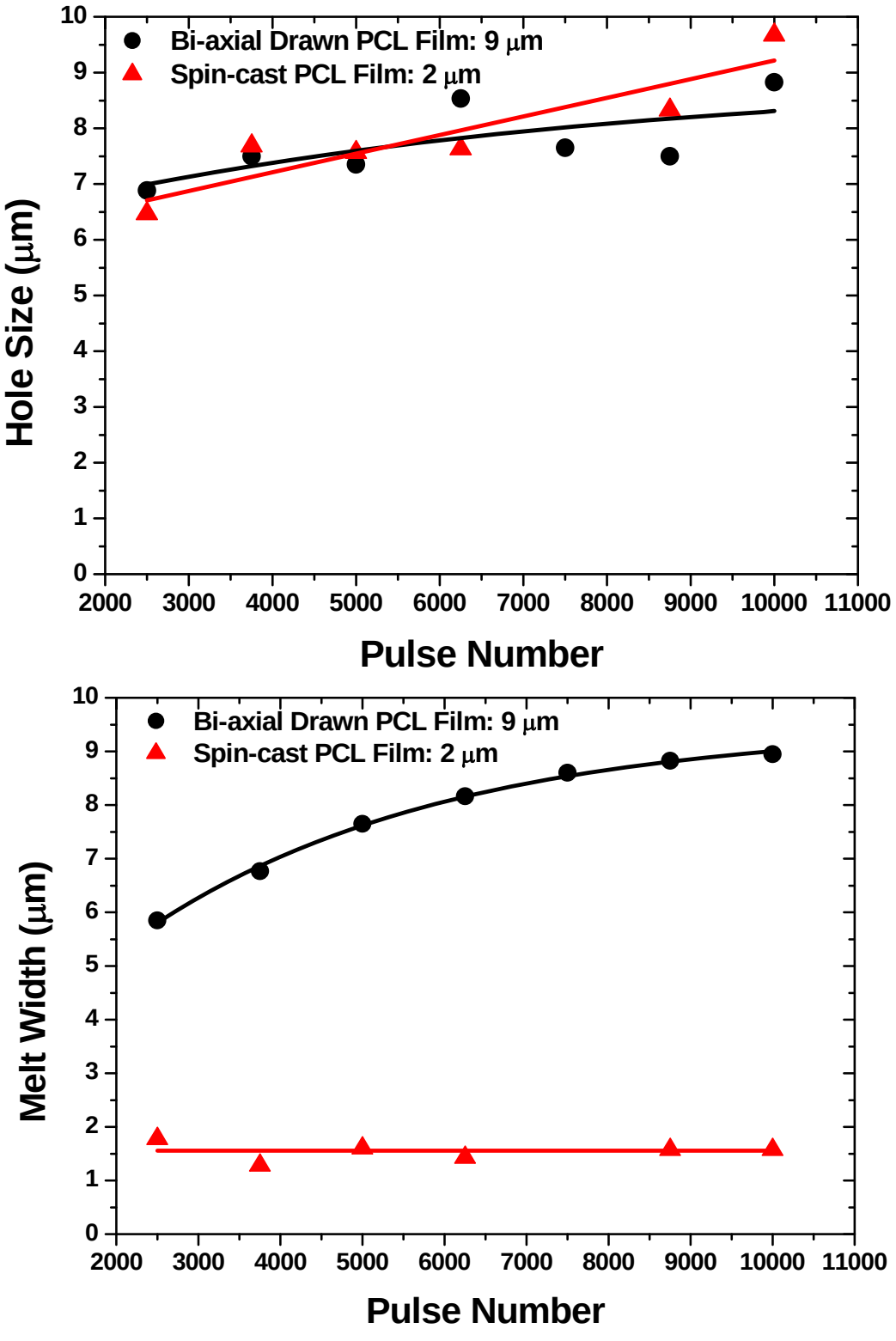

Fig. 4.7. Relationship between the dimension of the micro-pore and melt-width with pulse number at a laser fluence of 50 J/cm^2.

4.3.3 Theoretical simulation of temperature rise during laser micro-drilling

Small laser spot sizes when coupled with pulse rates that can reach up to tens of kilohertz or more may place the ablation in a very different regime as compared to larger laser spot sizes and low pulse rates. PCL film exposed to laser with a single pulse or short pulse repetition rate was able to form well-defined micro-size holes, even at a weak optical absorption at a wavelength of 532 nm. A higher optical absorption occurred at a wavelength of 355 nm. Mathematical simulation of the temperature rise produced by the laser ablation of PCL films take into consideration that only radial heat flow contributes to the cooling of the heated region.

The temperature-rise distribution T(r,t) produced by a nanosecond laser pulse is found by [94, 95]:

$$T(r,t) = T_0 \int_0^{\infty} e^{\frac{-z^2}{a^2}} e^{\frac{-(z^2+r^2)}{4\kappa t}} \times I_0\left(\frac{rz}{2\kappa t}\right)\frac{zdz}{2\kappa t}, \qquad \text{(Eq. 4.4)}$$

where I_0 is the zero-order Bessel function and κ is the thermal diffusivity of the polymer. The initial temperature rise is assumed to have a Gaussian distribution with value at r = 0 given by

$$T_0 = \frac{(1-R)\alpha F_0}{C}, \qquad \text{(Eq. 4.5)}$$

where C is the volume specific heat of the polymer and F_0 is the peak laser fluence. The above can be evaluated to be

$$T(r,t) = T_0 \frac{\left(e \frac{-r^2}{4\kappa t + a^2} \right)}{\left(\frac{4\kappa t}{a^2} + 1 \right)}, \qquad \text{(Eq. 4.6)}$$

The temperature rise produced by a train of pulses can then be found by the summation:

$$T(r,t) = \sum_{0}^{n-1} T(r, t + \frac{n}{\nu}), \qquad \text{(Eq. 4.7)}$$

where ν is the pulse repetition rate of the laser

Table 4.1. Thermal and optical properties of PCL

Thermal Diffusivity, κ	0.001 cm^2 s^{-1}
Volume specific heat, C	2.18 J cm^{-3} K^{-1}
Absorption Coefficient, α	at 532 nm: 2.1 cm^{-1} at 355 nm: 4.2 cm^{-1}
Reflection Coefficient, R	At 532 nm: 0.005 cm^{-1} At 355 nm: 0.005 cm^{-1}

Table 4.1 showed the optical and thermal properties of PCL. Fig. 4.8 showed a single pulse exposure on the biaxially-drawn PCL film using a 2nd harmonic generation Nd:YAG laser at 532 nm with the beam delivered through an objective lens that gives a laser spot size of a = 10 μm. A single laser shot was sufficient to produce micro-holes of 13 μm on the film. Fig. 4.9 showed the surface-temperature rise against time at r = 0 calculated as from the function T(*r*,*t*) as described earlier. At r = 0, the time constant for the cooling to half of the peak temperature was about 26 μs. By 10 ms, the ablated region and its surrounding would have cooled down to room temperature. Fig.

4.10 showed the radial heat distribution of the single shot ablation. At the centre region of the beam at r = 0, the temperature rise (of about 200 ^{o}C) was high enough to melt and vapourize the PCL film since the melting temperature of the PCL film was 60 ^{o}.

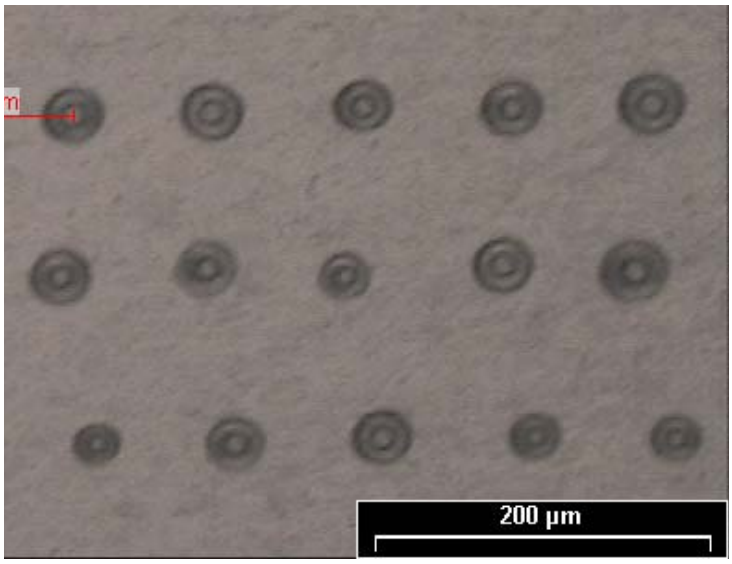

Fig. 4.8. Laser micro-drilling of micro-pores on 12 µm thin bi-axial stretched PCL film with single shot exposure using 532 nm laser at a laser fluence of 220 J/cm^2.

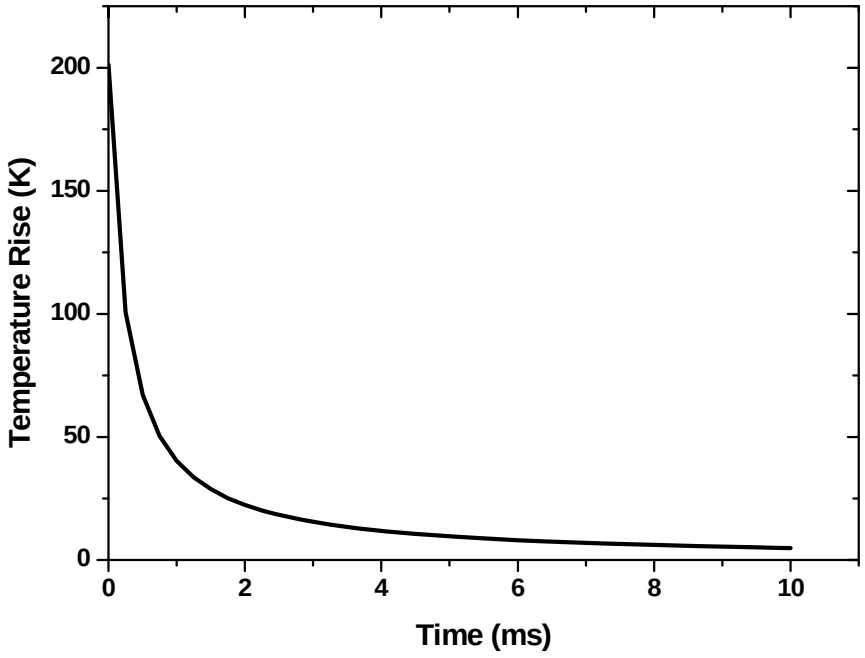

Fig. 4.9. Temperature decay as a function of time for a single pulse exposure at r=0. for 532nm laser at a fluence of 220 J/cm^2 on PCL film with a =10µm.

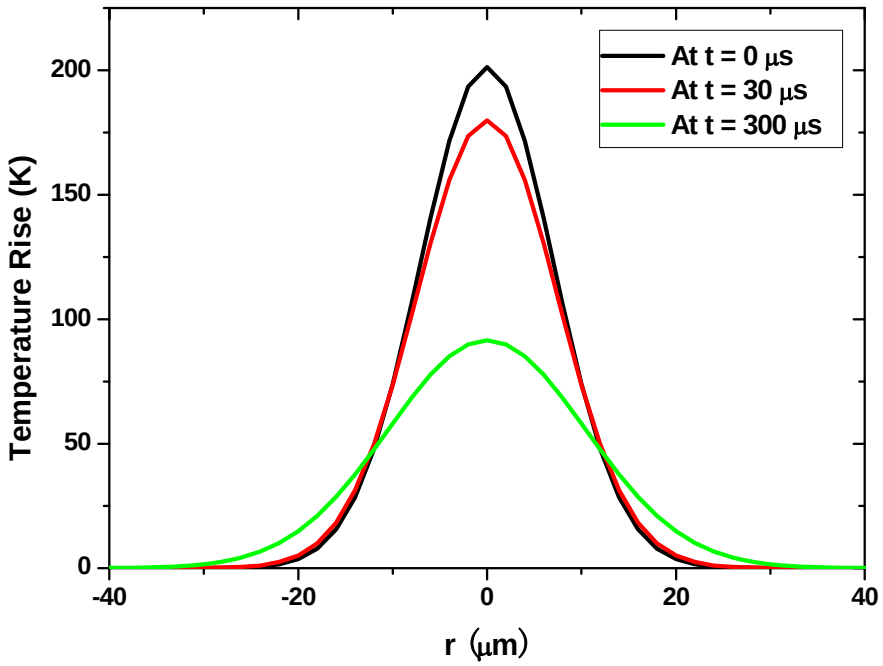

Fig. 4.10. Temperature rise calculated for a single pulse shot for 532 nm laser at a fluence of 220 J/cm^2 on PCL film with a = 10 μm.

At a low pulse rate, sufficiently high pulse energy can be generated to give a laser fluence that was large enough to produce a single shot ablation. However, a different result wouldl be obtained if the PCL film was subjected to a laser with a high pulse repetition rate (in the order of kHz). Fig. 4.11 showed the temperature rise for a single shot exposure on the film using 3rd harmonic generation Nd:YAG laser with a wavelength of 355 nm, laser fluence of 25 J/cm^2 and at a pulse repetition rate of 4 kHz. For this instance, the peak temperature rise was 46 K and this temperature rise was just above the melting point of the PCL. Hence no obvious ablation was observed. The time constant for cooling to 50% of its peak temperature rise was significantly longer at 1.2 ms due to larger spot size at a = 20 μm and thus, a longer time was required for the exposed area to be cooled down.

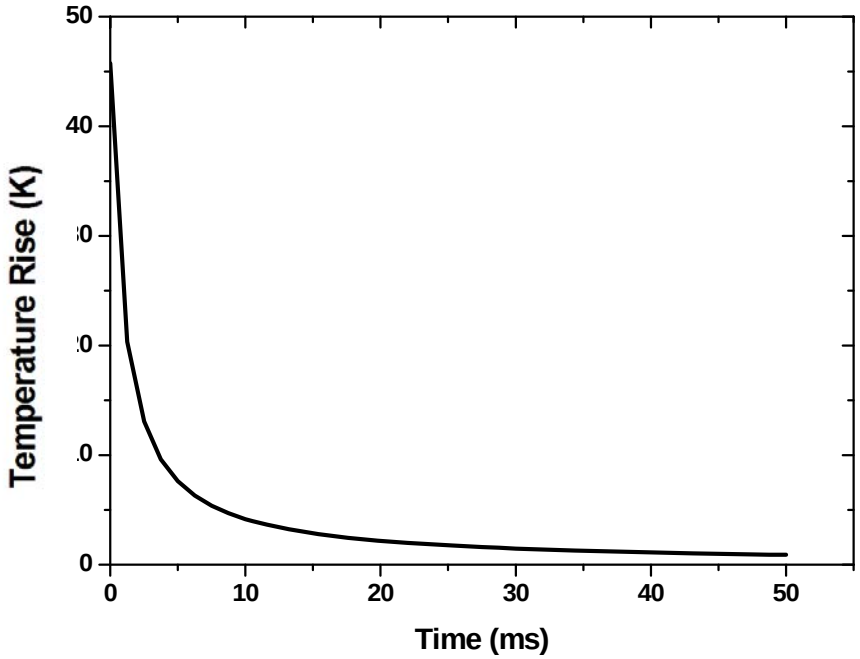

Fig. 4.11. Temperature decay as a function of time for a single pulse exposure at r = 0 for 355 nm laser at a fluence of 25 J/cm^2 on PCL film at 4 kHz and a = 20μm.

Since a single laser shot was insufficient to create micro-holes due to the slow increase in peak temperature, multiple shots would therefore be required to increase the peak temperature. Fig. 4.12 showed the temperature rise when 2000 laser pulses were irradiated on the PCL film with a calculated peak temperature rise of 1185 K within 500 ms based on cumulative heating. The temperature rise calculated in Fig. 4.12 corresponded to the micro-holes drilled as shown in Fig. 4.2, using plano-convex lens with a focal length of 50 mm and a focus spot size of 20 μm. This rise in temperature was sufficient to create a micro-hole on the PCL film. In fact the micro-holes created were large at about 85 μm in diameter. As the time duration to cool down was also significantly longer, the radial melt flow extended to a larger area, up to approximately 40 μm outwards from the micro-hole circumference.

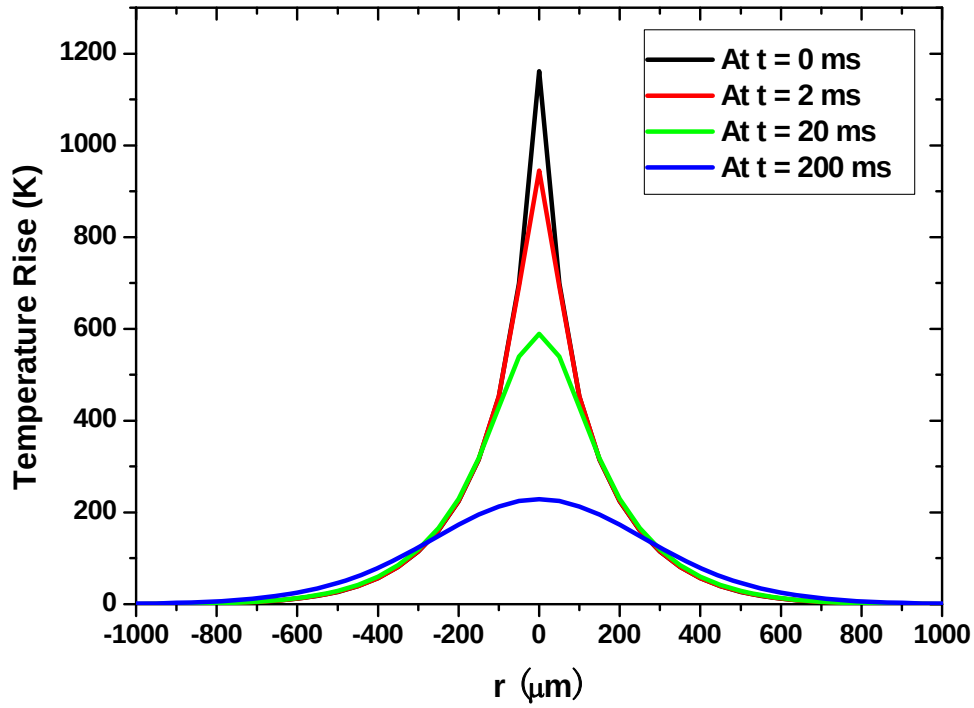

Fig. 4.12 Temperature rise calculated for 355nm laser irradiatated on PCL film using plano-convex lens with focal length of 50 mm at a fluence of 25 J/cm^2 on PCL film with a = 20 μm at 4 Khz and 2000 pulses

The use of high magnification objective lens with N.A. of 0.4 allowed the formation of smaller micro-holes due to a reduced focus spot size. Fig. 4.13 showed the temperature rise for a single laser pulse of laser spot size of a = 2 μm and 355nm wavelength. Due to a much smaller laser spot size, the time taken to cool became much faster. From the results calculated, it took approximately just 8.2 μs to cool down to 50% of its peak temperature rise. However, this initial temperature rise of 46K was not large enough to create a micro-pore during the exposure of a single laser pulse on the PCL film. In view of this, a train of pulses would therefore be required to increase the temperature rise. Due to the phenomenon of the rapid cooling, the accumulation of heat through a train of pulses at 5000 Hz could increase the temperature rise to 88 K, as shown in Fig. 4.14. This increase in temperature just exceeded the melting point of

the PCL film, and hence was able to produce micro-holes on the PCL film, shown in Fig. 4.3 showed. Due to this lower rise in temperature, the size of the micro-holes could be maintained up to 7 μm and the rapid cooling restricted the radial heat flow of the material to less than 4 μm outwards from the hole circumference.

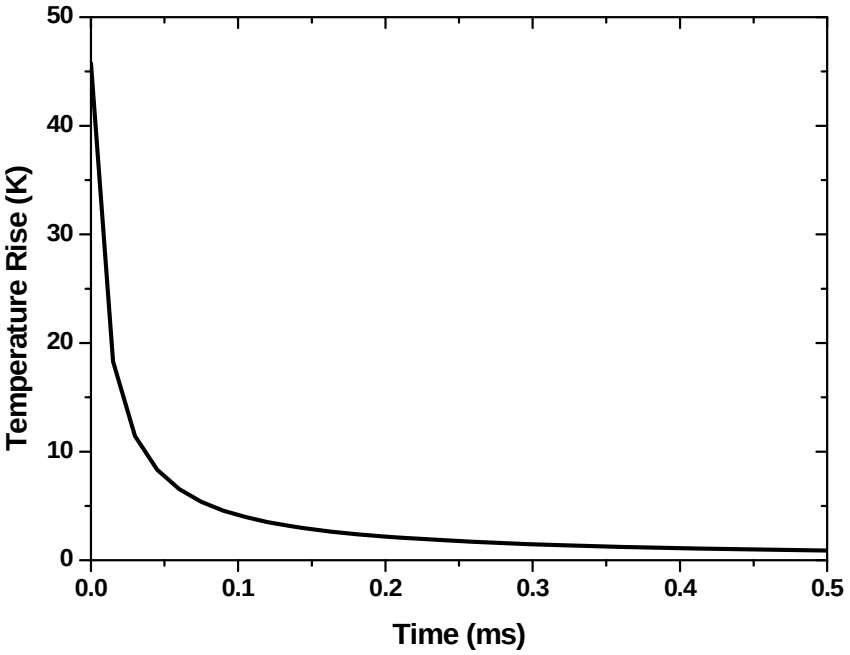

Fig. 4.13. Temperature decay as a function of time for a single pulse exposure at r = 0 for 355 nm laser at a fluence of 25 J/cm^2 on PCL film at 10 kHz and a = 2μm.

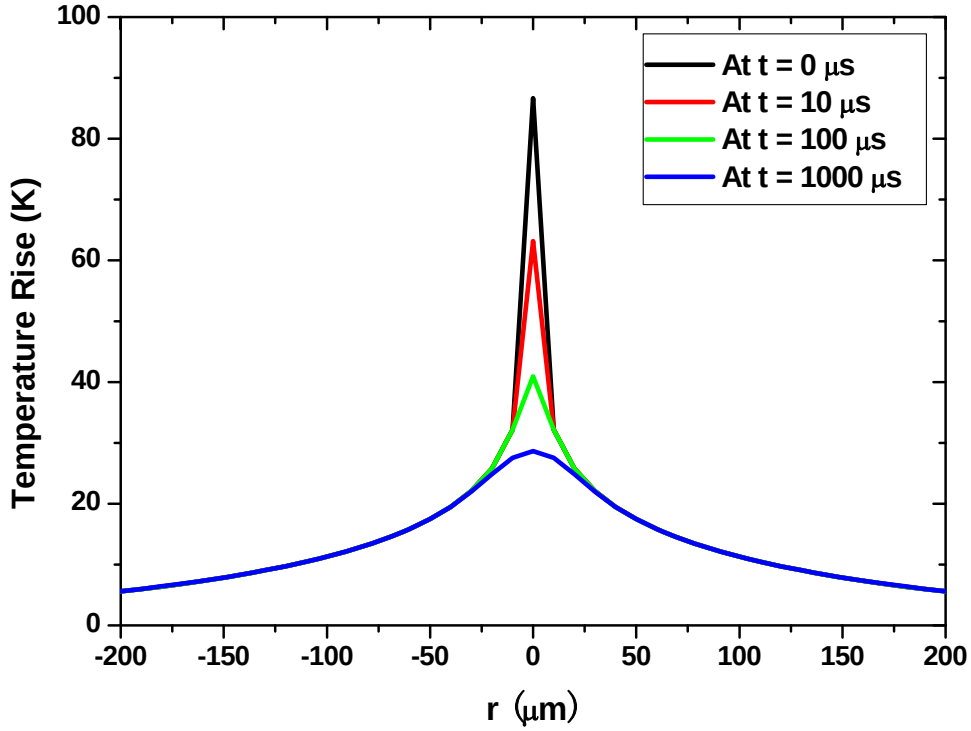

Fig. 4.14. Temperature rise calculated for 355nm laser irradiatated on PCL film using objective lens with focal length of 4 mm and N.A. 0.4 at a fluence of 25 J/cm^2 on PCL film with a = 2 μm at 10 Khz and 5000 pulses.

4.4 Summary

- Precision laser micro-processing on PCL films fabricated through spin-cast and biaxially drawn roll-mill techniques using the 3rd harmonic Nd:YAG laser delivered through different lens was able to perform precise micro-drilling and making fine micro-trenches.

- The melting of the thin polymer film was found to be insignificant for the 2 μm thick spin-cast PCL film but a slight extent of melting was observed in the thicker biaxially drawn roll-mill film. The thickness of the films plays an important role in the degree of melting due to a larger volume at higher thickness. At the same time,

laser beam delivered through different lens give different depths of focus and spot sizes and hence can affect the melting regions of the film as well.

- Mathematical simulation of the temperature-rise caused by the laser irradiation on PCL films showed that different focusing spot sizes delivered through different lens could affect the cooling rate of the material significantly. The laser which was delivered through plano-convex lens experienced a cooling time constant of 2 ms as compared to using a high N.A objective lens with a cooling time constant of 8.4 μs. Such a difference resulted in different accumulation of temperature rise, with slow cooling rate registering a high temperature rise of up to 1200 K while fast cooling rate registering only a temperature rise of 88 K. Consequently, the dimensions of the micro-holes produced and the radial heat flow around the micro-holes region would be affected.

Chapter 5:
Laser Micro-drilling of PCL Films

5.1 Introduction

In Chapter 4, mathematical simulation of the temperature-rise caused by laser irradiation on PCL films showed that different laser focusing spot sizes, number of laser pulses and wavelengths could affect the cooling rate of the material significantly. The cooling rate would in turn affect the accumulation of heat that could be sufficiently high enough to create a micropore on the PCL film. With this knowledge, the quality of the micro-pores drilled using different types of laser on the PCL film could then be expected.

Surfaces of polymeric membranes have been modified by chemical means for many years, but these methods require rigorous process control, can lead to undesirable surface changes such as severe surface roughening, excessive surface damage (cracks, and pitting, etc.), and surface contamination, and may cause environmental problems due to the chemical agents used. Laser treatments offer advantages over both chemical and other physical methods. They enable precise modification of certain surfaces that are difficult to treat with conventional chemical methods. The resulting modified surfaces are also contaminant-free and most importantly, the bulk properties of the materials remain intact. Laser treatment is therefore a relatively simple technique because it is easily controlled, environmentally clean and a safe process. The development of laser-assisted modification of polymer

surfaces is a rapidly growing and developing field that has gained considerable interest among scientists in the past decade.

The ability to modify surface of polymer films using excimer lasers has attracted much interest in this field. ArF and KrF excimer lasers were used to demonstrate that the ablation of solid PMMA and PI can improve interfacial adhesion of the materials via laser surface modification [85], while surface hydrophilicity and oleophilicity of fluororesin for coating applications can also being enhanced [84]. Laser surface modification of polypropylene (PP) film (of 40 μm thickness) has also been carried out successfully and reported to have good improvement of adhesive bond strength between the polymer and the epoxy resin adhesive [83]. In the biomedical field, modifying the surfaces of biocompatible polymers can lead to improved interactions between the polymer surface and the surface of cells. To be able to engineer the surface of biomaterials suitable for specific tissue engineering applications is therefore a challenge [96, 97].

The design and fabrication of thin membrane-like matrices are currently investigated by a number of research groups in the field of biomedical sciences. In one such effort by Hollander et al., hyaluronan-based 20 μm thick membranes with laser-drilled micro-perforations were used for cultivation of autologous keratinocytes and other cell types [98]. Laserskin^{TM} is a thin transparent membrane made of hyaluronan derivative (HYAFF) which is presented with two orderly arrays of laser-drilled micro-pores – one with a diameter of 40 μm and the other with macro-pores of diameter 500 μm. In an *in vitro* study of the development of a bi-layered skin substitute, Zacchi et al., reported that macro-pores of Laserskin membrane, allowed the keratinocytes to

migrate to the lower side at the interface between the natural polymer matrix and the plastic surface of the culture plate [99]. However, the relatively weak mechanical properties of hyaluronan base materials render them difficult to handle. To overcome this problem, Ng et al. have successfully developed biaxially stretched PCL membrane as a mechanical sound ultrathin template for membrane tissue engineering [26]. Khor et al. made use of this PCL membrane to conduct a cell culture study of human keratinocytes and has proved PCL membrane to be a suitable matrix material for tissue engineering an epidermal equivalent [67].

In order to make the surface more conducive for this purpose, Schantz et al. treated the PCL membrane with sodium hydroxide. In-vitro study using osteoblast-like cells on the sodium hydroxide treated membrane showed enhanced cell attachment and proliferation as compared to the non-treated membrane, thus demonstrating the improvement in surface hydrophilicity of the membrane after the chemical treatment [37]. As there is a tendency for the bulk material to deteriorate after the chemical treatment of membrane surface, physical methods may deem more desirable. Htay et al. developed perforated PCL membranes using needle-operated robot to improve the hydrophilicity of the membrane surface [43]. However, the flaps produced at the sites of needle punching tend to close when placed in cultured solution. Therefore in order to address this issue, laser processing is being attempted and is reported in this chapter.

5.2 Experimental Procedures

5.2.1 Femtosecond and Excimer Laser Systems

The PCL membranes fabricated as mentioned in Chapter 3 were processed by Spectra-Physics Millenia-Pumped Tsunami femtosecond laser and the Lambda Physik LPX 100 KrF excimer laser in standard room conditions. The femtosecond laser uses Ti:Sapphire doped crystal as the medium at a wavelength of 800 nm and pulse duration of 110 fs. The femtosecond laser beam was delivered through a Mitutoyo M Plan APO NIR objective lens with a numerical aperture of 0.26 and focal length of 20.0 mm.

The KrF excimer laser has a wavelength of 248 nm and a pulse duration of 23 ns. As this laser produces a large beam size of approximately 10 mm by 20 mm, a pre-fabricated mask with an array of holes of 50 μm in diameter was placed on top of the PCL film.

5.3 PCL Film Surface Characterization and Analysis

5.3.1 Optical Microscopy

The surface morphology of the laser processed PCL membranes were observed by an optical microscope as mentioned in Chapter 3.

5.3.2 Scanning electron microscopy (SEM)

Scanning electron microscopy (SEM) was performed on gold-sputtered laser-processed membranes using a JEOL JSM-5800 LV scanning electron microscope. Gold sputtering of the membrane samples was conducted in a vacuum chamber at a pressure of 8 MPa and a current of 10 mA for a period of 40 s.

5.3.3 Wettability

The wetting behaviour of the membranes was evaluated by determining the water contact angle formed between the water drop and the surface of the laser-perforated membrane using the VCA-optima Surface Analysis System. 10 picolitre of water was dispensed through a fine nozzle and the water droplet was directed on the laser-processed film. The water angle made with the non-laser perforated membrane was taken as the reference.

5.4 Results and Discussion

5.4.1 Surface Modification Using Femtosecond lasers

The main advantage of using ultra-short laser pulses is that there is little or no collateral damage due to shock wave and heat conduction produced in the materials being processed. In the laser ablation of polymers, heat diffusion into the polymer material is negligible and the energy loss into the sample is minimized [50]. Therefore,

high precision patterning of the sample without thermal damage of the surroundings is possible.

In laser ablation, energy has to be delivered in excess of the binding energy of the atom so as to remove the atom from the solid [100]. Thus, to ablate the same amount of materials in a short pulse, a higher laser intensity (or fluence) has to be applied, and this fluence is approximately inversely proportional to the pulse duration. At pulses in the range of femtoseconds, the fluence is able to ionize almost any target materials. Following the ionization, the laser energy is absorbed by the free electrons. These energetic electrons break free from the bulk materials and create a strong electric field due to charge separation with the parent ions. The magnitude of this electric field pulls the ions out of the solid target when the electron energy is larger than the binding energy of the ions, thus resulting in material removal.

5.4.1.1 Effect of Pulse Energy on Laser Drilling using Femtosecond Laser

The dimensions of the holes perforated were observed to be directly affected by laser pulse energy and pulse repetition rate. The microscopy images in Fig. 5.1 showed that the dimension of the holes drilled at N = 2 decreases from approximately (a) 80 μm at a pulse energy of 500 μJ to (f) 25 μm at a pulse energy of 100 μJ.

The energy intensity of the femtosecond laser takes the form of the Gaussian distribution. The intensity distribution I(r) of the pulse energy is related to Eq. 5.1 [101]**:**

$$I(r) = I_o e^{-\frac{2r^2}{w_o^2}}, \qquad \text{(Eq. 5.1)}$$

where I_o is the peak intensity, r the beam radius and w_o the beam radius at which the intensity has decreased to $\frac{1}{e^2}$ of the peak value. w_o is also known as the Gaussian beam radius.

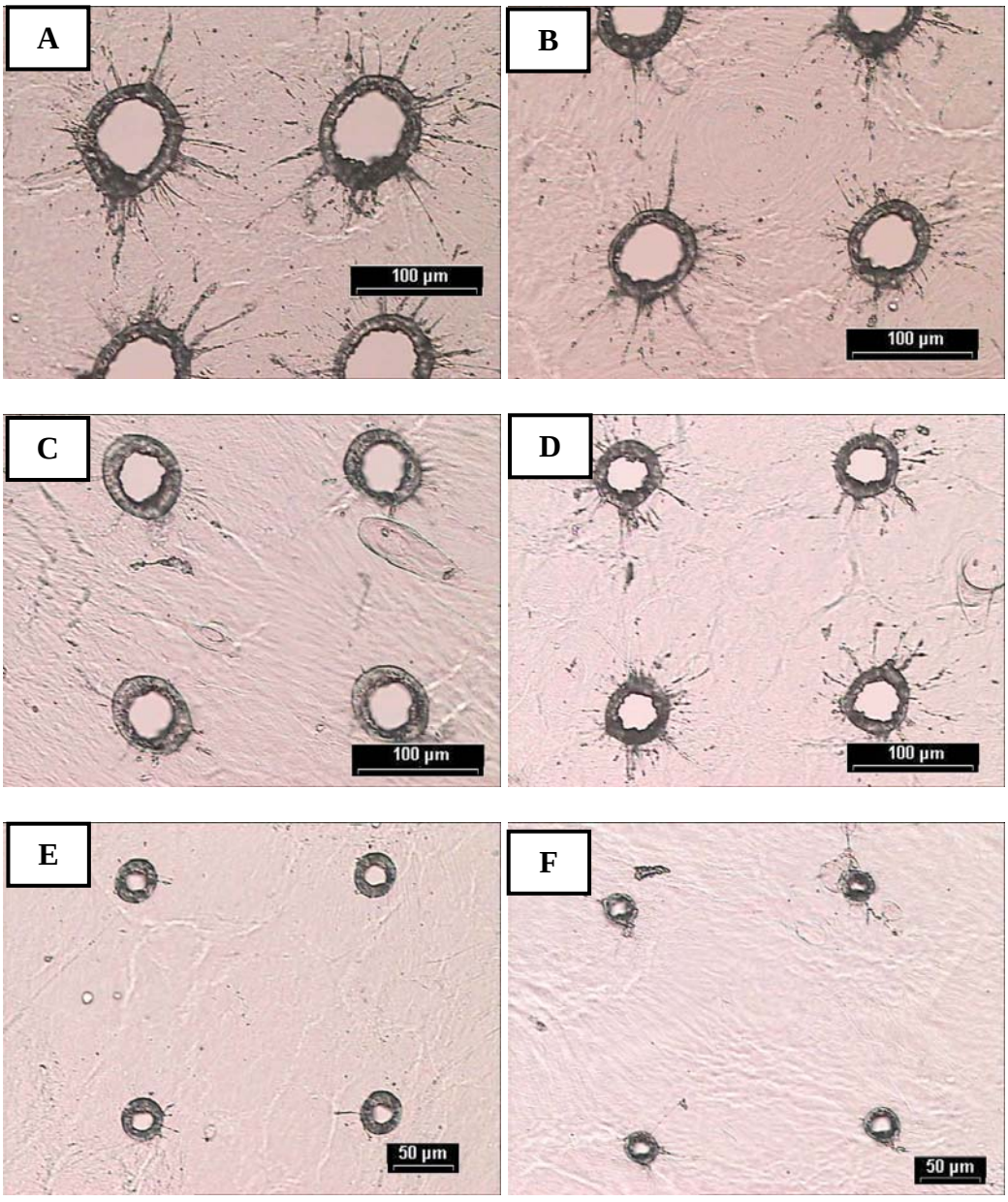

Fig. 5.1. Microscopy images of laser perforation on PCL membrane with different pulse energies at a pulse number of N = 2. {(A) E_{pulse} = 500 µJ, (B) E_{pulse} = 400 µJ, (C) E_{pulse} = 300 µJ, (D) E_{pulse} = 200 µJ, (E) E_{pulse} = 150 µJ and (F) E_{pulse} = 100 µJ}

5.4.1.2 Effect of Pulse Number on Laser Drilling using Femtosecond Laser

To study the effect of pulse number N on laser drilling, the PCL membrane was perforated at a pulse energy of 600 μJ from N = 200 to N = 5. The microscopy images in Fig. 5.2 (A) – (D) showed the result of laser perforation with increasing values of N and the SEM images in Fig. 5.3 (A) – (C) showed clearer pictures of the result of the perforation.

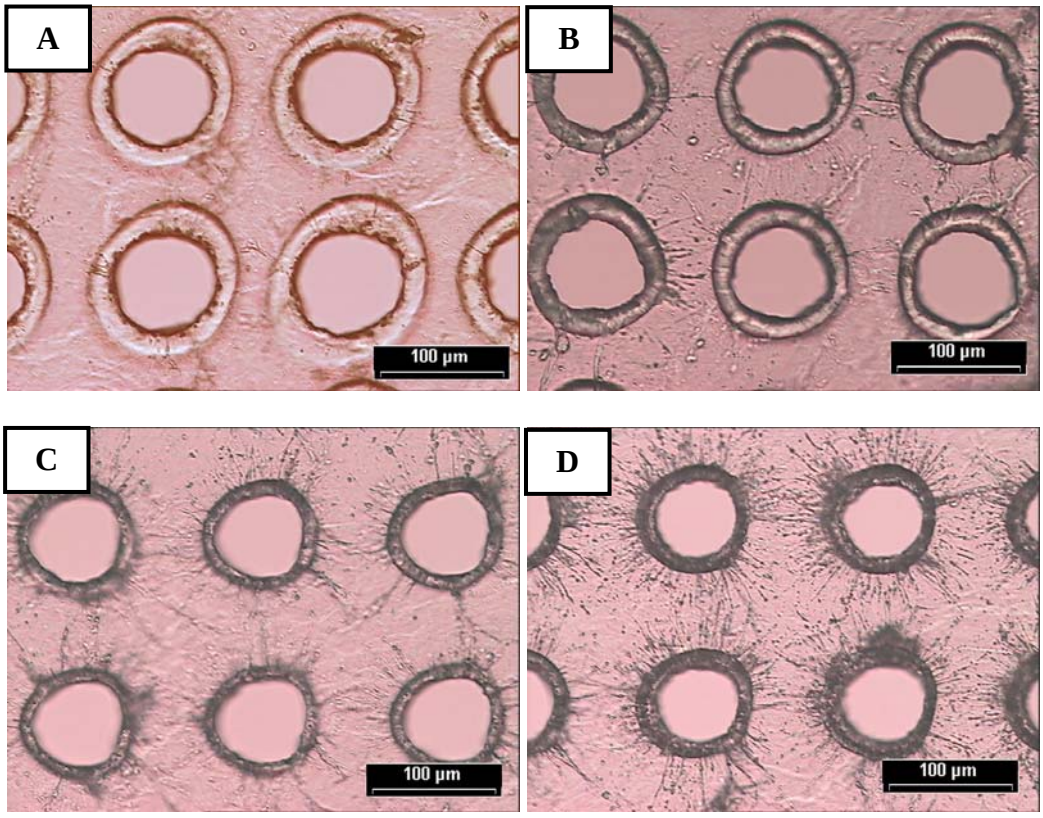

Fig. 5.2 Microscopy images of laser perforation on PCL membrane with different pulse numbers at a pulse energy of E_{Pulse} = 600 μJ.

{(A) N = 200, (B) N = 100, (C) N = 20 and (D) N = 5.}

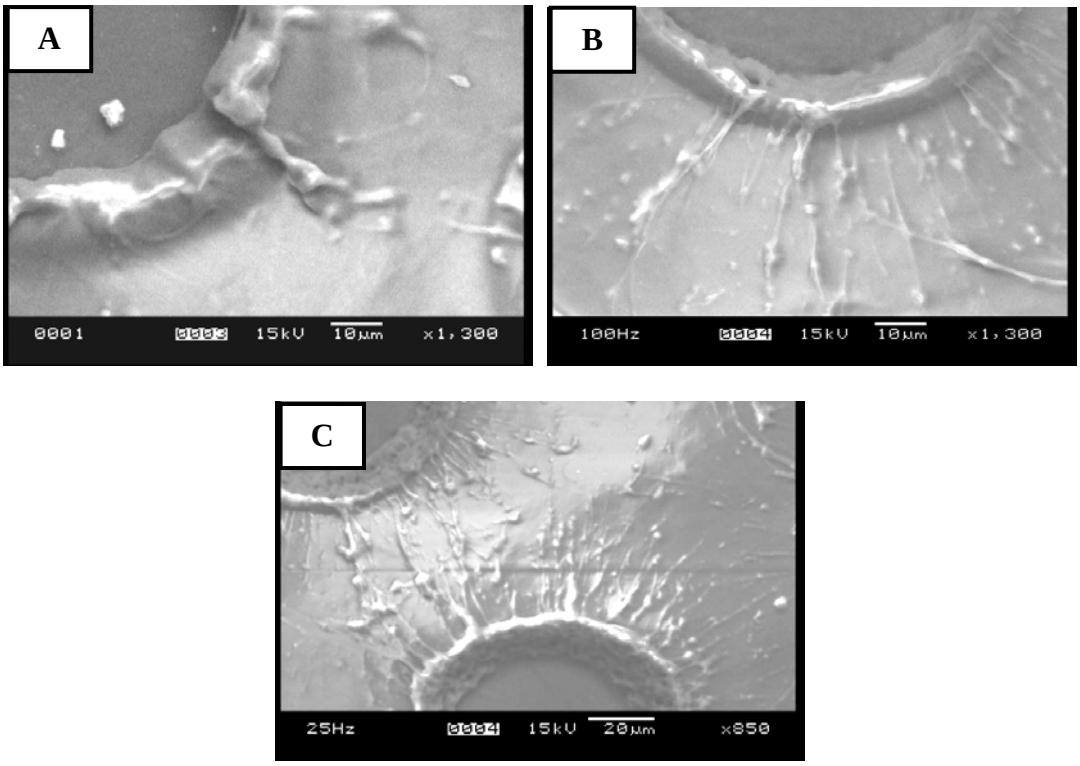

Fig. 5.3. SEM images of laser perforation on PCL membrane with different pulse numbers at a pulse energy of E_{Pulse} = 600 µJ.

{(A) N = 100, (B) N = 20 and (C) N = 5.}

The laser pulses that impinged on the PCL material surface resulted in concurrent disintegrations and formation of gaseous products such as CO_2 which led to a localized bursting of the surface and ejection of melt. It could be seen that at N = 20 and N = 5 (from Fig. 5.2 and Fig. 5.3), there was ejection of melt at the circumferential area of the holes, and that the melt ejection was more prominent in membrane being irradiated with fewer pulses. At pulses above N = 100 as in Fig. 5.2 (A) and (B), there was almost no melt ejection being observed. This could be due to the fact that at higher pulses, the concurrent disintegration of PCL took place at a much faster rate and before the melt could land on the membrane surface, it would have already been disintegrated

by the high number of pulses. Hence this explained why there was less melt ejection at higher values of N.

Laser ablation on other optically transparent polymers using ultra-short pulse lasers in air have also been reported, and the organic polymers involved during testing included engineering thermoplastic polyetheretherketone (PEEK) membranes of 550 μm thick, polytetrafluoroethylene (PTFE) membranes of 100 μm thick which was used in microelectronic and biomedical applications, and polycarbonate (PC) membrane of 100 μm thick that was used in advanced artificial organs [50]. The extent of ablation on the surfaces of these polymers was found to be directly dependent on the wavelength and pulse duration of the laser. The threshold fluence was very low for the lasers in visible and infra-red regions while the ablation rate was higher for pulse duration of pico- or femtosecond lasers.

5.4.2 Surface Modification using KrF Excimer Laser

Preliminary results from the irradiation of PCL films with KrF excimer laser showed excellent surface-patterning micro-features. The surface patterning design was a replication of the array of holes on the pre-fabricated stainless steel mask. The dimensions of the circular structures were approximately 50 μm diameter.

Morphological observation of the PCL thin film in Fig. 5.4 suggested possibly the effects of thermal compressive stresses imparted to the laser-irradiated regions of the PCL film during the experiment. It caused the surrounding PCL film surface to

experience tensile stress on the PCL film. These regions eventually cracked as a result of thermal stress relaxation and the stress exerted on the circular structures.

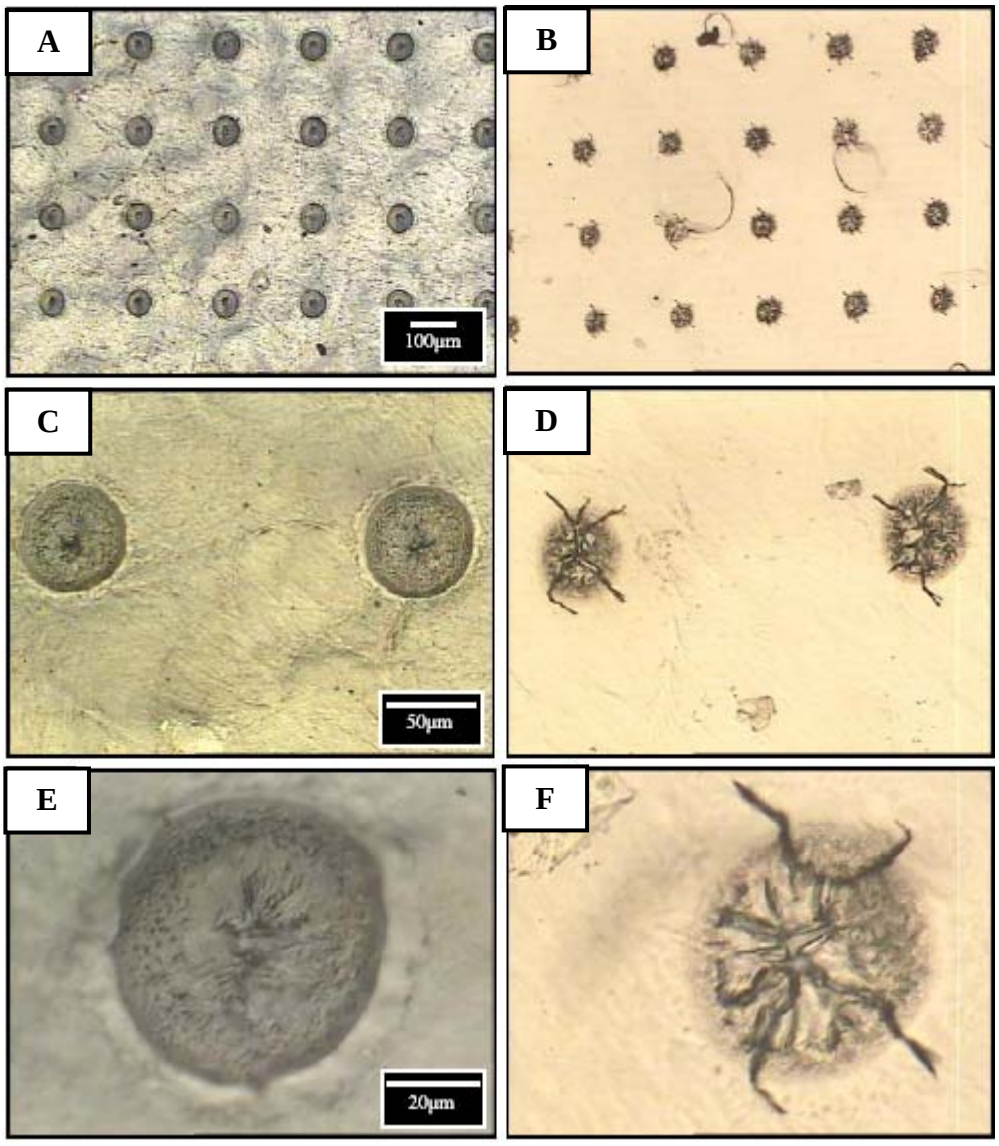

Fig. 5.4. (A-C): Microscopy images of laser surface-patterned PCL thin film with 248 nm KrF excimer laser at 210 mJ energy, 2 Hz repetition rate, and 300 s irradiation time. (D-F): Micrographs of the same laser surface-patterned PCL thin film observed with backlight illumination.

Further analysis of these star-like radiating structures were made with SEM, as shown in Fig. 5.5. The SEM images later confirmed the observations of the phase contrast microscope of the surface morphology. The surface morphology had irregularly varying depths and varying patterns throughout the array of circular structures that were laser-patterned onto the PCL film.

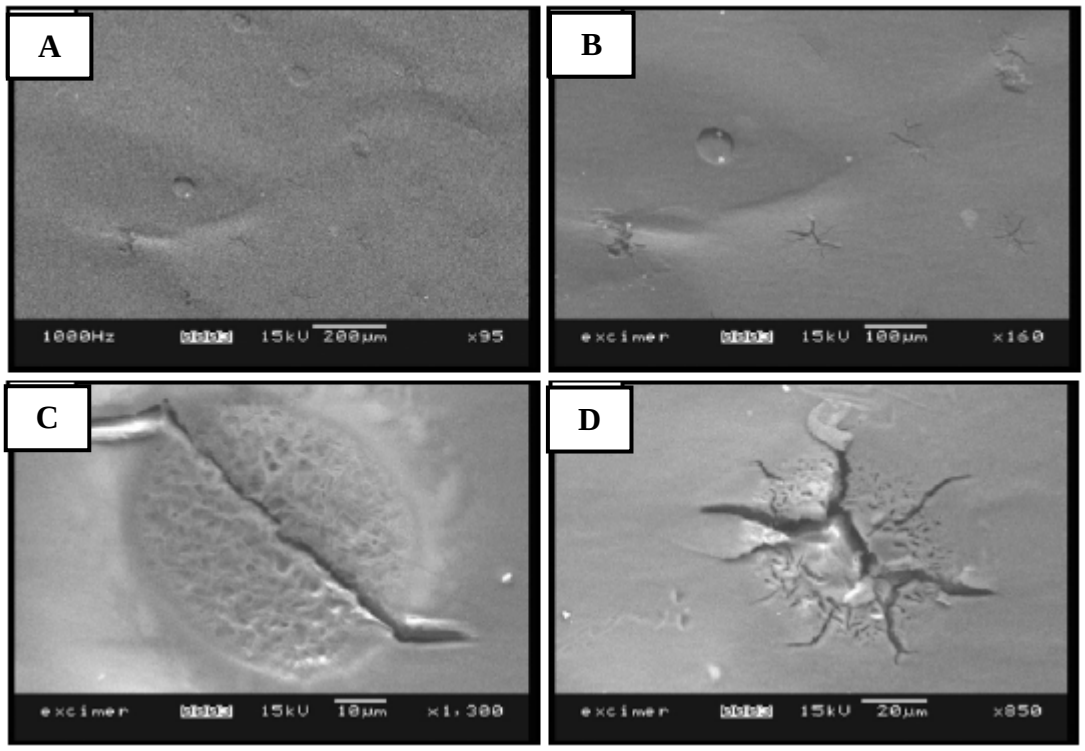

Fig. 5.5. SEM images of the laser-patterned PCL thin film showing irregularly varying depths and patterns throughout the array of circular structures.

5.4.3 Surface Wettability of Laser-Processed Membranes

The wettability of the surface of the laser perforated PCL membrane can be determined by the measurement of the water contact angle. Hydrophilic and hydrophobic surfaces are indicated by high or low surface energies, respectively. For a

hydrophobic surface, the water contact angle is large as the water tends to minimize its area of contact with the material. Fig. 5.6 shows the three interfacial lines of tension when a water droplet is in contact with a solid substrate surface. The three interfacial lines of tension are:

- γ_{lv} , the liquid-vapour interfacial tension,
- γ_{sv} , the solid-vapour interfacial tension and
- γ_{sl} , the solid-liquid interfacial tension .

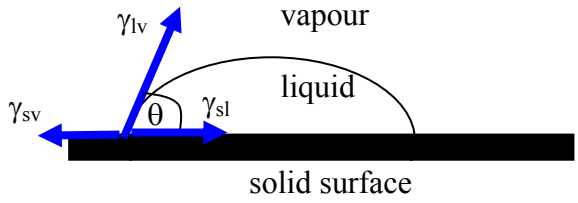

Fig. 5.6: Illustration of contact angle on surface of solid substrate [68].

Laser micro-perforation and processing of the PCL membrane caused the surface to be filled with asperities due to melt ejection or particles accumulation. These defects can influence the water droplet and particle interaction forces by modifying the van der Waals interaction [102]. These surface asperities can stimulate rupture of the thin liquid membrane between a particle and a bubble. The movement of the three phase contact line over a rough surface can also rupture the thin liquid membrane.

5.4.3.1 Wettability of Femtosecond Laser Perforation Membranes

The water contact angle measurement was carried out to determine the wettability of the PCL membranes after the laser perforation. The results of the water contact angle at 200 pulses and varying values of E_{Pulse} were shown in Fig. 5.7. Fig.

5.8 showed the relationship between water contact angle and the hole dimension with respect to E_{Pulse} from Fig. 5.7.

The contact angle (at time = 0 s) for non-perforated PCL membrane was found to be in the range of 74 ~ 78^{o}. In Fig. 5.7 and Fig. 5.8, when the membrane was irradiated at pulse energies between 100 and 300 μJ at N = 200, the water contact angle dropped to its lowest value of 58 ~ 60^{o}. This corresponded to an external hole diameter between 40 and 60 μm. The contact angle began to increase at pulse energies beyond 300 μJ at which the external hole diameter increased beyond 60 μm. At 400 μJ – 500 μJ, there was no significant change in the water contact angle as compared to the non-perforated membrane.

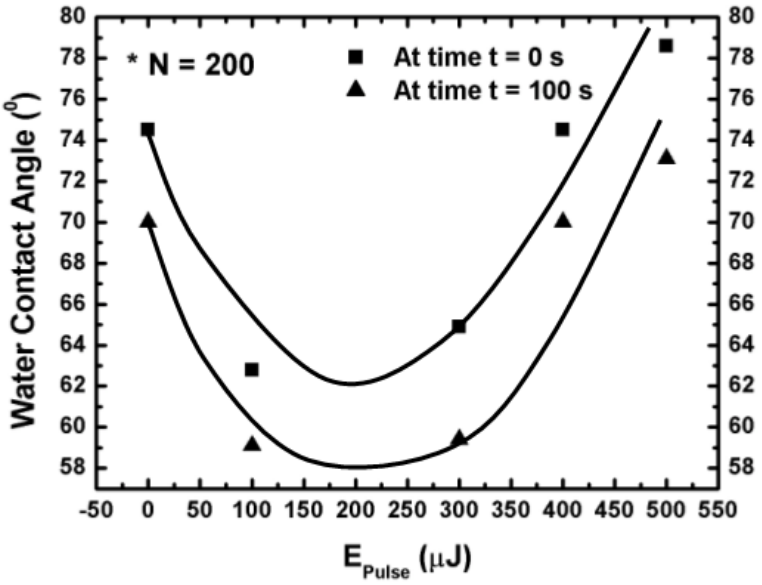

Fig. 5.7. Graph of changes in water contact angle of membrane at N = 200 with E_{Pulse} at time t = 0 s and t=100 s.

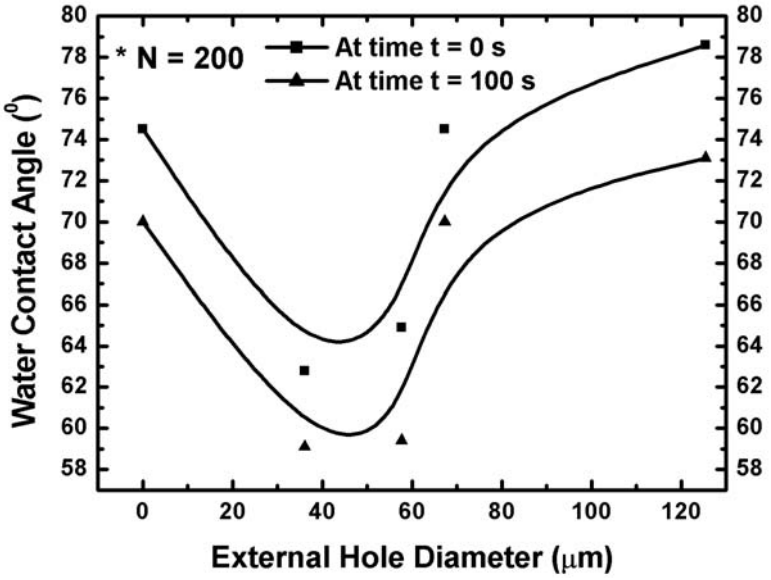

Fig. 5.8. Graph of changes in water contact angle of membrane at N = 200 with respect to external hole diameter at time t = 0 s and t = 100 s.

When the PCL membrane was irradiated at a constant pulse energy of 500 μJ at varying pulse N, the water contact angle was reduced by an average of 10 ~ 20^{o} with pulses in the range of N = 1 to 20, as illustrated in Fig. 5.9. At high pulses, the water contact angle remained relatively the same as the non-perforated membrane. From the results, it could be deduced that the PCL membranes with holes perforated at lower pulse numbers have higher surface energies. This could be explained that at lower pulses, the degree of surface roughness was higher because there were more surface asperities due to greater "splattering" effect. These asperities could have ruptured the liquid membrane that held the liquid together. This could be the reason for its increase in hydrophilicity.

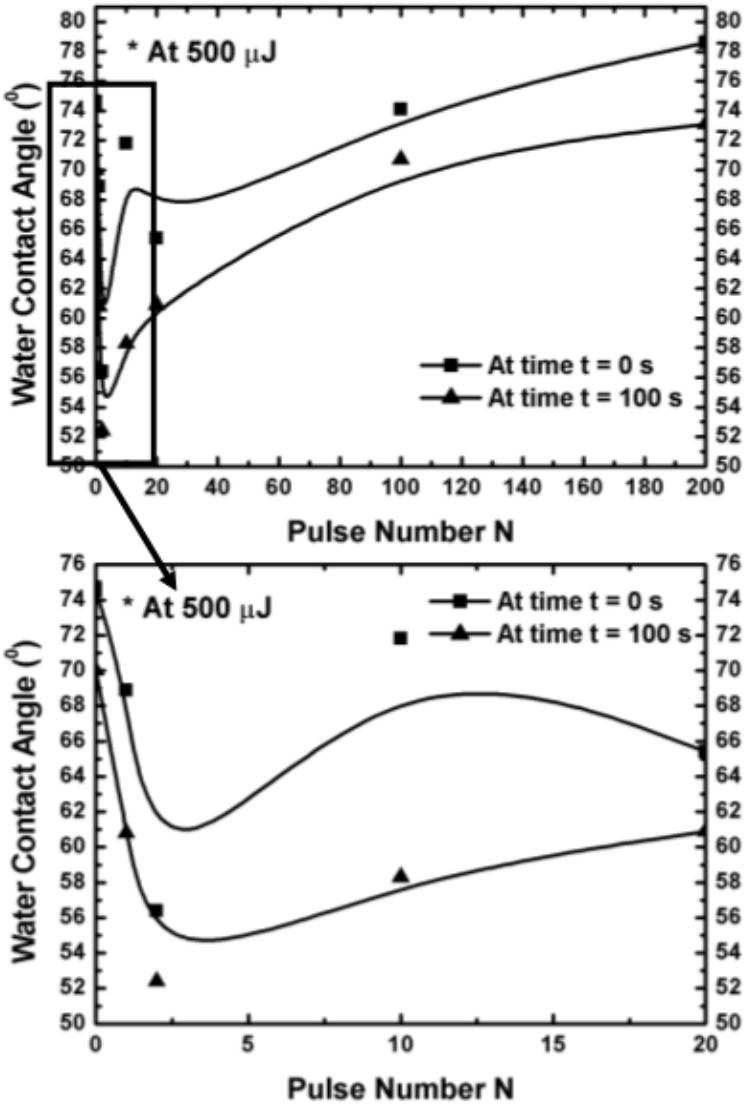

Fig. 5.9. Graph of changes in water contact angle of the membrane at E_{Pulse} = 500 μJ with N at time t = 0 s and t = 100 s [68].

5.4.3.2 Wettability of KrF Excimer Laser Surface Modified Membrane

Water contact angle measurement was conducted for two varying parameters. In the first two experiments, the 248 nm KrF excimer laser energy was kept constant at 78 mJ and 171 mJ, respectively, while the laser irradiation time was increased from 8 to 12 minutes, in incremental value of 2 minutes. This was done to observe how the water contact angle for the PCL thin film would change as a function of time, at lower

energies (78 mJ) and at higher energies (171 mJ). Fig. 5.10 showed the change in contact angle as the laser pulse number increases from 4800 to 7200 at a pulse energy of 78 mJ. The contact angle was observed to drop at a faster rate at higher pulse numbers of 6000 and 7200 (corresponding to longer laser irradiation times: t = 10 minutes and t = 12 minutes), compared to the contact angle at lower pulse number 4800 (t = 8 minutes). In both cases, the contact angle values dropped from 64^{o} to 50^{o}, and from 67^{o} to 50^{o}, respectively. A difference of 14^{o} and 17^{o} respectively, indicated a significant change in water contact angle. At 4800 pulse number, the contact angle reduction was approximately only 7.5^{o} (half that of the other two contact angle difference), from 67.5^{o} to 60^{o}.

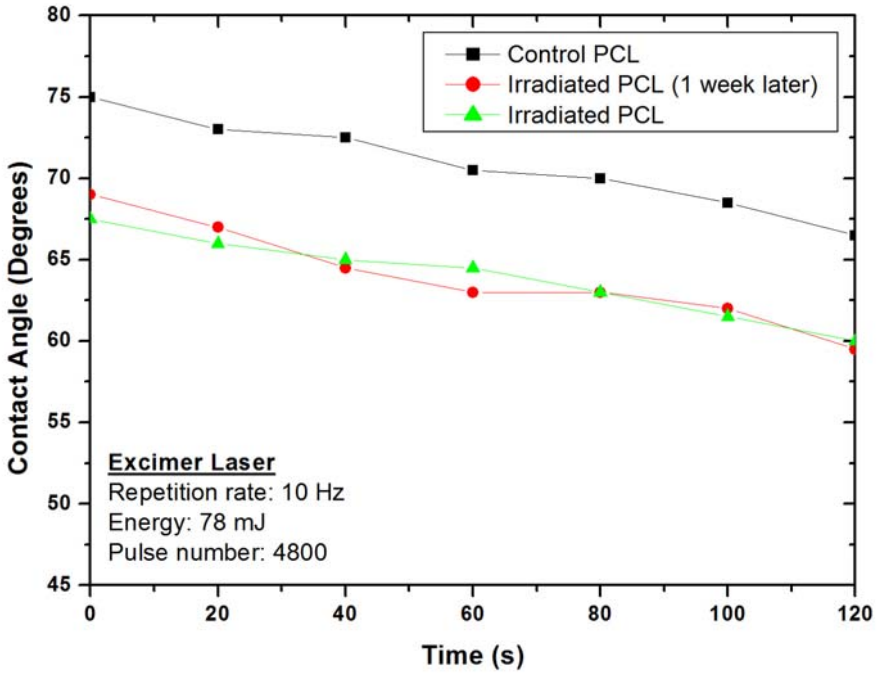

Fig. 5.10a. Graphs of water contact angle plotted for a 2 minute test duration for biaxially-stretched ultra-thin PCL film irradiated with 248 nm KrF excimer laser at a repetition rate of 10 Hz, 78 mJ energy and pulse number of 4800.

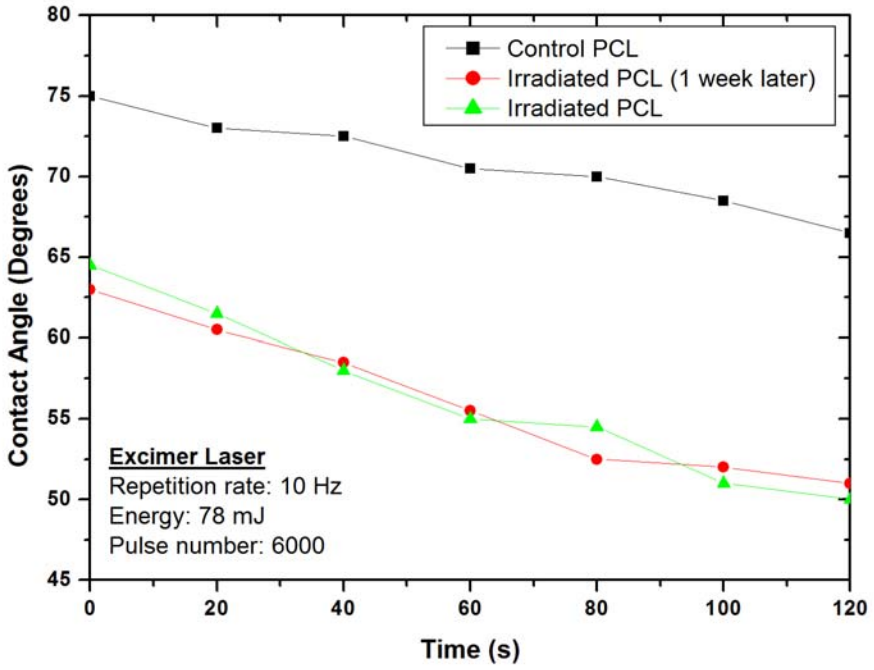

Fig. 5.10b. Graphs of water contact angle plotted for a 2 minute test duration for biaxially-stretched ultra-thin PCL film irradiated with 248 nm KrF excimer laser at a repetition rate of 10 Hz, 78 mJ energy and pulse number of 6000.

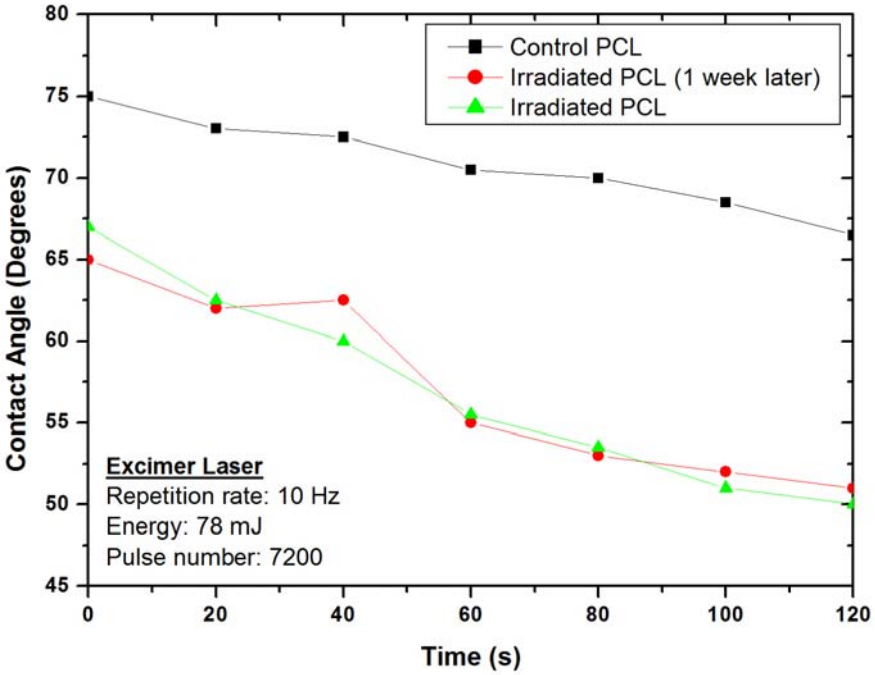

Fig. 5.10c. Graphs of water contact angle plotted for a 2 minute test duration for biaxially-stretched ultra-thin PCL film irradiated with 248 nm KrF excimer laser at a repetition rate of 10 Hz, 78 mJ energy and pulse number of 7200.

These results suggested that increasing the pulse number (corresponding to prolonged laser irradiation time) at low laser energy of 78 mJ increased the surface hydrophilicity of the PCL. The water droplet on the laser-patterned PCL thin film exhibited greater static advancing of its contact angle within the 2 minute test duration. Comparing these values to the contact angle values for non-lasered PCL, KrF excimer laser-patterning had indeed improved the PCL surface hydrophilicity significantly.

The improvement in surface hydrophilicity after the laser irradiation was an expected phenomenon. The intense energy from the excimer laser beam focused on the PCL thin film, would have provided energy sufficient to overcome the bond strength of the PCL chemical structure at these irradiated regions. As the laser patterning was conducted in ambient conditions, oxidation reaction could have developed at these regions via photo-decomposition, photo-substitution or photo-lytic mechanisms. This change in the chemical structure of the PCL would also affect its wettability property.

Fig. 5.11 showed the change in contact angle as the pulse number was increased from 4800 to 7200 at a pulse energy of 171 mJ. The contact angle was observed to have reduced at approximately the same rate for all pulse number of 4800, 6000 and 7200. For pulse number of 4800 and 6000, both the contact angles were reduced to approximately 55^{o}, from 72^{o} and 67^{o} initial contact angles respectively. A difference of 17^{o} and 12^{o} respectively, indicated a significant change in water contact angles. At a pulse number of 7200, the contact angle reduction was approximately 19^{o}, from 67^{o} to 48^{o}.

Comparing the experiments of using pulse energies of 78 mJ and 171 mJ, results from the use of higher laser energy suggested an improvement of surface hydrophilicity of the PCL.

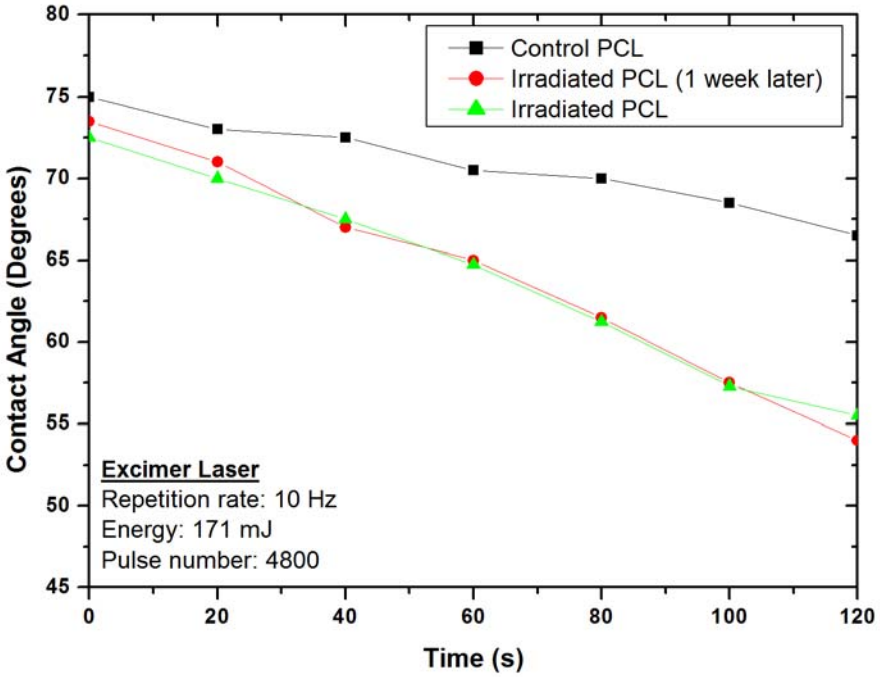

Fig. 5.11a. Graphs of water contact angle plotted for a 2-minute test duration for biaxially-stretched ultra-thin PCL film irradiated with 248 nm KrF excimer laser at a repetition rate of 10 Hz, 171 mJ energy and pulse number of 4800.

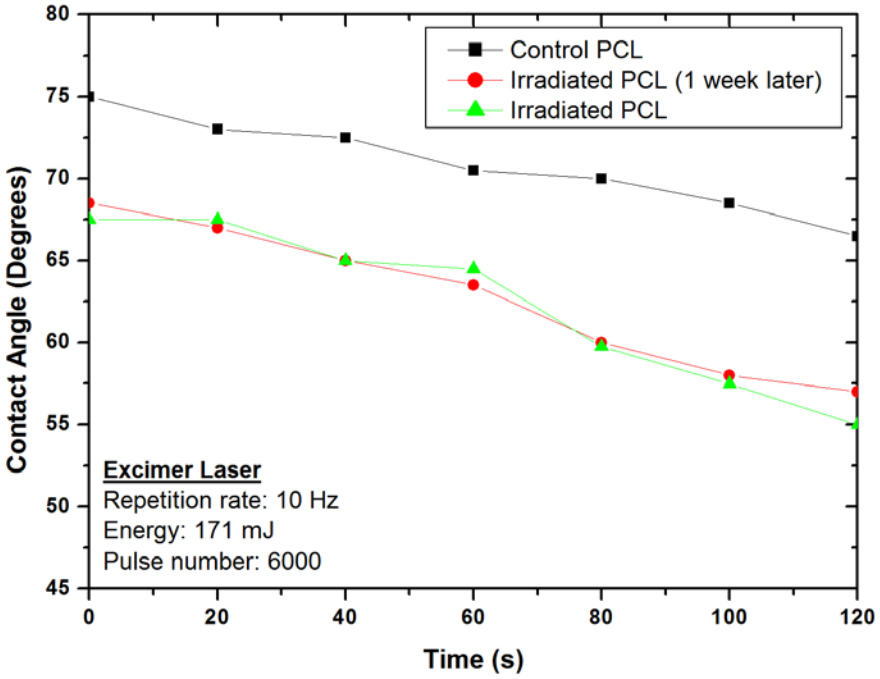

Fig. 5.11b. Graphs of water contact angle plotted for a 2-minute test duration for biaxially-stretched ultra-thin PCL film irradiated with 248 nm KrF excimer laser at a repetition rate of 10 Hz, 171 mJ energy and pulse number 6000.

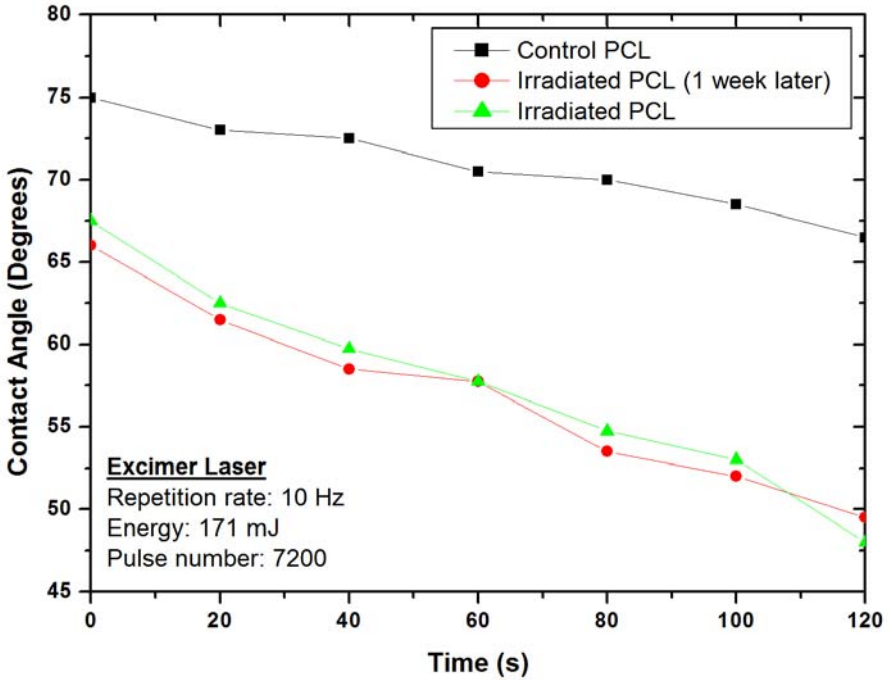

Fig. 5.11c. Graphs of water contact angle plotted for a 2-minute test duration for biaxially-stretched ultra-thin PCL film irradiated with 248 nm KrF excimer laser at a repetition rate of 10 Hz, 171 mJ energy and pulse number of 7200.

5.5 Summary

- Femtosecond and excimer lasers were used to modify the surface of PCL membranes and the results showed satisfactory results in terms of enhancing the wettability of the hydrophobic nature of the PCL membranes.

- In the micro-perforation of PCL membrane using femtosecond laser, the pulse energy E_{Pulse} of the femtosecond laser directly affect the size of the holes. A higher E_{Pulse} generally led to a larger hole being drilled and this result corresponded to the Gaussian distribution. The pulse number N could also affect the quality of the holes produced as low pulses irradiation generated greater ejections of melt on the circumferential areas of the holes, which subsequently led to higher degree of surface roughness.

- In the experiment laser micro-perforation on PCL film using femtosecond laser, the contact angle was found to be directly dependent on pulse energy and repetition rates. Water contact angle was at its minimal at pulse energies from 100 ~ 300 μJ when the external hole diameters were in the range of 40 ~ 50 μm, and at values between 2 ~ 5 pulses in which the surface roughness was at its maximum. At high values of pulse energy and repetition rates, there was no significant change in the contact angle as compared to non laser-perforated membrane. A correlation could thus be drawn that the perforated membranes produced by femtosecond laser were most hydrophilic when the membranes were irradiated using parameters of low pulse energy and pulse repetition rate.

- Irradiation of the PCL films using KrF excimer laser with the aid of a mask with an array of drilled micro-holes showed excellent surface modification results. The water contact angle measurement of the laser-patterned region showed a significant change (reduction) in water contact angle.

Chapter 6:

Laser Degradation Study of PCL

6.1 Introduction:

In Chapter 5, femtosecond and excimer lasers were used to modify the surface of PCL membranes and the results showed satisfactory results in terms of enhancing the wettability of the hydrophobic nature of the PCL membranes. Different number of pulses by femtosecond laser was used to create micro-pores on the PCL film. The results showed that low number of laser pulses created more surface roughness and hence, better wettability. This could be due to the deposition of the materials being ejected out of the surface during ablation. In using KrF excimer laser to micro-patterned the PCL surface, better wettability results were also showed. This could be due to chemical changes induced during the ablation process. More study on the degradation and chemical changes caused by lasers will be presented in this chapter.

The development of biodegradable polymers is increasing in importance in the field of biomedical science, especially in tissue engineering and controlled drug delivery [103, 104]. The surface properties of a biomaterial are of paramount importance as they control the interactions between the material and the biological environment exposed to. Hence, biomaterials must show excellent biocompatibility, biodegradability and cell adhesion properties. However, the success of tissue engineering has been very much limited to avascular or thin tissues, such as skin and cartilage due to the ability to sustain cell viability where oxygen and nutrients can be easily diffuse into the biomaterial implant [105-107]. As the tissue grows and becomes

thicker over the biomaterial implant, cells and tissues located more than a few hundred microns away from the nearest blood capillaries suffer from hypoxia, a condition of deficiency in oxygen, after which it may then eventually trigger apoptosis and necrosis of tissue [108]. Thus, the development of complex tissues or organs through tissue engineering biomaterial construct still remains a huge challenge. The ability to induce controlled vascularization of engineered tissues is an important consideration, such that a biomaterial implant can not only allow the growth and proliferation of cells and tissue around it, it must also be able to sustain and retain its functionality.

In addition, the biomaterial must encompass mechanical properties, such as durability, stress resistance, flexibility and good elasticity. Synthetic polymers, such as polycarbonate, poly(ε-caprolactone), polyethylene and polyethylene terephthalate, are preferred over natural materials due to their availability, low cost and the ability to be shaped easily [16, 41]. However, such polymers tend to have low surface energy and hence exhibit hydrophobic property. Thus, selective surface modification to enhance the hydrophilicity has to be carried out on such materials to enhance cell adhesion and proliferation.

The use of lasers in the surface modification of polymers offers many advantages over chemical and physical methods. Laser processing allows precise modification of the surface and keeps the bulk properties of the materials intact while ensuring that the resulting modified surfaces are free from contaminants [68]. The maintenance of the bulk properties of the polymer is essential in preserving the biological and structural properties of the biomaterials which allow it to repair, maintain or enhance the bodily structure and function [20].

Studies have also been conducted to improve the surface wettability of polymer films. Our research found that using different laser parameters to generate different surface morphologies and sizes of perforation on PCL films were able to reduce the water contact angle, hence improving the wettability of the film [68]. Revez et. al. reported that the photochemical treatment of PTFE using excimer lasers caused the surface to become hydrophilic as well [109]. Others have also reported on the effect of irradiation wavelength and atmospheric gases on the polymers. Lippert et. al. studied the effect of irradiation wavelength of triazenopolymer and discovered that chemical modification and micro-structural change are dependent on both wavelength and threshold fluence of the polymer [110]. Bityurin et. al. demonstrated that both modification and etching kinetics of PMMA were strongly influenced by ambient atmosphere [111].

Besides enhancing the surface properties of the polymer to cater for specific requirements, the choice of the materials used for tissue engineering applications is also very critical. As mentioned earlier, the chosen materials must be mechanically sound to bear the type of load that is to be applied on and at the same time exhibits biocompatibility properties [67]. PCL has been made into ultra-thin membranes suitable for membrane tissue engineering applications, and many research studies have been focused on utilizing and developing this thin PCL film [26, 35, 37, 45, 67, 68, 89]. Chapter 3 has shown that biaxially drawing the PCL films can physically enhance and alter its properties. For instance, there was a significant effect on the melting behaviour of the PCL films, such as increasing the melting temperature caused by the forming of larger or thicker lamellae that was formed during the annealing of the biaxially drawn PCL film [26, 27, 42, 43, 78]. The degree of crystallinity was also

found to be 4 ~ 6 % lower and was understood to be caused by the destruction of crystalline materials as the large lamellae (folded chain structures) were subjected to drawing to form micro-fibrils (extended chain structures).

Apart from altering its thermal properties, another important enhancement is its water vapour permeability. This property determines its mass transport property, and hence is an important aspect in the search for good tissue engineering scaffold that allows efficient diffusion of nutrients and waste products. Conventional single layer biaxial drawn solvent cast films has the lowest water vapour transmission rate (WVTR) at 38.24 g/h.m^2 while this value can be as high as 74.96 g/h.m^2 for biaxial drawn spin cast PCL film.

Biaxially drawn films also exhibited higher tensile strength while those of non-biaxially drawn films exhibited greater elongation. At the same time, the modulus of the films increased due to the strain-hardening stage. Strain hardening upon biaxial drawing also resulted in the tensile strength of all PCL films to increase. The distinct enhancement in the modulus and tensile strength of the biaxial drawn PCL films could be attributed to the effect of annealing after biaxial drawing where the stress imposed on the micro-fibrils was relaxed.

The interest in the investigation of the micro- and nano-topgraphy on surface is increasing in recent years. This is because the ability to micro-structure the film surface with micro-pores, lines or other patterns are known to induce cell orientation, proliferation and differentiation [90-92]. This phenomenon has the capability to engineer cell and tissue growth and/or repair and is seen as a vital alternative pathway

for organ regeneration. Moreover, the potential to use the biaxially drawn PCL films, as mentioned previously, as a thin matrix would also limit the mass of bioresorbable polymer implanted, thus limiting the quantity of degradation by-products so that the immunological reactions can be reduced [67]. At the same time, incorporating the use of laser to irradiate the surface for chemical surface enhancement will increase the impact for the use of such films in membrane tissue engineering. Hence, this area of research in unique fabrication and surface modification of biodegradable polymer films proves to be important in biomedical applications.

6.2 Experimental Procedure

6.2.1 Laser systems

Laser micro-perforation on PCL films fabricated as described in Chapter 3 was carried out using Coherent AVIA 355-1500 diode-pumped solid-state 3rd harmonic Nd:YAG laser (355 nm, 30 ns), with the laser delivered through a Mitutoyo M Plan NUV-Plan objective lens of 50× magnification with a focal length of 4 mm. The micro-wells were formed using Lambda Physik LPX 100 KrF excimer laser (248 nm, 23 ns) with a pre-fabricated stainless steel mask with holes of 50 μm in diameter. In the laser degradation study of PCL film, the film surface was exposed to the above-mentioned lasers via a ScanLab laser scanning galvanometer at a speed of 50 mm/min. The lasers used in this laser degradation study also include Spectra-Physics Hippo Q-switched Nd:YAG Laser (1064 nm, 80 ns), and a Lightwave diode-pumped Q-switched 2nd harmonic generation Nd:YAG laser (532 nm, 45 ns) with their respective ScanLab laser galvanometers.

6.3 PCL Films Characterizations

6.3.1 X-Ray Photon Spectroscopy

Laser-induced surface chemical modification of the laser-irradiated PCL films was studied using the PHI Quantera XPS with Al Kα X-ray source (1486.6 eV photons). Survey scan spectra were taken and surface elemental stoichiometries were determined from peak-area ratios while narrow scan spectra for carbon-bonded species (C-H, C=O, O-C=O) were compared.

6.3.2 Gel Permeation Chromatography

The weight-average (M_w) and number-average (M_n) molecular weight of the processed PCL films were determined by gel permeation chromatography (GPC), which comprised of a Water Alliance 2690 separations module, a Water 996 photodiode array detector and a Water 2420 ELS detector. In this analysis, an area of 5 mm x 5 mm of pristine and laser-processed PCL films were dissolved in separate vials consisting of 3 ml of tetrahydrofuran (THF). Five samples of each type of laser-processed PCL films were carried out.

6.4 Results and discussions

6.4.1 Laser drilling of PCL films using Nd:YAG laser (at λ=355 nm) and excimer laser (at λ=248 nm)

The PCL films fabricated were subjected to different laser irradiation using Nd:YAG laser (at λ = 355 nm) and KrF excimer laser (at λ = 248 nm) to produce micro-structures. Fig. 6.1 (A) shows the laser micro-drilling of micro-pores on ultra-thin PCL film fabricated through spin-casting of nearly 1 μm in thickness using Nd:YAG laser (at λ = 355 nm) delivered through a high magnification objective lens [28]. Neat array of micro-pores of size 4 ~ 5 μm in diameter were produced with no obvious melting around its periphery was observed. In order to ensure that film surface was flat for the laser processing to be carried out, the film was stretched to keep taut such that radial tension was acting on the film. This tension acting on the film could be the reason that the pore size becomes stretched and slightly deformed. Fig. 6.1 (B) shows the result of producing micro-size pores in thicker PCL films of thickness of ~ 10 μm. The micro-pores of approximately 4 ~ 5 μm in diameter were again produced but at this instance, surrounding ring of annulus structure was formed around each micro-pore. From Fig. 6.1 (B), melting occurred during the laser irradiation as the ring structure was formed due to melting of the material. The pores drilled were also found to be more circular in shape as compared to Fig. 6.1 (A). Hence, film thickness could affect the degree of melting and deformation during laser irradiation: a thicker film had a larger volume that could allow more material to flow and subsequently form a periphery ring during the laser irradiation. A thicker film would also mean that it had substantial mass to withstand the tearing of the film while the film was irradiated at its tensile state. When the film was exposed to 10 pulses of KrF excimer laser through the

use of a mask perforated with micro-sized holes, matters such as atoms, molecules and ions were ejected out of the surface as plasma plumes, and the end result was the formation of well-defined micro-wells or craters, as shown in Fig. 6.1 (C). Since it took approximately 24 laser pulses at a laser fluence of 0.25 J/cm^2 to completely ablate through the 10 μm thick film, the depth of the micro-wells formed were thus estimated to be at about 4 μm.

Other techniques, such as photolithography or e-beam lithography, have been widely used for patterning of surfaces, especially in the semi-conductor industry. Photolithography involves a series of steps that requires the exposure of photo-sensitive polymers to UV light source and followed by developers to wash off either the exposed or unexposed area, hence leaving behind the desired patterns. However, such biocompatible photosensitive polymers are limited and the use of developers may contaminate the polymer. E-beam lithography offers patterning of substrates in the nanometer scale, but the speed of patterning is very slow and coupled with the high cost of the equipment, is not an economically feasible process. Using lasers to direct write or pattern polymer substrates in normal room conditions or even vacuum chamber offers a much more direct and convenient process. Laser processing, in this case, also offers other versatilities such as the ability to vary different sizes, depths and the pitches of the trenches formed by using different types of mask and the number of laser pulses the film is exposed to. Besides the ability of the laser to produce discrete micro-structures on PCL film, Fig. 6.1 (D) also showed that micro-channels of 2 μm wide could be created on the PCL film by laser “direct-write” method. Dense inter-connecting networks of channels could also be easily fabricated on the film.

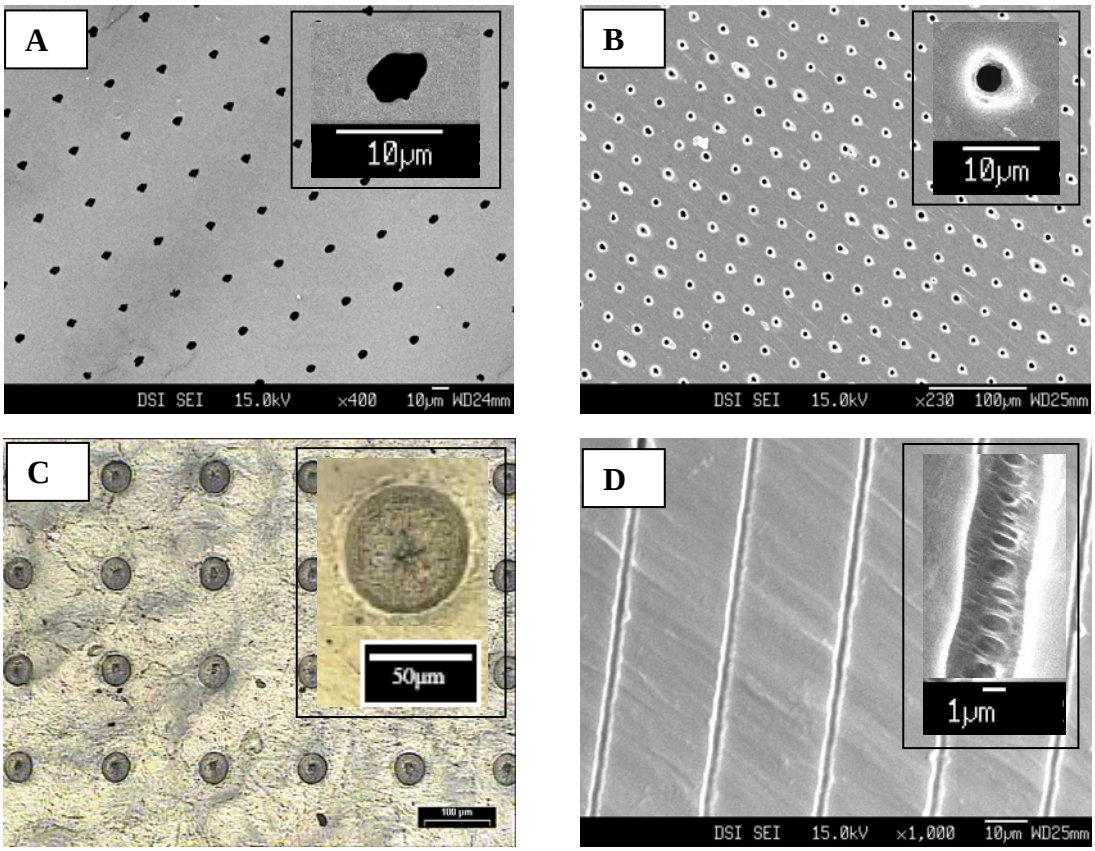

Fig. 6.1. Pictures of laser surface-patterned PCL thin films showing **(A)** micro-perforations using Nd:YAG laser (at λ = 355 nm) with uniformed array of micro-size perforations on 1 µm thick PCL film; **(B)** 'donut-like' array of micro-size perforations on 10 µm thick PCL film; **(C)** micro-wells formed using KrF excimer laser (at λ = 248 nm) with mask; **(D)** laser "direct-writing" on PCL film forming micro-channels of about 2 µm wide.

The micro-wells formed from KrF excimer laser exposure can find potential applications in areas of cell trapping and/or isolation or drug encapsulation. The micro-size perforation created by Nd:YAG laser can help to improve film porosity, and hence able to achieve a better permeability and diffusivity to solvent and solute particles in the application of membrane tissue engineering. Coupled with the use of micro-channels formed on PCL films by laser "direct-writing" and the ability to photo-graft favourable functional groups on the surface by UV laser, there is a great potential for this to become a suitable biomaterial scaffold that may help promote cell growth as well as controlled vasculogenesis and/or angiogenesis, and hence develop into complex tissues and organs which can be sustainable. While this has yet to be proved to be the right formula to achieve the ultimate goal of engineering complex tissues and/or organs, the versatility of lasers to produce micro-architectural structures, photo-chemical modifications on the PCL films together with the advancement of tissue engineering methods, could be the major step forward towards achieving this success.

6.4.2 XPS analysis of PCL film surface chemistry

While the use of lasers can physically or chemically alter the surface properties, detailed study of the chemical changes during laser processing of the PCL films is vital. As different material has different optical absorption, the extent of optical absorption during processing with lasers of different wavelengths is an important factor to consider. From the information of the degree of optical absorption on the material, the kind of laser-material interaction can then be predicted. Fig. 6.2 showed the UV-Vis spectrum of PCL films in which UV lasers of 248 nm and 355 nm registered higher optical absorptions of 0.5267 cm^{-1} and 0.0262 cm^{-1} respectively, as compared to other

lasers of longer wavelengths of 532 nm and 1064 nm that showed significant lower optical absorptions of 0.0090 cm^{-1} and 0.0011 cm^{-1} respectively.

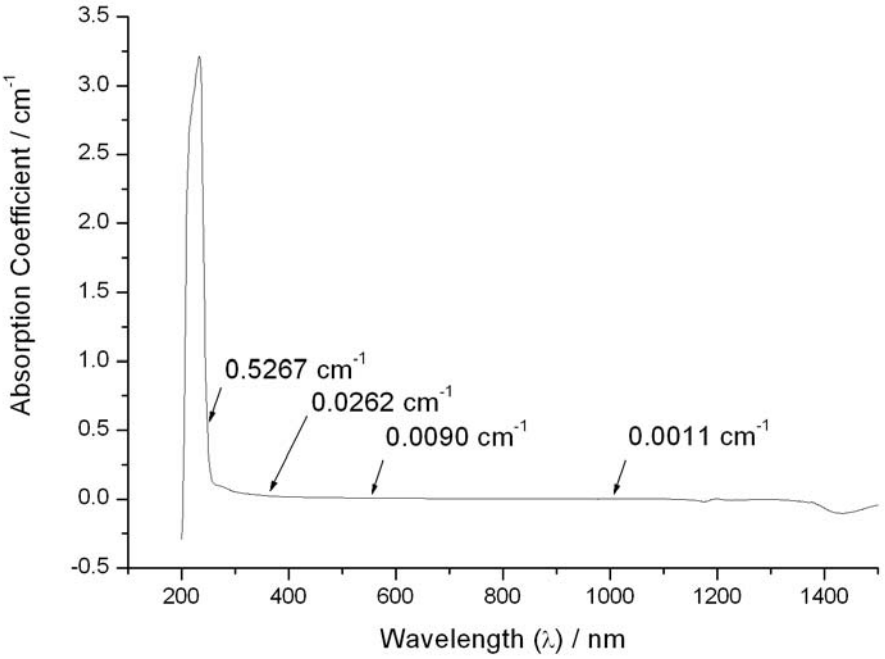

Fig. 6.2. UV-Vis spectrum showing optical absorption of PCL film across wavelengths of 200 – 1400 nm. The absorption coefficient values correspond to optical absorption of PCL film at laser wavelengths of 248 nm, 355 nm, 532 nm and 1064 nm, in descending order.

To characterize the chemical changes, the films fabricated were placed directly under Nd:YAG laser (at wavelengths 1064, 532 and 355 nm respectively) and scanned over an area of 2 X 2 cm using a laser scanning galvanometer. As for irradiation by an excimer UV laser (at wavelength of 248 nm), the PCL film was exposed to an area of 1 X 2 cm for 10 pulses at a repetition rate of 2 Hz.

X-ray photon spectroscopy (XPS) wide-scan spectrum showed the presence of carbon and oxygen signals while the narrow scan spectrum revealed the presence and composition of C-H, C=O and O-C=O species. The spectra in Fig. 6.3 showed the various species composition through the narrow scans of the laser-processed and pristine PCL films. From the results of the XPS analysis, the compositional changes of organic species C-H, C=O and O-C=O were significant. Generally, an increase in the composition of both C=O and O-C=O species were observed from an increase in the C=O and O-C=O resolved curves as compared to the pristine PCL film while that of C-H species showed a significant reduction across all laser-processed films.

The increase in the composition of C=O and O-C=O revealed that the films had undergone significant surface oxidation after the laser irradiation. The general reduction in composition of the main chain C-H could also have implied that part of it had oxidized to form C=O and O-C=O. This conversion could be due to the effect of photo- and thermal-oxidative degradation of the PCL films after exposure to the excimer and Nd:YAG lasers, respectively. The issue of oxidative development plays an important part in theory of polymeric materials degradation and stabilization [112]. The general mechanism of thermal oxidative degradation starts with the initial reaction, where energy is absorbed and bond cleavage occurs to form reactive free radicals on the main chain. These radicals can then react with oxygen in chain propagation reactions. Chain branching reactions follow leading to chain scission. Finally, the reaction terminates when the radicals combine in cross-linking reactions to become inactive products. Thermal- and photo-oxidation differ such that in the former, initiation results from thermal dissociation of chemical bonds while in the latter, initiation results from photo-dissociation of chemical bonds [113].

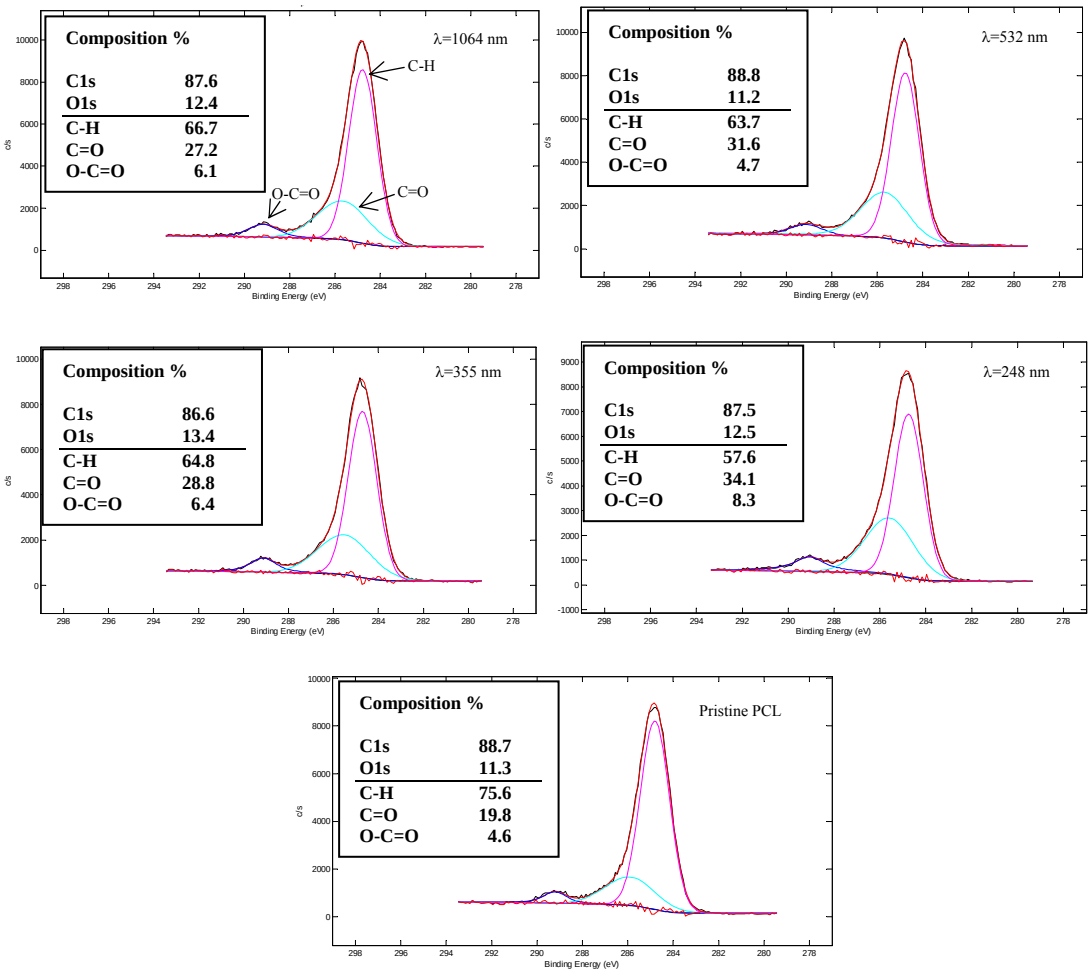

Fig. 6.3. XPS narrow-scan spectra showing the various species compositions of laser-processed and pristine PCL films. A significant change was observed when the PCL film was exposed to KrF excimer laser (at λ = 248 nm) in which the composition of the main chain C-H dropped to 57.6% while that of the species C=O and O-C=O increased to 34.1% and 8.3% respectively. The rest of the films subjected to Nd:YAG lasers (at λ = 355, 532, 1064 nm) showed less compositional changes to C-H, C=O and O-C=O.

The largest increase in surface oxidation was seen in PCL films that were exposed to excimer laser (at wavelength of 248 nm). This was evident from the increase in composition of C=O from 19.8% to 34.1% and O-C=O from 4.6% to 8.3% while the main C-H chain decreased from 75.6% to 57.6% after the laser irradiation.

This was expected since PCL has a high optical absorption at 248 nm, as shown previously in Fig. 6.2. This is very near the optical absorption of PCL at approximately 220 nm [114]. The degree of film oxidation of the PCL films irradiated with Nd:YAG lasers at wavelengths 1064, 532 and 355 nm was milder as compared to the films irradiated with excimer laser. This could be attributed to the lower photon energies from the three Nd:YAG lasers that were not high enough to warrant a more intense photo-thermal oxidative degradation, as compared to photo-chemical oxidative degradation from excimer laser.

The degree of oxidation in polymers is also known to be dependent on its percentage crystallinity [112]. Oxidation of polymers generally occurs in the amorphous regions and hence the higher the percentage crystallinity, the lower the radiation yield of oxygen absorption and formation of oxygen containing products. Since roll-milled and biaxially stretched PCL films were found to have 47 % crystallinity [42], oxidation could have occurred in the remaining 53 % of amorphous structure.

According to Fedynyshyn [115], polymer degradation can be caused by the mechanism of Norrish Type 2 cleavage. This occurs when the polymer main chain cleaves, leading to two new shorter polymer chains of decreased molecular weight. The polymer can then undergo a bond scission reaction which leads again to an initial carbon radical on the polymer main chain, which then undergoes further reactions that lead to polymer cross-linking. This may be a possible method to cleave the PCL main chain. The tertiary carbon radical formed after cleavage is free to react with any oxygen available to carry out further oxidative degradation, hence resulting in the

increase in the ratios of C=O and O-C=O with respect to C, as seen in the XPS analysis. Both thermal and/or photo-chemical degradation can also be initiated by the presence of external free radicals, which are formed from thermolysis and/or photolysis of some impurities, additives or photo-initiators [113]. From the results of increased surface oxidation due to laser exposure, especially KrF UV excimer laser, the photo-oxidation of the PCL film can also help to create localized useful functionalities, such as carboxyl (-COOH), hydroxyl (-OH), amine ($-NH_2$) and amide ($-CONH_2$) groups on the PCL films to enhance cell adhesion and induce favourable cell differentiation [116].

6.*4.3 Analysis of molecular weight distribution after laser processing*

Since laser irradiation of PCL films is capable of producing photo-induced chain scission and subsequent branching caused by the radicals formed, there is a need to track the molecular weight distribution of PCL films upon laser irradiation via gel permeation chromatography. The molecular weight distribution affects the polymer's crystalline structure, physical properties (such as density, tensile and bending strength, elongation at break, modulus, viscosity and etc.) and its rheological properties. Therefore, the degradation of PCL caused by the changes in molecular weight distribution is of great consequence in preserving its properties [112].

There are two ways to describe the molecular weight of a polymer. Number-average molecular M_n weight in Eq. 6.1 is defined as the total weight of all polymer molecules in a sample and divided by the total number of polymer molecules. Weigh-average molecular weight M_w in Eq. 6.2 is calculated in a more complicated way that

emphasizes on the mass of the polymer molecules such that the heavier molecules are given a higher probability factor.

$$M_n = \frac{\Sigma_i N_i M_i^2}{\Sigma_i N_i} \qquad \text{Eq. 6.1}$$

$$M_w = \frac{\Sigma_i N_i M_i^2}{\Sigma_i N_i M_i} \qquad \text{Eq. 6.2}$$

where N_i is the number of molecules and M_i the molecular weight

The ratio of M_w and M_n is the measure of the polydispersiy index a polymer mixture; the range of distribution of the molecular weights in the mixture. A ratio of 1 indicates that the range of molecular weights in the mixture is narrow while a high ratio indicates that the range is wide.

The resulting changes in the molecular weight distribution and polydispersity index of the PCL films after laser irradiation were shown in Fig. 6.4. Pristine PCL film has a M_w of 158, 000 and a M_n of 97,000. For PCL films irradiated with 355 nm Nd:YAG laser, the M_w decreased slightly to 149,000 while the M_n increased to 149,000. These two values suggested that a slight degradation of the PCL film had occurred and that the molecular weight, as well as the number of polymer chains, was reduced. The polydispersity index decreased from 1.62 to 1.00 and showed a tremendous narrowing down of molecular weight distribution due to the narrowing of M_w and the number of polymer chains.

For films irradiated with 532 nm Nd:YAG laser, the M_w was found to have increased to 184,000 and the M_n increased to 120, 000. The increase in both of these values suggested that cross-linking of the macromolecules had taken place. However

the polydispersity index was reduced from 1.62 to 1.54. This could be due to a large increase in M_n. Hence, cross-linking of the polymer chain seemed to be more dominant over chain scission. However, the molecular weight of the polymer chains after cross-linking remained small, causing the polysdispersity index to fall. PCL films irradiated with fundamental Nd:YAG laser at 1064 nm showed a slight increase of M_w to 157,000 while a slight drop of M_n to 94,000, thus giving a marginal increase of polydispersity index from 1.62 to 1.67. These values suggested that no significant chain scission or cross-linking occurred when the PCL films were irradiated.

A more significant impact was observed when PCL films were irradiated with 248 nm excimer laser. The M_w decreased to 126,000 while the M_n decreased to 53,000. Due to the significant reduction in M_n, the polydispersity index increased significantly to 2.36. During the exposure of excimer laser on the PCL films, chain scission had become the predominant process, which resulted in smaller polymer chains with a molecular weight smaller than the original value. Upon irradiation with lasers, polymers could undergo a photo-induced chain scission reaction in which either the polymer main chain or side chain was cleaved. Main chain scission would lead to a reduction of molecular weight while side chain scission was an established pathway to form acrylate and methacrylate esters [115].

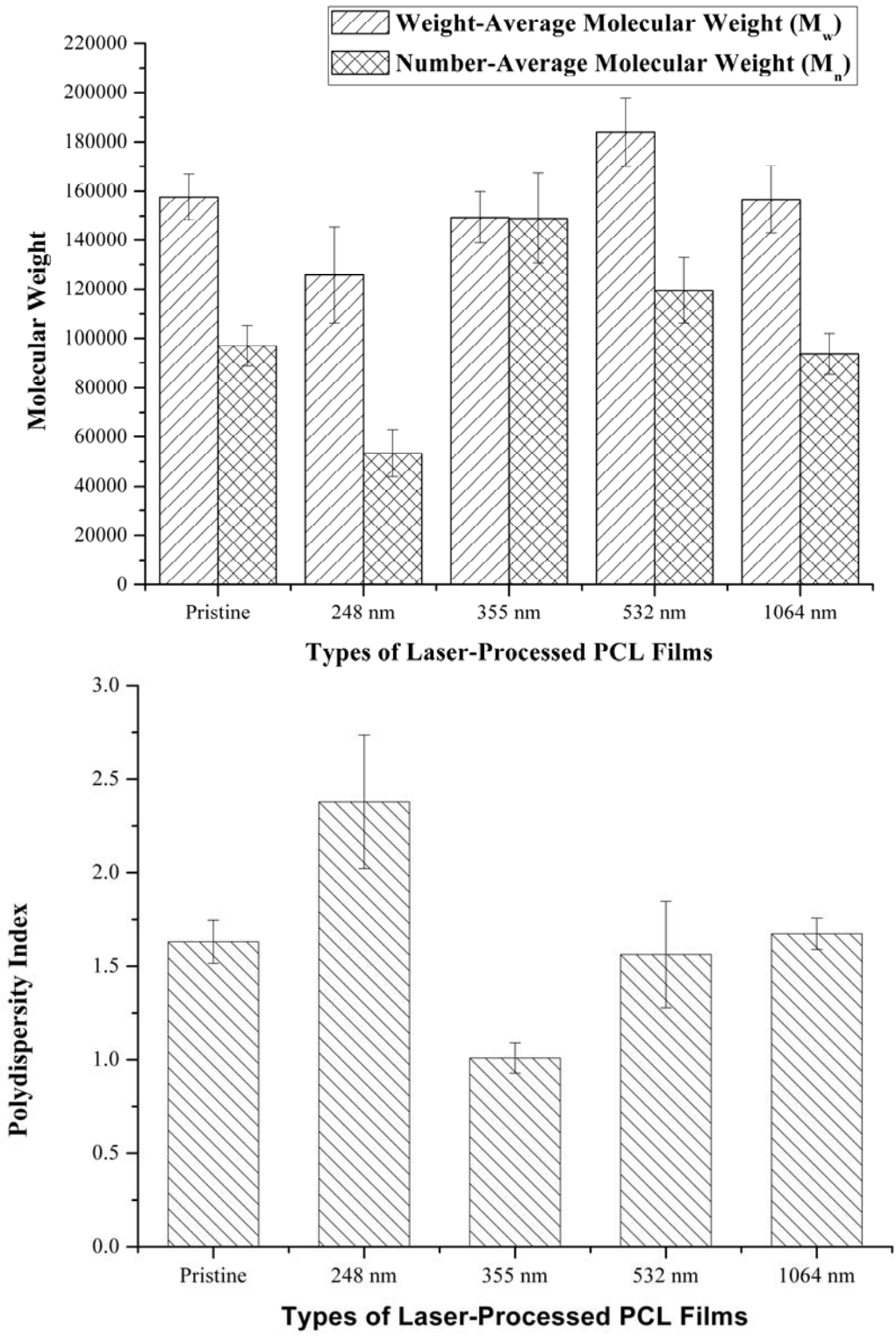

Fig. 6.4. Comparison of values of M_w and M_n and polysdispersity index of pristine and irradiated PCL films at various laser wavelengths.

6.5 Summary

- A study on the laser degradation of the PCL films revealed that photochemical oxidative degradation occurred for the excimer laser while thermo-oxidative degradation occurred for the Nd:YAG lasers. The pre-cursor to final surface oxidation was useful in creating functional groups which could help to enhance protein adsorption, cell behavior and tissue responses at the cell-biomaterial interface.

- PCL film irradiated by excimer laser was found to exhibit the highest amount of degradation due to large increase in surface oxidation and large reduction in M_n and $M_{w,}$ which subsequently resulted in a large increase in the polydispersity index. These results showed that the PCL film had undergone extensive surface oxidation and chain scission which led to bulk degradation of the PCL films.

- PCL films exposed to Nd:YAG lasers (at λ = 355 and 532 nm) also experienced surface oxidation and an increase in M_n suggested that cross-linking of the macromolecules took place.

- PCL films irradiated by Nd:YAG laser (at λ = 1064 nm) showed the least amount of surface oxidation while the M_n and M_w showed little change and hence its polydispersity index remained relatively unchanged. These results suggested that the PCL films did not undergo much bulk degradation due to poor energy absorption by PCL at this particular wavelength.

Chapter 7:
Conclusion

7.1 Conclusion and Research Contributions

In this extensive research study, the various fabrication techniques of PCL films, through the initial steps of dissolution, spin-casting and two-roll milling, followed by compression into thin, uniform and homogenous sheets, and finally the bi-axial drawing of the sheets into ultra-thin membranes, were carried out. All films were biaxially drawn to its limit and were found that films made from two-roll mill have the highest drawing ratio while that of spin cast films has the lowest drawing ratio.

The fabrication of sub-micrometer ultra-thin PCL films was also successfully carried out through biaxial drawing of the spin-cast films. The morphology of all the biaxial drawn films studied showed similar fibrillar networks due to chain orientation induced by biaxial drawing. The mechanical properties of the biaxially drawn PCL thin films determined through the tensile test showed that upon biaxial drawing, all films exhibited a reduction in elongation, increase in tensile strength and increase in modulus. This was largely due to the polymer chain extension and orientation during the biaxial stretching process. Due to the reduction in film thickness, the water vapour transmission rate was also increased significantly to allow better bidirectional gas and moisture diffusion through the film.

From the results, biaxial drawn two-roll mill films not only possessed the preferred mechanical properties, it also offered reduced thickness as compared to the

solvent cast films due to a higher drawing ratio. With its good mechanical properties, this can match the commercially available wound dressings such as Omiderm® [117]. However, taking into consideration the benefits of administering less foreign materials over a same surface area, biaxial drawn spin-cast films could also prove important in membrane tissue engineering applications since this method could produce PCL films with a thickness of 1 μm. The transport of water vapour was also much faster and hence, mass transport of ions necessary for cell proliferation and nutrient/waste transfer could be carried out efficiently. Thus the fabrication method via spin-cast, coupled with biaxial drawing, seems to offer potential benefits for membrane tissue engineering applications.

Precision laser micro-processing on PCL films by 3rd harmonic Nd:YAG laser delivered through different lens was able to perform precise micro-drilling and produce fine micro-trenches. Melting of the thin PCL film caused by heat accumulation around the micro-pores are not visible for the 2 μm thick spin-cast PCL film but a slight extent of the melting was observed in the thicker bi-axial drawn roll-mill film. Hence, this shows that the thickness of the films played an important role in the degree of melting due to a larger volume at higher thickness. Mathematical simulation in predicting the temperature-rise caused by laser irradiation on PCL film was evaluated and the results showed that different focusing spot sizes delivered through different lens could affect the cooling rate of the material significantly. The laser which was delivered through plano-convex lens with long focal length and smaller NA experienced a cooling time constant of 2 ms. A high NA objective lens and short focal length experienced a cooling time constant of 8.4 μs. These differences resulted in different accumulation of temperature rise, with the film experiencing slow cooling rate registering a high

temperature rise of up to 1200 K while that of film experiencing fast cooling rate registering only a temperature rise of 88 K. Consequently, this affected the dimensions of the micro-holes produced and the radial heat flow around the micro-holes region. Therefore, laser processing with small focal spot size was advantageous and enabled more well-defined micrometer-sized features to be created.

Surface properties of biomaterials, such as porosity, surface charge, surface topography, wettability, are known to play an important role in the adhesion process of cells. In general, hydrophilic surfaces display better affinity for cells but lower affinity for proteins than hydrophobic surfaces. The material PCL chosen for this research, although biodegradable and biocompatible in nature, is also hydrophobic. In order for cells to attached, differentiate and proliferate on the PCL films effectively, attempts to physically and chemically modify the surface via laser processing were carried out. Femtosecond laser and KrF excimer laser were used to physically modify the surface by producing arrays of micro-perforations. At higher pulse energy, the width of the Gaussian beam profile widened and enlarged the micro-pores drilled on the PCL film while lower pulse number increased the deposition of ejected materials on the film surface. These micro-pores, together with the material deposits, were believed to have caused the rupture of a thin liquid membrane that resulted in substantial reduction in the water contact angle by up to 30%, thereby enhancing the surface wettability.

Lasers can also be used to induce chemical modifications through photo-chemical reactions. A study on the laser degradation of the PCL films revealed that photochemical oxidative degradation occurred for the excimer laser while thermo-oxidative degradation occurred for the Nd:YAG lasers. The pre-cursor to final surface

oxidation can be proved to be useful in creating functional groups which can help enhance protein adsorption, cell behavior and tissue responses at the cell-biomaterial interface. PCL film irradiated by excimer laser was found to exhibit the highest amount of degradation due to large increase in surface oxidation and large reduction in M_n and $M_{w,}$ which subsequently resulted in a large increase in polydispersity index. This showed that the PCL film had undergone extensive surface oxidation and chain scission which led to bulk degradation of the PCL films. PCL films which were exposed to Nd:YAG lasers (at λ = 355 and 532 nm) also experienced surface oxidation and an increase in M_n suggested cross-linking of the macromolecules had taken place. PCL films irradiated by Nd:YAG laser (at λ = 1064 nm) showed the least amount of surface oxidation as the M_n and M_w showed little change and hence, its polydispersity index remained relatively unchanged. These suggested that the PCL films did not undergo much bulk degradation due to poor photon absorption by PCL at this particular wavelength.

The detailed research study presented in this thesis would see femtosecond laser as the preferred tool for laser surface modification of PCL films due to its ability to produce micrometer-sized pores ranging from 10 – 100 μm by simply adjusting the power of the laser. As such, the film porosity can be customized to different types of experiment requiring different film porosities. The surface wettability were enhanced as a result of increased surface roughness. The bulk properties of the film were retained because the interaction of femtosecond laser with PCL was caused by multi-photon absorption and hence, chemical changes on the film caused by heat and photon were considered to be negligible.

7.2 Future research directions

Currently the PCL used in this research takes a fair amount of time (about two to three years) to fully degrade and absorb into the biological environment. This lengthy process may not be necessary or suitable for some membrane tissue engineering applications for fear of invoking inflammatory and toxic response. To accelerate the rate for biodegradation, PCL can blend in or co-polymerize with other biodegradable polymers with hydrolytical unstable linkages in the main chain. Such polymers include [118]:

- Polyglycolide (PGA) – simplest linear aliphatic polyester which exhibits high strength and modulus. It will lose 50% of its strength after two weeks, 100% of it in four weeks and totally absorbed into the body in four to six months.
- Polylactide (PLA) – cyclic dimer of lactic acid. Poly(l-lactide) is semi-crystalline. It exhibits high tensile strength and low elongation and is suitable for high load bearing applications, but it takes more than two years to be fully absorbed into the body. Poly(dl-lactide), on the other hand, is amorphous and has lower tensile and higher elongation, and degrades more rapidly than poly(l-lactide).
- Poly(dioxanone) – a semi-crystalline polyester that loses half of its strength in three weeks and fully absorbed in six months.
- Other polymers that include poly(trimethylene carbonate), polyanhydrides, polyorthoesters, polyphosphazines, and etc.

With the new blend or copolymer in different compositions, the desired degradation time can be tailored to match the required applications. However, renewed efforts are required in finding the suitable method with optimal processing parameters to fabricate the polymer blend into ultra-thin sheets.

The laser micro-perforation of the PCL films was carried out through a time-consuming process in which the holes were drilled through individually. This process can be significantly hastened through the use of a laser galvanometer or microlens array setup.

1. Fast scanning laser galvanometer

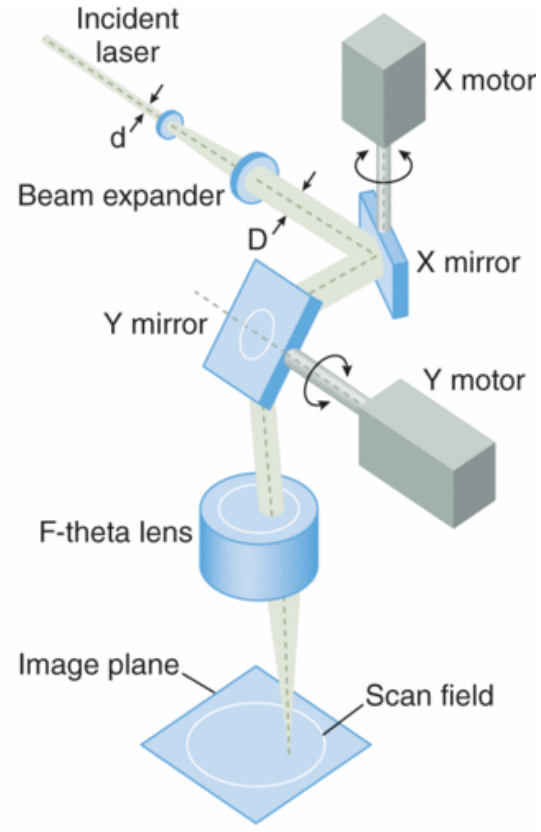

Fig.7. 1. A laser galvanometer uses a mirror pair sized to the input beam aperture over a range of rotation angles for the required scan field.

A fast scanning laser galvanometer enables process to be carried out at scanning speed of up to 2000 mm/s, that is to say that it needs approximately ten minutes to fully fabricate a porous film a film measuring 30 cm x 30 cm of 50 μm pore size with a pitch of 100 μm. Such scanning system facility is available to Nd:YAG lasers in the laboratory but is not suitable for fabricating micro-perforated films. This is because the mentioned fabrication method requires a single pulse to fully drill through the film and that the energy from a single pulse from Nd:YAG lasers is not strong enough to achieve that. However, if the laser scanning system is applied to a femtosecond laser, this will become possible. Coupled with the favourable feature of the femtosecond laser in that it reduces (or almost completely eliminate) heat accumulation over the processed surface to a minimum and the bulk properties of the surrounding micro-pore region remains the same, this can be seen as a the one of the ideal methods to fabricate a fully porous biodegradable PCL film effectively and efficiently for membrane tissue engineering.

2. Microlens array

A microlens array can act as a collective set of very small lens in the order of tens to hundreds of micrometer. Each microlens array of 1 cm X 1 cm can have up to few or tens of thousands of small lenses, determined by its diameter and pitch. As such, a single laser exposure will be able to form an array of patterns. This method offers a very quick way of achieving patterns on the film. Fig. 7.2 shows the schematic setup of the laser micro-patterning or micro-perforation on the PCL film with the use of a microlens array. However, there are a few considerations in using this method. First, the microlens array has a very small focal length of tens to hundreds of micrometer and

therefore, focusing the laser through the microlens on to the PCL film must be very exact as a slight displacement of the film from the focal plane of the microlens can happen easily. Second, as the focal length is very small, material ejection from the PCL surface during laser ablation may contaminate the microlens, and lead to eventual damage. Hence, microlens patterning and perforation has to be done on photo-sensitive materials which upon laser irradiation, will change the chemical structure instead of ablation, and these areas that are exposed to laser can then either be retained or wash off in subsequent chemical treatment. The availability of such photo-sensitive materials which require it to be biocompatible and biodegradable is, however, limited. Hence, the use of microlens setup to produce patterned films efficiently requires the use of this photo-polymer in order for it to be effective.

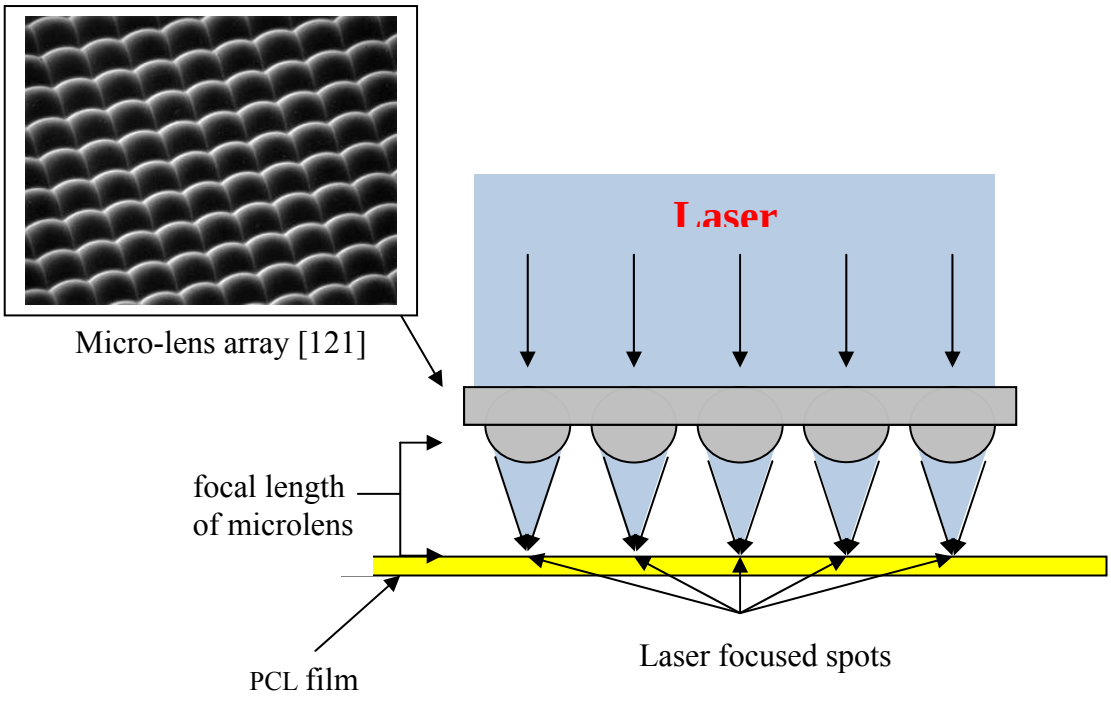

Fig. 7.2 Schematic design of microlens array laser micro-processing and micro-patterning.

Lastly, to assess the potential use of such films for membrane tissue engineering, it is recommended for the micro-perforated PCL films to undergo in-vitro experiments.

References

1. Hecht, J., Understanding Lasers: An Entry-Level Guide (IEEE Press Understanding Science & Technology Series). 2nd Ed. ed. New Jersey: John Wiley & Sons. 2001.
2. Chan, C.M., T.M. Ko, and H. Hiraoka. Polymer surface modification by plasmas and photons, Surf. Sci. Rep., *24*, pp. 1 - 54. 1996.
3. Khorasani, M.T., H. Mirzadeh, and P.G. Sammes. Laser induced surface modification of polydimethylsiloxane as a super-hydrophobic material, Radiat. Phys. Chem., *47*, pp. 881 - 888. 1996.
4. Khorasani, M.T., H. Mirzadeh, and P.G. Sammes. Laser surface modification of polymers to improve biocompatibility: HEMA grafted PDMS, in vitro assay – III. , Radiat. Phys. Chem., *55*, pp. 685 - 689. 1999.
5. Dadsetan, M., H. Mirzadeh, and H. Sharifi. Effect of CO2 laser radiation on the surface properties of polyethylene terephthalate. , Radiat. Phys. Chem., *56*, pp. 597 - 604. 1999.
6. Viville, P., S. Beauvois, G. Lambin, G. Lazzaroni, J.L. Bredas, K. Kolev, and L. Laude. Excimer laser-induced surface modifications of biocompatible polymer blends, Appl. Surf. Sci. , *96 - 98*, pp. 558 - 562. 1996.
7. Black, J., Biological performance of materials. 2nd Ed. ed. New York: Marcel & Dekker. 1992.
8. Dec, K.C., D.A. Puleo, and R. Bigirs, An introduction to tissue-biomaterial interactions. New York: John Wiley & Sons. 2002.
9. Greco, R.S., Implantation biology: the host response and biomedical devices. London: CRC Press. 1994.

10. Hill, D., Design engineering of biomaterials for medical devices. New York: John Wiley & Sons. 1998.

11. Jamison, R.D. and L.N. Gilbertson, Composite materials for implant applications in the human body (ASTM STP1144). Philladelphia, USA: American Society of Testing and Materials. 1993.

12. Park, J.B. and R.S. Lake, Biomaterials - an introduction. 2nd ed. ed. New York: Plenum Press. 1992.

13. Ratner, B.D., A.S. Hoffman, F.J. Schoen, and J.E. Lemons, Biomaterials science: an introduction to materials in medicine, ed. eds. New York: Elsevier Sci. 1996.

14. St.John, K.R., Particulate debris from medical implants (ASTM STP1144). Philladelphia, USA: American Society of Testing and Materials. 1992.

15. Teoh, S.H., *Introduction to biomaterials engineering and processing -- an overview*, in *Engineering Biomaterials for Medical Applications*, S.H. Teoh, Editor. 2004, World Scientific Publishing Co. Pte. Ltd.: Singapore.

16. Hutmacher, D.W., T. Schantz, I. Zein, K.W. Ng, S.H. Teoh, and K.C. Tan. Mechanical properties and cell cultural response of polycaprolactone scaffolds designed and fabricated via fused deposition modeling, J. Biomed. Mater. Res. , *55*, pp. 203 - 216. 2001.

17. L'Heureux, N., S. Paquet, R. Labbe, L. Germain, and F.A. Auger. A completely biological tissue-engineered human blood vessel, FASEB J., *12*, pp. 47-56. 1998.

18. Shimizu, T., M. Yamato, Y. Isoi, T. Akutsu, T. Setomaru, K. Abe, A. Kikuchi, M. Umezu, and T. Okano. Fabrication of pulsatile cardiac tissue grafts using a

novel 3-dimensional cell sheet manipulation technique and temperature-responsive cell culture surfaces, Circulation Res., *90*, pp. E40-E48. 2002.

19. Perrin, D.E. and J.P. English, *Polycaprolactone*, in *Handbook of biodegradable polymer*, A.J. Domb, J. Kost, and D.M. Wiseman, Editors. 1997, CRC Press. p. 63-78.

20. Tang, Z.G., R.A. Black, J.M. Curran, J.A. Hunt, N.P. Phodes, and D.F. Williams. Surface properties and biocompatibility of solvent-cast poly[ε-caprolactone] films, Biomaterials, *25*, pp. 4741 - 4748. 2004.

21. Kweon, H.Y. and M.K. Yoo. A Novel Degradable Polycaprolactone Networks for Tissue Engineering, Biomaterials, *24*, pp. 801-808. 2003.

22. Coombes, A.G.A. and S.C. Rizzi. Precipitation Casting of Polycaprolactone for Applications in Tissue Engineering and Drug Delivery, Biomaterials, *9*, pp. 315-325. 2003.

23. Marra, K.G., J.W. Szem, P.N. Kumta, P.A. DiMilla, and L.E. Weiss. In Vitro Analysis of Biodegradable Polymer Blend/Hydroxyapatite Composites for Bone Tissue Engineering, J.Biomed. Mater. Res. A, *47*, pp. 324-335. 1999.

24. Heath, D.J., P. Christian, and M. Griffin. Involvement of Tissue Transglutaminase in the Stabilization of Biomaterials/Tissue Interfaces Important in Medical Devices, Biomaterials, *23*, pp. 1519-1526. 2002.

25. Ashby, M.F. and D.R.H. Jones, Engineering materials 1: An introduction to their properties & applications: Butterworth Heinemann. 2001.

26. Ng, C.S., S.H. Teoh, T.S. Chung, and D.W. Hutmacher. Simultaneous biaxial drawing of poly (ε-caprolactone) films, Polymer, *41*, pp. 5855-5864. 2000.

27. Sakai, Y. and K. Miyasaka. Biaxial drawing of dried gels of ultra-high molecular weight polyethylene, Polymer, *29*, pp. 1608-1614. 1988.

28. Sakai, Y. and K. Miyasaka. Development of fibrillar texture during simultaneous biaxial drawing of ultra-high-molecular-weight polyethylene dried gels, Polymer, *31*, pp. 51-57. 1990.

29. Sakai, Y., K. Umetsu, and K. Miyasaka. Mechanical properties of biaxially drawn films of ultra-high molecular weight polyethylene dried gels, Polymer, *34*, pp. 318-322. 1993.

30. Taraiya, A.K., G.A.J.Orchard, and I.M. Ward. Barrier properties of biaxially oriented polypropylene films, Plast. Rubber Compos. Process Appl., *19*, pp. 273-278. 1993.

31. Chu, F., T. Yamaoka, H. Ide, and Y. Kimura. Microvoid formation process during the plastic deformation of -form polypropylene, Polymer, *35*, pp. 3442-3448. 1994.

32. Gerrits, N.S.J.A. and P.J. Lemstra. Porous biaxially drawn ultra-high molecular weight polyethylene films, Polymer, *32*, pp. 1770-1775. 1991.

33. Zhu, W., X. Zhang, C. Zhao, W. Wu, J. Hou, and M. Xu. A novel polypropylene microporous film., Polym. Advan. Technol., *7*, pp. 743-748. 1996.

34. Zhang, X. and A. Ajji. Biaxial orientation behaviour of polystyrene: orientation and properties, J. Appl. Polym. Sci., *89*, pp. 487-496. 2003.

35. Ng, K.W., D.W. Hutmacher, J.T. Schantz, C.S. Ng, H.P. Too, T.C. Lim, T.P. Phan, and S. Teoh. Evaluation of Ultra-Thin Poly(ε-Caprolactone) Films for Tissue-Engineered Skin, Tissue Eng., *7*, pp. 441-455. 2001,.

36. Khor, H.L., K.W. Ng, A.S. Htay, J.T. Schantz, S.H. Teoh, and D.W. Hutmacher. Preliminary study of polycaprolactone membrane utilized as epidermal substrate, J. Mater. Sci.-Mater. Med., *14*, pp. 113-120. 2003.

37. Schantz, J.T., D.W. Hutmacher, K.W. Ng, H.L. Khor, T.C. Lim, and S.H. Teoh. Evaluation of a tissue-engineered membrane-cell construct for guided bone regeneration, Int. J. Oral Maxillofacial Implants, *17*, pp. 161-174. 2002.

38. Serrano, M.C., R. Pagani, M. Vallet-Regí, J. Peña, A. Rámila, I. Izquierdo, and M.T. Portolés. In vitro biocompatibility assessment of poly(ε-caprolactone) films using L929 mouse fibroblasts, Biomaterials, *25*, pp. 5603-5611. 2004.

39. Yang, S.F., K.F. Leong, Z.H. Du, and C.K. Chua. The Design of Scaffolds for Use in Tissue Engineering, Tissue Eng., *7*, pp. 679-689. 2001.

40. L. Lu, C.A. Garcia, and J.o.B.M.R. A. G. Mikos, 1999. 46, pp.236. In vitro degradation of thin poly(DL-lactic-co-glycolic acid) films, J. Biomed. Mater. Res. A, *46*, pp. 236-244. 1999.

41. Suggs, L.J., J.K. West, and A.G. Mikos. Platelet adhesion on a bioresorbable poly(propylene fumarate-co-ethylene glycol) copolymer, Biomaterials, *20*, pp. 683 - 690. 1999.

42. Tiaw, K.S., S.H. Teoh, R. Chen, and M.H. Hong. Processing methods of ultrathin poly(ε-caprolactone) films for tissue engineering applications, Biomacromolecules, *8*, pp. 807-816. 2007.

43. Htay, A.S., S.H. Teoh, and D.W. Hutmacher. Development of perforated microthin poly(ε-caprolactone) films as matrices for membrane tissue engineering J. Biomater. Sci. Polymer Edn, *15*, pp. 683-700. 2004.

44. Zhu, Y.B., C.Y. Gao, X.Y. Liu, and J.C. Shen. Surface modification of polycaprolactone membrane via aminolysis and biomacromolecule immobilization for promoting cytocompatibility of human endothelial cells, Biomacromolecules, *3*, pp. 1312-1319. 2002.

45. Cheng, Z. and S.H. Teoh. Surface modification of ultra thin poly (ε-caprolactone) films using acrylic acid and collagen Biomaterial *25*, pp. 1991-2001. 2004.

46. Ozdemir, M. and H.A. Sadikoglu. New and emerging technology: Laser-induced surface modification of polymers, Trends Food Sci. Tech., *9*, pp. 159 - 168. 1998.

47. McKenzie, A.L. and J.A.S. Carruth. Lasers in surgery an medicine, Phys. Med. Biol., *29*, pp. 619-641. 1984.

48. Cammarata, F. and M. Wautelet. Medical lasers and laser-tissue interactions, Phys. Educ., *34*, pp. 156-161. 1999.

49. Sato, H. and S. Nishio. Polymer Laser Photochemistry, Ablation, Reconstruction, and Polymerisation, J. Photochem. Photobiol. C-Photochem. Rev., *2*, pp. 139-152. 2001.

50. Serafetinides, A., M.I. Makropoulou, C.D. Skordoulis, and A.K. Kar. Ultra-short pulsed laser ablation of polymers, Appl. Surf. Sci., *180*, pp. 42-56. 2001.

51. Jandeleit, J., G.Urbasch, H.D.Hoffmann, H.G. Treusch, and E.W. Kreutz. Picosecond laser ablation of thin copper films, Appl. Phys. A-Mater. Sci. Process., *63*, pp. 117-121. 1996.

52. R.Srinivasan and V. Mayne-Banton. Self-developing photoetching of poly(ethylene terephthalate) films by far-ultraviolet excimer laser radiation, Appl. Phys. Lett., *41*, pp. 576-578. 1982.

53. Kosmidis, C.E. and C.D. Skordoulis. Dopant-enhanced ablation of nitrocellulose by a nitrogen laser, Appl. Phys. A-Mater. Sci. Process., *56*, pp. 64-68. 1993.

54. Skordoulis, C.D., M.I. Makropoulou, and A.A. Serfetinides. Ablative etching of nitrocellulose with infrared and ulra-violet laser-radiation, Opt. Laser Technol., *27*, pp. 185-189. 1995.

55. Skordoulis, C.D., M.I. Makropoulou, and A.A. Serfetinides. Ablation of nylon-6,6 with UV and IR lasers Appl. Surf. Sci., *86*, pp. 239-244. 1995.

56. Viville, P., S. Beauvois, G. Lambin, R. Lazzaroni, J.L. Brēdas, K. Kolev, and L. Laude. Excimer Laser-Induced Surface Modifications of Biocompatible Polymer Blends, Appl. Surf. Sci., *96-98*, pp. 558-562. 1996.

57. Srinivasan, R. and B. Braren. Ultraviolet laser ablation of organic polymers, Chem. Rev., *89*, pp. 1303-1316. 1989.

58. Roberts, M.A., J.S. Rossier, P. Bercier, and H. Girault. UV Laser Machine Polymer Substrates for the Development of Microdiagnostic Systems, Anal. Chem., *69*, pp. 2035-2042. 1997.

59. Korte, F., S. Nolte, B.N. Chichkov, T. Bauer, G. Kamlage, C. Fallnich, and H.Welling. Far-field and Near-field Material Processing with Femtosecond Laser Pulses, Appl. Phys. A-Mater. Sci. Process., *69*, pp. S7-S11. 1999.

60. Bado, P., W. Clark, and A. Said. *Ultrafast lasers for science, industry and micromachining*. [cited; Available from: http://www.cmxr.com/index.htm.

61. Farag, M.M., Polymeric materials and their processing. New York: Prentice Hall. 1989.

62. Kalpakjian, S., Manufacturing Processes for Engineering Materials. 3rd ed ed. Massachusetts: Addison-Wesley. 1984.

63. Khan, T.A., K.K. Peh, and H.S. Ch'ng. Mechanical, Bioadhesive Strength And Biological Evaluations Of Chitosan Films For Wound Dressing, J. Pharm. Pharm. Sci, *3*, pp. 303-311. 2000.

64. Yudanova, T.N. and I.V. Reshetov. Modern wound dressings: Manufacturing and properties Pharmaceut. Chem. J., *40*, pp. 85 – 92. 2006.

65. Ang, L.P.K., Z.Y. Cheng, R.W. Beuerman, S.H. Teoh, X. Zhu, and D.T.H. Tan. The Development of a Serum-Free Derived Bioengineered Conjunctival Epithelial Equivalent Using an Ultrathin Poly(ε-Caprolactone) Membrane Substrate, Invest. Ophthamol. Vis. Sci. , *47*, pp. 105-112. 2006.

66. Matsuda, T. Recent Progress of Vascular Graft Engineering in Japan, Artif. Organs, *28*, pp. 64 – 71. 2004.

67. Khor, H.L., K.W. Ng, J.T. Schantz, T.T. Phan, T.C..Lim, S.H. Teoh, and D.W. Hutmacher. Poly(ε-caprolactone) films as a potential substrate for tissue engineering an epidermal equivalent, Mater. Sci. Eng. C, *20*, pp. 71-75. 2002.

68. Tiaw, K.S., S.W. Goh, M. Hong, Z. Wang, B. Lan, and S.H. Teoh. Laser surface modification of poly(ε-caprolactone) (PCL) membrane for tissue engineering applications, Biomaterials, *26*, pp. 763-769. 2005.

69. Prucker, O., S. Christian, H. Bock, J. Rühe, C.W. Frank, and W. Knoll. On the glass transition in ultrathin polymer films of different molecular architecture, Macromol. Chem. Phys. , *199*, pp. 1435-1444. 1998.

70. Crescenzi, V., G. Manzini, G. Calzolari, and C. Borri. Thermodynamics of fusion of poly-β-propiolactone and poly-ε-caprolactone. comparative analysis of the melting of aliphatic polylactone and polyester chains, Eur. Polym. J, *8*, pp. 449-463. 1972.

71. Ruiz-Cardona, L., Y.D. Sanzgiri, L.M. Benedetti, V.J. Stella, and E.M. Topp. Application of benzyl hyaluronate membranes as potential wound dressings: evaluation of water vapour and gas permeabilities, Biomaterials, *17*, pp. 1639-1643. 1996.

72. Savitskii, A.V., B.Y. Levin, and V.P. Demicheva. Regularities of the orientational drawing of crystallizing polymers, Polym. Sci U.S.S.R., *15*, pp. 1446-1451. 1973.

73. Persenaire, O., M. Alaxandre, P. Degée, and P. Dubois. Mechanisms and Kinetics of Thermal Degradation of Poly(ε-caprolactone), Biomacromolecules, *2*, pp. 288 - 294. 2001.

74. Ruseckaite, R.A. and A. Jiménez. Thermal degradation of mixtures of polycaprolactone with cellulose derivatives, Polm. Degrad. Stab., *81*, pp. 353 – 358. 2003.

75. Sivalingam, G. and G. Madras. Thermal degradation of poly (ε-caprolactone) Polym. Degrad. Stab., *80*, pp. 11 – 16. 2003.

76. Sivalingam, G., K. R., and G. Madras. Blends of poly(ε-caprolactone) and poly(vinyl acetate): mechanical properties and thermal degradation Polym. Degrad. Stab., *84*, pp. 345 – 351. 2004.

77. Marco, Y., L. Chevalier, and M. Chaouche. WAXD study of induced crystallization and orientation in poly(ethylene terephthalate) during biaxial elongation, Polymer, *43*, pp. 6569-6574. 2002.

78. Lüpke, T., S. Dunger, J. Sänze, and H.-J. Radusch. Sequential biaxial drawing of polypropylene films, Polymer, *45*, pp. 6861-6872. 2004.

79. Narh, K.A., J.A. Odell, A. Keller, and G.V. Fraser. The effect of nucleation density on the kinetics of crystallization and on the resulting structure and thermal properties of polymers crystallized during cooling J. Mater. Sci *15*, pp. 2001-2009. 1980.

80. Lackey, J.C., R.G. Marchand, and M.K. Kumaran, *A Logical Extension of the ASTM Standard E 96 to Determine the Dependence of Water Vapour*

Transmission on Relative Humidity, in *Insulation Materials: Testing and Applications*, R.S. Graves and R.R. Zarr, Editors. 1997, ASTM International: West Conshohocken, PA 19428-2959 USA. p. 456-472.

81. Hu, Y., V. Topolkaraev, A. Hiltner, and E. Baer. Measurement of water vapor transmission rate in highly permeable films, J. Appl. Polym. Sci. , *81*, pp. 1624-1633. 2001.

82. Cussler, E.L., Diffusion: Mass Transfer in Fluid Systems. 2nd edn ed: Cambridge University Press. 1997.

83. Breuer, J., S. Metev, and G. Sepold. Photolytic surface modification of polymers with UV-laser radiation, J. Adh. Sci. Technol., *5*, pp. 185 - 197. 1994.

84. Murahara, M. and K. Toyoda. Laser-induced photochemical modification and adhesion improvement of a fluororesin surface, J. Adh. Sci. Technol., *8*, pp. 213 - 221. 1995.

85. Zhang, J.Y., H. Esrom, U. Kogelschatz, and G. Emig. Modifications of polymers with UV excimer radiation from lasers and lamps, J. Adh. Sci. Technol., *8*, pp. 153 - 184. 1994.

86. Bityurin, N., B. Luk'yanchuk, M.H. Hong, and T.C. Chong. Models for laser ablation of polymers Chem. Rev., *103*, pp. 519-552. 2003.

87. Ashkenasi, A., G. Müller, A. Rosenfeld, R. Stoian, I.V. Hertel, N.M. Bulgakova, and E.E.B. Campbell. Fundamentals and advantages of ultrafast micro-structuring of transparent materials, Appl. Phys. A, *77*, pp. 223-228. 2003.

88. Stuart, B.C., M.D. Feit, S. Herman, A.M. Rubenchik, B.W. Shore, and M.D. Perry. Nanosecond-to-femtosecond laser-induced breakdown in dielectrics, Phys. Rev. B, *53*, pp. 1749 - 1761. 1996.

89. Tiaw, K.S., M.H. Hong, T.S. Ong, Q. Xie, and S.H. Teoh, *Laser micro-structuring of newly-developed ultra-thin poly(e-caprolactone) films*, in *6th International Symposium on Laser Precision Microfabrication - Science and Applications*. April 4 - 8, 2005: Williamsburg, Va, USA.

90. Curtis, A. and C. Wilkinson. Topographical control of cells, Biomaterials *18*, pp. 1573 - 1583. 1997.

91. Ito, Y. Surface micropatterning to regulate cell functions, Biomaterials, *20*, pp. 2333 - 2342. 1999.

92. Rajnicek, A.M., S. Britland, and C. McCaig. Contact guidance of CNS neurites on grooved quartz: influence of groove dimensions, neuronal age and cell type, J. Cell Sci, *110*, pp. 2905 - 2913. 1997.

93. Hecht, E., Optics. 4th ed. ed: Addison Wesley. 2001.

94. Carslaw, H.S. and J.C. Jaeger, Conduction of Heat in Solids. 2nd ed. Oxford: Oxford Scientific Publications. 1990.

95. Dyer, P.E., M. Pervolaraki, and T. Lippert. Experimental studies and thermal modelling of 1064- and 532-nm Nd:YVO4 micro-laser ablation of polyimide Appl. Phys. A, *80*, pp. 529-536. 2004.

96. Teoh, S.H., *Scaffolds in cardiovascular tissue engineering ultra thin layer by layer*, in *Cardiovascular Tissue Engineering Symposium, World Congress Biomechanics*. 4-9 Aug 2002: Calgary, Canada.

97. Teoh, S.H. Tissue engineering issues and challenges: the asian perspectives, Tissue Eng., *9 (Sup 1)*, pp. S1 - S3. 2003.

98. Hollander, D.A., C. Soranzo, S. Falk, and J. Windolf. Extensive traumatic soft tissue loss: Reconstruction in severely injured patients using cultured hyaluronan-based three-dimensional dermal and epidermal autografts, J. Trauma-Injury, Infect. Crit. Care, *50*. 2001.

99. Zacchi, V., C. Soranzo, R. Cortivo, M. Radice, P. Brun, and G. Abatangelo. In vitro engineering of human skin-like tissue, J. Biomed. Mater. Res. A, *40*. 1998.

100. Gamaly, E.G., A.V. Rode, V.T. Tikhonchuk, B. Luther-Davies, and A.S.S. 704. Electrostatic mechanism of ablation by femtosecond lasers, Appl. Surf. Sci., *198*, pp. 699 - 704. 2002.

101. Pendroitti, F.L. and L.S. Pendroitti, Introduction to Optics. 2nd ed: Prentice Hall 1991.

102. Ralston, J., D. Fornasiero, and N. Mishchuk. The Hydrophobic Force in Flotation - A Critique, Colloids and Surfaces A, *192*, pp. 39 - 51. 2001.

103. Hutmacher, D.W. Scaffolds in tissue engineering bone and cartilage, Biomaterials, *21*, pp. 2529 - 2543. 2000.

104. Langer, R. and J.P. Vacanti. Tissue engineering, Science, *260*, pp. 920-926. 1993.

105. Atala, A., S.B. Bauer, S. Soker, J.J. Yoo, and A.B. Retik. Tissue-engineering autologous bladders for patients needing cystoplasty, Lancet, *367*, pp. 1241-1246. 2006.

106. Jain, R.K., P. Au, J. Tam, D.G. Duda, and D. Fukumura. Engineering vascularized tissue, Nat. Biotechnol., *23*, pp. 821-823. 2005.

107. Oberpenning, F., J. Meng, J.J. Yoo, and A. Atala. De novo reconstitution of a functional mammalian urinary bladder by tissue engineering, Nat. Biotechnol., *17*, pp. 149-155. 1999.

108. Patel, Z.S. and A.G. Mikos. Angiogenesis wih biomaterial-based drug- an cell-delivery systems, J. Biomat. Sci. Polym. Ed., *15*, pp. 701-726. 2004.

109. Revez, K., B. Hopp, and Z. Br. Excimer laser induced surface chemical modification of polytetrafluoroethylene, Appl. Surf. Sci. , *109 - 110*, pp. 222 - 226. 1997.

110. Lippert, T., T. Nakamura, H. No, and A. Yabe. Laser induced chemical and physical modifications of polymer films: dependence on the irradiation wavelength, Appl. Surf. Sci., *109 - 110*, pp. 227 - 231. 1997.

111. Bityurin, N., S. Muraviov, A. Alexandrov, and A. Malyshev. UV laser modifications and etching of polymer films (PMMA) below the ablation threshold, Appl. Surf. Sci., *109-110*, pp. 270-274. 1997.

112. Emanuel, N.M. and A.L. Buchachenko, New Concepts in Polymer Science: Chemical Physics of Polymer Degradation and Stabilization. 1st English Edn. ed: VNU Science Press. 1987.

113. Rabek, J.F., Photodegradation of Polymers. Physical Characteristics and Applications: Springer. 1996.

114. Gupta, A., R. Liang, F.D. Tsay, and J.Moacanin. Characterization of a dissociative excited state in the solid state: Photochemistry of poly(methyl methacrylate). Photochemical processes in polymeric systems. 5, Macromolecules, *13*, pp. 1696 - 1700. 1980.

115. Fedynyshyn, T.H., R.R. Kunz, R.F. Sinta, R.B. Goodman, and S.P.Doran. Polymer photochemistry at advanced optical wavelengths, J. Vac. Sci. Technol. B, *18*, pp. 3332 - 3339. 2000.

116. Thevenot, P., W. Hu, and L. Tang. Surface chemistry influences implant biocompatibility, Curr. Top. Med. Chem., *8*, pp. 270-280. 2008.

117. Lanir, Y., Handbook of Bioengineering. New York, NY: McGraw-Hill. 1987.

118. Kohn, J. and R. Langer, Bioresorbable and bioerodible materials. Biomaterials Science, ed. B.D. Ratner, et al. New York: Academic Press. 1996.